Characterization of MRE11 mutants provides insight into human genetic disease, cancer, and clinical intervention.

by

Joshua A. Regal

**A dissertation submitted in partial fulfillment
of the requirements for the degree of
Doctor of Philosophy
(Molecular and Cellular Pathology)
in the University of Michigan
2013**

Doctoral Committee:

**Associate Professor David O. Ferguson, Chair
Professor Eric R. Fearon
Associate Professor Mats E.D. Ljungman
Associate Professor Xiaochun Yu**

ACKNOWLEDGEMENTS

This work was supported by National Institutes of Health [R01 HL079118 to DOF, T32 GM007863 to JAR, and T32 CA009676 to JAR]. I would like to acknowledge my mentor, David Ferguson, M.D., Ph.D., for his guidance through this endeavor. I also appreciated the feedback of my other dissertation committee members, Eric Fearon, M.D., Ph.D.; Mats Ljungman, Ph.D.; and Xiaochun Yu, Ph.D. Thanks to Todd Festerling, M.S., of the Ferguson lab for help with experiments. Also, Jeff Buis, Ph.D., of the Ferguson lab was indispensible in the development of this project. Yipin Wu, Ph.D., of the Fegusion lab and Kishore Chiruvella, Ph.D., of the Thomas E Wilson lab provided technical assistance. Many of the Medical Scientist Training Program, Molecular and Cellular Pathology, and the Cancer Biology Training Program aided me through my career as a graduate student until this point, namely Ron Koenig, M.D., Ph.D.; Nick Lukacs, Ph.D.; Mike Imperiale, Ph.D.; Ellen Elkin, Laura Hessler, Laura Labut, and too many others to name. Last but not least, I would like to express my gratitude to Tehmina Masud, M.B.B.S., Ph.D., for her support and thoughtful input throughout this process.

TABLE OF CONTENTS

LIST OF FIGURES

is a loading control. (A-F) Immunoblots are representative of at least three independent experiments. (A) Comparison of empty-vector and wild-type controls. Whereas only weak pKAP or pCHK1 induction was observed in empty-vector controls, these species were robustly induced in cells with wild-type MRE11. The extent of induction was similar across the range of wild-type MRE11 levels seen. (B) Induction of these phosphoproteins was ATM-dependent. (C,D) Induction of pATM and pKAP1, but not pCHK1, was partially abrogated in ATLD17-expressing clones. (D)ASM-expressing cells showed dramatic defects in pKAP1 and pCHK1 induction. (E,F) GRM expression largely complemented pATM and pKAP1 induction; however, GRM complemented pCHK1 induction to a much lesser extent. (F) Cells expressing ATLD1 displayed wild-type levels of pKAP1 and pCHK1 induction. (G-J) Quantitation of pKAP S824 and pCHK S345 induction by cell line (G, I) or cell type (H, J). After accounting for protein loading, induction was normalized to the weighted mean induction of the wild-type lines. Each bar represents at least three independent experiments. Error bars represent standard error of the mean.

Figure 10: Ionizing radiation-induced apical kinase activation and activity, dose-response and time-course studies, 33

(A) ATLD17 expression failed to fully complement pKAP1 induction over a wide range of IR doses. (B) Early pKAP1 induction was not fully complemented by ATLD17 expression. (C) ATLD17 expression fully complemented pCHK1 but not pATM or pKAP1 levels 30 minutes to 8 hours post-IR. (D) ASM-associated defects in pKAP1 and pCHK1 induction persisted 30 minutes to 8 hours post-IR. (E) Over the duration of several hours post-IR, GRM complemented pATM and pKAP1 induction but failed to fully complement pCHK1 induction.

Figure 11: G_2/M checkpoint assay, 35

MEFs were either mock treated or treated with 10 Gy IR and allowed to recover for an hour. Cells were stained for the mitosis-specific p-histone H3 S10 modification. Mitotic index was obtained by comparison of the percentage of pH3-positive IR-treated cells to that for mock-treated cells for each cell line. Results are shown by cell line (A) or cell type (B). A minimum of three independent experiments were performed for each cell line shown. Error bars represent standard error of the mean. At least 80% of wild-type-expressing MEFs that would otherwise be in mitosis were not in mitosis 1h post-IR, consistent with efficient IR-induced G_2/M checkpoint activation. In contrast, IR treatment reduced the proportion of MRE11- or ATM-deficient cells in mitosis to a much lesser extent, which suggests a G_2/M checkpoint defect. ATLD17-, GRM-, or ATLD1-expressing cells all appeared checkpoint proficient while ASM-expressing cells displayed a pronounced checkpoint defect.

Figure 12: MRE11/RAD50/NBS1 molar ratios, 37

(A) MRN complex component levels in empty-vector controls and wild-type MRE11- or mutant-expressing MEF clones. Though ATLD17- and ASM-expressing cells had a wild-type-like RAD50:MRE11, NBS1:MRE11 was reduced in these cells. In contrast, both RAD50:MRE11 and NBS1:MRE11 were wild-type-like in GRM- and ATLD1-expressing cells. GAPDH was used as a loading control. (B-C) Quantitation of cellular MRN complex component levels. MRE11, RAD50 (B), and NBS1 (C) levels were normalized to those in wild-expressing clone 1 (WT 1) whole cell lysate after accounting for protein loading. Each data point represents a

slightly but consistently abrogated. ASM-NBS1 interaction was not appreciated. No defects were detected in GRM or ATLD1 interaction with NBS1.

Figure 16: MRE11 homodimerization and direct interaction with NBS1 by yeast two-hybrid, supplemental, 44

(A) ASM fusion protein levels were similar to wild-type fusion protein levels. Bait and prey were fused to a MYC-tag or HA-tag, respectively. Tubulin was used as a loading control. (B) and (C) Quantitation of bait and prey levels. Fusion protein levels are presented relative to wild-type MRE11 fusion protein levels after accounting for loading. Error bars represent the standard error of the mean for three clones per bait-prey combination. (D) MRE11 homodimerization showing full plates except for where a row or two were cropped out. (E) MRE11-NBS1 interaction showing full plates except for where a row or two were cropped out.

Figure 17: Dimerization mutant, 46

(A) MRE11 stick diagram and alignment showing L72, the residue changed in the DM. (B) *Hs*MRE11 phosphodiesterase domain dimer showing L72 (pink), W243 (violet), and residues 340-366 (mocha). One MRE11 protomer is depicted as light gray while the other is light blue. Note that the latching loops in these structures were mostly disordered and therefore are not shown. The two images shown are rotated ~90° about the long axis of M_2 from each other. (C) DM homodimerization was similar to background by yeast two-hybrid colorimetric assay. (D) Y2H colony growth assay revealed substantially abrogated DM homodimerization. (E) Direct interaction between DM and NBS1 was reduced by 59% compared to wild-type by α-galactosidase assay. (F) DM-NBS1 interaction was slightly but reproducibly reduced by Y2H colony growth assay.

Figure 18: Model depicting ionizing radiation-induced apical kinase activity in mutant-expressing cells, 49

Schematics are shown for cells expressing ATLD17 (A), ASM (B), or GRM (C). Thick arrows represent normal flux whereas thin arrows represent suspected deficiency.

LIST OF TABLES

ABSTRACT

DNA double strand breaks (DSBs) pose a serious threat to cellular and organism well-being. In response to DSBs, MRE11/RAD50/NBS1 (MRN) initiates DNA repair and facilitates signaling via ataxia-telangiectasia mutated (ATM) and ataxia-telangiectasia- and rad3-related (ATR) kinases. Though alteration of any one of several MRE11 protein interaction partners contributes to human genetic disease and/or carcinogenesis, the role *MRE11A* mutation plays in these processes remains unclear. I have set out to clarify this role with potential implications in cancer prevention, prognostication, and treatment.

I studied four human disease-associated MRE11 mutants. Mutants had altered phosphodiesterase domain (MRE11 W243R (ATLD17) and MRE11 Del340-366 (ASM)), glycine-arginine-rich (GAR) motif (MRE11 R572Q (GRM)), or cyclin-dependent kinase (CDK) 2-interacting motif (MRE11 R633X (ATLD1)). Murine versions of the mutants were expressed to physiologic MRE11 levels in murine embryonic fibroblasts, and conditional deletion abolished wild-type MRE11 expression. In this context, I assessed the mutant proteins' abilities to facilitate DSB response (DSBR) signaling.

Each cancer-associated mutant had distinct effects on ionizing radiation (IR)-induced DSBR. ATLD17, ASM, and GRM were defective in facilitating ATM, ATM and ATR, and ATR activity, respectively. Only the impact of ASM obviously disabled the G_2/M checkpoint. No defect in ATLD1-facilitated kinase activity was detected. Whereas ATLD17- and ASM-associated deficits appeared to be attributable to varying disruptions in the MRN complex, no such disruptions were evident with GRM or ATLD1.

MRE11 functional roles clarified include those of the phosphodiesterase domain and homodimerization motif in ATM activation and those of the MRE11 GAR and CDK2-interacting motifs in DSBR signaling. Physiologic MRE11 levels were found to be crucial for optimal DSBR signaling. Because our findings concern the influences of MRE11 protein levels, protein folding, protein-protein interactions, and post-translational modifications on fundamental cellular processes, these findings may broadly inform understanding of MRE11 and protein complexes containing MRE11 in normal and disease states.

CHAPTER 1: INTRODUCTION

1.1: Damage happens

DNA damage is commonplace; each human cell sustains on the order of 10^4-10^6 lesions per day, yet cellular and organism viability rely upon maintenance of genomic integrity for survival and reproduction [1]. Damage can arise from endogenous processes. DNA is subject to nonenzymatic alkylation, or DNA can undergo uncatalyzed hydrolytic production of deaminated bases or abasic sites [2-6]. Cellular respiration gives rise to an abundance of intracellular reactive oxygen species (ROS) [7]. Some ROS invariably make it to the DNA and cause damage. ROS - along with nitrogen species - are made even more abundant during inflammation [8]. Additionally, DNA is damage-prone during replication. In part because ribonucleotides are far more prevalent than deoxyribonucleotides – even during DNA replication, ribonucleotides are often misincorporated [9]. This constitutes by far the most common cause of endogenous nucleotide base lesion in proliferating cells. After being incorporated, ribonucleotides are more susceptible than their deoxy counterparts to undergoing hydrolysis to produce SSBs [10]. Additionally, deoxyribonucleotides can be misincorporated during replication, resulting in base mismatches [11]. Replication of highly repetitive regions of DNA can be problematic and - through processes such as polymerase slippage - can result in addition to or deletion of repetitive elements [12]. In addition, abortive topoisomerase activity can produce SSBs or DNA double strand breaks (DSBs) that require additional cell machinery to be fixed [13-16]. DNA damage can also be programmed. Lymphocyte development requires DNA breaks or alteration during V(D)J recombination, class-switch recombination, and somatic hypermutation [17]. Moreover, DNA breaks are required for crossing over during meiosis in gametes [18].

The genome is under constant assault from exogenous agents. Ultraviolet radiation (UV) is ubiquitous and is capable of producing 10^5 lesions per exposed cell per hour [19]. UV light produces cyclobutane dimers and pyrimidine-(6-4)-pyrimidone photoproducts [20]. Exposure to

chemicals, such as those in tobacco products, heterocyclic amines in over-cooked meats, and aflatoxins in moldy food, can result in DNA adduct formation [21]. Infectious agents often cause DNA damage indirectly through incitement of inflammation and replication stress as well as interference with DNA maintenance machinery, but they can also directly cause damage – e.g. via viral integration [22]. Iatrogenic DNA damage arises from use of cancer chemotherapeutic agents including alkylating agents, antimetabolites, and topoisomerase inhibitors [23-25].

Ionizing radiation (IR) is another exogenous cause of DNA damage. IR can arise from natural sources or iatrogenically. Naturally occurring radioisotopes can decay into radon, which accumulates in some basements and exposure to which has been associated with lung cancer [26]. Iatrogenic sources of IR include computed tomography scans, plain film X-rays, fluoroscopy, and nuclear medical imaging using ^{123}I, ^{99m}Tc, and ^{18}F [27,28]. Though DSBs are not necessarily the most common type of damage caused by IR, DSBs are a particularly cytotoxic result of IR exposure [29]. Because of this trait, IR is often used therapeutically [30]. ^{131}I is use to treat benign and malignant thyroid diseases. Common cancer treatments include photon therapy and brachytherapy using ^{137}Cs, ^{60}Co, ^{192}Ir, ^{125}I, ^{103}Pd, or ^{106}Ru. Finally, nuclear weapons use at Hiroshima, Nagasaki, and test sites around the world and nuclear meltdowns the likes of Chernobyl and Fukushima serve as tangible if somber reminders of the damaging powers of ionizing radiation.

1.2: The DNA damage response (DDR)

The DNA damage response (DDR) encompasses DNA lesion detection, signaling of lesion presence, and mediation of DNA repair.

DNA repair, overview

To deal with the myriad DNA lesions, cells have evolved a diverse array of complementary and sometimes overlapping DNA repair pathways. O^6-alkyguanines undergo direct reversal, i.e. dealkylation [31]. The mismatch repair machinery detects DNA mismatches and insertion/deletion loops and performs nicking of a single strand; the mismatch is subsequently resolved by nuclease, polymerase, and ligase activities [32]. Abnormal DNA bases and simple

base adducts may be handled by base excision repair (BER) which begins with glycolytic base removal followed by nuclease, polymerase, and ligase activities [33]. Single strand breaks – such as those which might occur with backbone hydrolysis following ribonucleotide misincorporation, oxidative damage, and abortive topoisomerase I activity commonly feed into the BER pathways. Helix-distorting base lesions, e.g. bulky base adducts and UV photoproducts, undergo nucleotide excision repair (NER) [34]. Difficulty transcribing across lesions can result in transcription-coupled NER. A global NER pathway also exists. In either case, nucleolytic activity results in excision of 22-30 bases which is followed by polymerase and ligase activity. Replication fork blockage can be bypassed by translesion synthesis polymerases [35].

Double strand break (DSB) repair occurs by one of two types of mechanisms: non-homologous end-joining (NHEJ) and homology-directed repair (HDR) (Figure 1) [36,37]. Classical NHEJ (C-NHEJ) involves detection by the highly abundant KU70/80 complex, signal transduction by DNA-dependent protein kinase catalytic subunit (DNA-PKcs) activation and activity, Artemis nuclease, X-ray repair cross-complimenting protein (XRCC) 4, ligase (LIG) 4, and XRCC4-like factor (XLF). KU70/80 and XRCC4/LIG4 are considered the NHEJ core and are sufficient for blunt end ligation. DNA-PKcs and Artemis are responsible for processing non-blunt ends prior to ligation. Unlike C-NHEJ, alternative end-joining (A-EJ) remains poorly defined. Though no proteins have been identified as functioning exclusively in A-EJ, several proteins - including ADP-ribosyl transferases (ARTs, more commonly known as PARPs), meiotic recombination (MRE) 11, C-terminal binding protein-interacting protein (CTIP), Werner syndrome helicase (WRN), LIG1, and LIG3 - have been implicated in A-EJ. C-NHEJ and A-EJ – but especially the latter - are considered error-prone. NHEJ can occur during any phase of the cell cycle but especially predominates during G_1/G_0, and C-NHEJ is relatively fast and efficient. Consequently, C-NHEJ is the predominate means of general DSB repair in mammalian cells. V(D)J rearrangements and class-switch recombination (CSR) are also catalyzed by C-NHEJ and C-NHEJ or A-EJ, respectively [38].

Homology-directed repair includes homologous recombination (HR) [37]. For HR, a complex of MRE11, RAD50, and Nijmegen breakage syndrome (NBS) 1 (MRN) and CTIP promote resection to yield ssDNA intermediates. RAD51, breast and ovarian cancer susceptibility protein (BRCA) 1, and BRCA2 are involved in invasion of the resulting 3′-ssDNA into the homologous

sister chromatid sequence. Polymerases, nucleases, helicases, and ligase all subsequently cooperate in substrate resolution and ligation. HR results in high-fidelity repair. HR is restricted to S and G_2 phases of the cell cycle, when a sister chromatid is present; during that time, HR is the predominant general DSB repair pathway. Components of the HR machinery are also involved in DNA replication restart at stalled replication forks, resolution of inter-strand cross-links, A-EJ, and meiotic recombination.

Figure 1: DNA double strand break repair pathways, overview

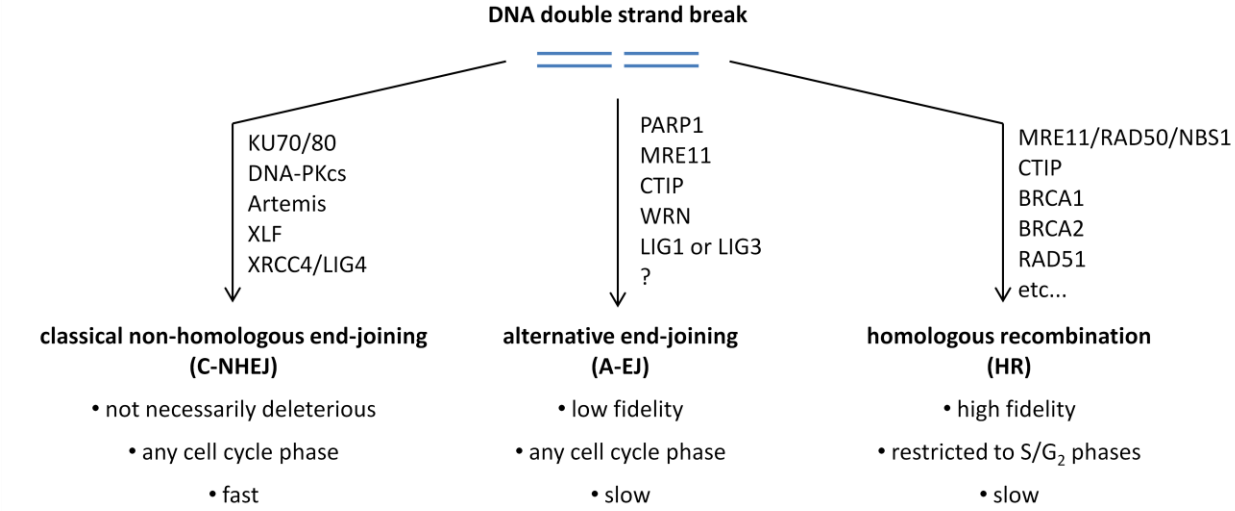

DNA damage response signaling, overview

In addition to activating various DNA repair pathways, DNA breaks can activate apical phosphatidylinositol 3-kinase-related kinases: DNA-PKcs, ataxia-telangiectasia mutated (ATM), and/or ataxia telangiectasia- and rad3-related (ATR) (Figure 2) [39]. After DSBs are sensed by KU70/80 or MRN, DNA-PKcs or ATM is activated, respectively. DSB resection results in replication protein A (RPA)-coated ssDNA, ATR interacting protein (ATRIP) and ATR recruitment, and ATR activation [40,41]. Following activation, these kinases target proteins containing their (S/T)Q consensus sequence [42-44]. Amongst ATR and ATM targets are

checkpoint kinase (CHK) 1 and CHK2 which together regulate cyclin-dependent (CDK) kinase activity [45-48]. DNA damage-induced CDK inhibition results in delays at G_1/S, intra-S, and G_2/M checkpoints which allows cells more time to repair damaged DNA [49]. Apical kinases also activate DNA repair: They induce DNA repair protein activity either through transcriptional upregulation or post-translational modification, and they promote recruitment of factors for damage repair. Recent studies point to the vastness of the ATM and ATR kinomes, suggesting these kinases actually regulate many other cellular processes [44].

Following successful repair, DDR signaling activates its own downregulation [50-54]. If damage persists, chronic DDR can often activate cellular senescence or apoptosis [55]. Erroneous DNA repair potentially results in a loss of cell functioning- including the ability to accurately repair future DNA lesions – and other oncogenic changes [56].

Figure 2: DNA double-strand break response signaling, overview

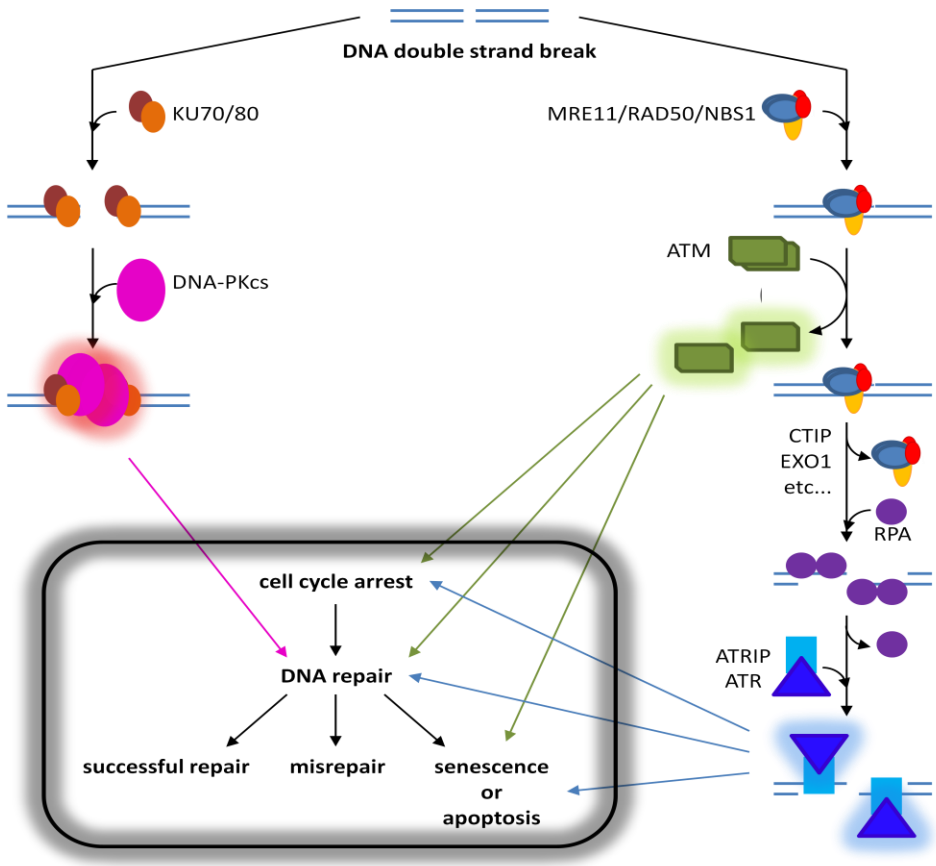

1.3: The MRE11/RAD50/NBS1 (MRN) complex: A key regulator of double strand break response signaling and repair

The MRN complex is a key mediator of the cellular DSB response (DSBR). MRN senses DSBs, activates the ATM and ATR apical kinases, mediates homology-directed repair during S and G_2 phases of the cell cycle and meiosis, promotes DSB resection, and serves a broader role in tethering DNA ends together [57].

MRE11/RAD50/NBS1 structure

MRE11 and RAD50 are highly conserved; orthologues are found in bacteriophages, eubacteria, archaea, and eukarya. NBS1 is part of a family limited to eukarya which includes Xrs2 in the budding yeast *Saccharomyces cerevisiae* [58].

MRE11 consists of an ordered and conserved N-terminal phosphodiesterase domain and a disordered and somewhat less conserved C-terminus (Figure 3A) [59]. The phosphodiesterase domain includes the nuclease or catalytic domain and the capping domain. The nuclease domain includes five nuclease motifs. These nuclease motifs contain residues responsible for coordination of 2 Mn^{2+} ions per nuclease active site. A mechanism of nucleolytic cleavage has been proposed based on archaea *Pyrococcus furiosus* Mre11-nucleotide structures [60-62]. The active site residues directly involved in Mn^{2+} coordination and transition state stabilization are conserved between archaea and humans, suggesting the same mechanism may be applicable to *Homo sapiens* MRE11 [59]. While one Mn^{2+} ion stabilizes the substrate DNA backbone, the other Mn^{2+} ion binds the hydroxide ion nucleophile. *Pf*Mre11 H85 (*Hs*MRE11 H129) is presumed to be involved in stabilization of the pentacovalent transition state and proton donation to the 3′-OH leaving group.

The MRE11 nuclease domain is also involved in homodimer formation. Though many residues involved formation of the hydrophobic dimer interaction sites are conserved between eukarya and prokarya, the structures are otherwise divergent. The primary dimerization interface in prokaryotic Mre11 is a four-helix bundle [61,63,64]. In contrast, the primary dimerization interface of *Hs*MRE11 consist of interaction of an extend α2-β3 latching loop – not found in

prokarya – and helices H2 and H3 of the opposite protomer [59]. Together this loop and these helices have extensive hydrophobic interactions, a water-mediate H-bond, and a disulfide bond. Another *Hs*MRE11 dimerization interface occurs by packing of the β3-α3 loop of one protomer with the S4-S5 loop – which is much shorter than that found in prokaryotic Mre11 - of the opposite protomer.

*Pf*Mre11 co-crystallization with synaptic and branched DNA structures revealed six binding loops in the *Pf*Mre11 phosphodiesterase domain, and DNA-interacting residues in five of these six loops are conserved between humans and *P. furiosus* [62]. However, when synaptic DNA was modeled onto *Hs*MRE11, a much different DNA binding configuration was predicted [59]. Furthermore, branched DNA was sterically hindered from binding to *Hs*MRE11 in a manner similar to that seen for *Pf*Mre11. These modeling studies, the increased compaction of the *Hs*MRE11 phosphodiesterase domain, and the differences in homodimer configuration between *Pf*Mre11 and *Hs*MRE11 together suggest that DNA binding modes are quite different for *Hs*MRE11 and prokaryotic Mre11. The disordered mammalian MRE11 C-terminus includes a glycine-arginine-rich (GAR) motif – which has no equivalent in prokaryotic Mre11 – that has been implicated in DNA binding [65]. Other C-terminal motifs have also been implicated [66]. However, the nature of mammalian MRE11 DNA binding is otherwise poorly understood.

The MRE11 C-terminus may also be involved in binding to RAD50. The prokaryotic Mre11 C-terminus and capping domain are critical for interaction with the Rad50 coiled-coil and ATPase domains, respectively [63,67,68]. The Mre11 C-terminus forms a helix-loop-helix motif that fits orthogonally across the end of the Rad50 coiled-coil domain. Conservation of Mre11 C-terminal residues suggests the mammalian MRE11 C-terminus could be similarly involved though this interaction remains to be defined.

In addition to potentially being involved in DNA and RAD50 binding, the MRE11 C-terminus may serve as a flexible tether to mediate other MRE11-protein interactions. MRE11 has been recently shown to interact with CDK2 and enable CDK2-mediate CTIP phosphorylation and activity [69].

MRE11 and RAD50 form are able to form a heterotetrameric DNA binding and processing core [61,70]. RAD50 consists of an ATPase domain connected via a long coiled-coil domain to a

Zn^{2+}-coordinating hook domain (Figure 3B) [71]. The hook domain can either contribute to RAD50 homodimerization within an M_2R_2 complex or interact with other M_2R_2 complexes to bridge DNA ends as far away as 1200Å [70,72]. The coiled-coil domains are involved in MRE11 binding, DNA binding, and communication of hook domain and ATPase domain binding statuses across the complex. In addition to hydrolyzing ATP, the ATPase domain interacts with MRE11 and is the primary domain responsible for RAD50 homodimerization.

NBS1 includes an N-terminal Forkhead homology (FHA) domain and tandem BRCA C-terminal (BRCT) domains (Figure 3C). These domains are responsible for interaction with DSBR phosphoproteins such as CTIP and mediator of DNA damage checkpoint (MDC) 1. Like MRE11, NBS1 has a disordered, flexible C-terminus. The NBS1 C-terminus includes an MRE11 binding motif and an ATM binding motif. The fission yeast *Schizosaccharomyces pombe* Nbs1 Mre11 binding motif has been shown to interact with the *Sp*Mre11 capping domain and latching loops [73]. This interaction is asymmetrical in nature with only one *Sp*Nbs1 molecule making contacts with the latching loops of both *Sp*Mre11 protomers. Disruption of the *Sp*Mre11 or *Hs*MRE11 latching loops was found to compromise interaction with *Sp*Nbs1 or *Hs*NBS1, respectively, consistent with the importance of the latching loops in MRE11-NBS1 interaction [59,73].

Figure 3: MRE11, RAD50, and NBS1 structures

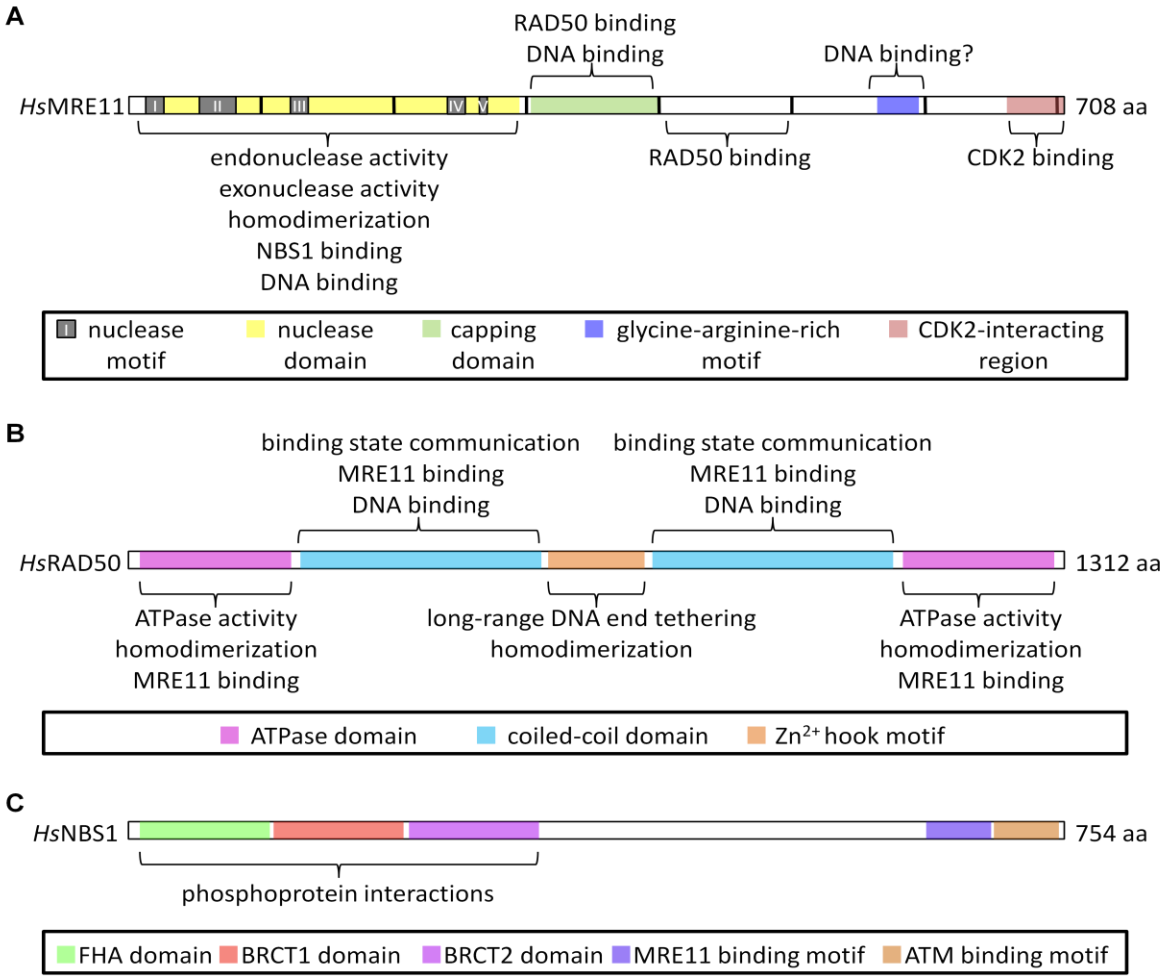

MRE11/RAD50/NBS1 in DNA metabolism and repair

MRN facilitates general DSB repair through enzymatic and architectural activities. MRE11 and MRN possess Mn^{2+}-dependent 3′-5′ exonuclease, ssDNA endonuclease, and hairpin opening activities *in vitro* [74,75]. Paradoxically, this nuclease activity is required for efficient completion of HR, which requires production of a 3′ tail for strand invasion [76]. MRN-CTIP nuclease activity appears to be involved in nicking DNA up to a few hundred bases away from DSBs and thereby provides sites for other nucleases, e.g. EXO1 or DNA2, to complete DNA resection and produce a 3′ tail [77,78]. Meanwhile, MRN is able to tether DNA ends over short or long distances so that they may eventually be rejoined [79]. Part of MRN's usefulness in

initiation of DSB resection may lie in its ability to cleave 3′ adducts from DNA ends [80]. Hence, abortive topoisomerase II activity can be repaired with the help of MRN nuclease activity. MRN processing could also work to favor HR over C-NHEJ. DNA-PK favors binding to dsDNA ends, so DNA end processing could discourage DNA-PK binding and C-NHEJ. The functions of MRN in HR promotion are critical for cellular homeostasis. HR is critical during proliferation with HR defects resulting in impaired development and stem cell function [81]. Furthermore, accumulation of unrepaired DSBs is associated with cellular senescence or loss and aging [82].

MRN nuclease and tethering activities also appear to play roles in facilitating NHEJ. B cells expressing the nuclease-dead MRE11 H129N mutant were found to be defective in class switch recombination (CSR), an NHEJ process [38]. The loss of MRN further decreased CSR efficiency, consistent with MRN tethering of DSBs being important for general DSB repair. MRN mediation of class switch recombination and NBS1 and ATM promotion of V(D)J rearrangement collectively promote effective adaptive immunity.

In addition to its role in general DSB repair, MRN participates in DSB prevention. MRN facilitates resection at stalled replication forks to prevent replication fork collapse [83]. Also, MRN is able to cleave 3′-phosphotyrosyl bonds and thereby prevent abortive topoisomerase I activity from being encountered by a replication fork and becoming a DSB [84].

Furthermore, MRN is involved in telomere homeostasis [85-87]. MRN binds to telomeres in S and G_2 phases of the cell cycle where it could be involved in production of leading strand 3′ overhangs. With the assistance of other components of the HR machinery, these overhangs can subsequently be used to form t-loops. T-loop formation, in turn, prevents recognition of chromosome ends as DSBs. In this manner, MRN and ATM activity prevent NHEJ-mediated telomeric fusions. However, these proteins can also support neoplasia through mediation of HR-based alternative lengthening of telomeres.

DNA processing by MRN is also required in meiosis [88,89]. During initiation of crossing over, the topoisomerase II-like enzyme SPO11 creates DSBs and remains covalently attached to the DNA ends. MRN is required for SPO11 removal and production of ssDNA. The complete set of HR machinery, including ATM, participates in progression of HR during meiosis. Additionally,

evidence exists that suggests MRN tethering is required for SPO11-mediated DSB induction, reinforcing the importance of MRN tethering [90].

MRE11/RAD50/NBS1 in signaling

MRN plays a crucial role in DSB signal transduction. MRN mediates ATM kinase recruitment to DSBs [91,92]. Upon ATM recruitment, ATM autophosphorylates, monomerizes, and is activated. ATM targets include the CHK2 kinase, the tumor suppressor p53, histone H2AX, MRN, CTIP, and KRAB-interacting protein (KAP) 1. MRN also indirectly activates ATR and CHK1 through its activities promoting DNA resection. These events and others combine to delay progression through the cell cycle, promote repair, and – if necessary – trigger senescence or apoptosis.

The NBS1 C-terminus has been reported to be sufficient and necessary for ATM interaction; however, NBS1 lacking an MRE11 binding motif showed decreased interaction with ATM [40]. This observation is consistent with ATM relying upon multiple contacts with MRN for activation and activity. Furthermore, absence of an NBS1 C-terminus was associated with intact ionizing radiation (IR)-induced ATM autophosphorylation but deficiencies in IR-induced CHK2 and p53 phosphorylation, abrogated γH2AX foci formation, radiosensitivity, and radioresistant DNA synthesis. Moreover, MR was sufficient for ATM interaction and activation in biochemical assays while the NBS1 N-terminus and MRE11 C-terminus appeared important for MRN-ATM interaction [91]. These observations are consistent with the NBS1 C-terminus being important for directing ATM activity towards certain substrates but not necessarily for ATM activation *per se*. Therefore, contacts between ATM and MRN sites other than the NBS1 C-terminal ATM interacting motif are required for ATM activation in cells.

ATM activity is important for DNA damage-induced cell cycle checkpoint activation, senescence, and apoptosis. ATM can target and activate the CHK2 [46]. CHK2 phosphorylates the CDK phosphatase CDC25. This phosphatase is required for CDK-cyclin complex activity, and inhibitory phosphorylation of CDC25 prevents CDK-cyclin activity and cell cycle progression. ATM and CHK2 both target the tumor suppressor p53. P53 phosphorylation activates transcriptional programs specifying DNA repair and cell cycle arrest. Chronic DSBR signaling can prolong p53 activation and result in senescence or apoptosis [55,93,94].

Another ATM target is the histone variant H2AX [95]. As a result, γH2AX is able to recruit mediator of DNA damage checkpoint (MDC) 1. MDC1 is able to recruit additional MRN and ATM thereby closing a positive feedback loop. MDC1-null cells have normal levels of ATM autophosphorylation but still display evidence of defective DSBR signaling suggesting that MDC1-mediated recruitment is required for appropriate directing of ATM activity [96]. MRN recruitment by MDC1 depends upon MDC1 phosphosite interaction with the NBS1 N-terminal FHA and BRCT domains [97], and disruption of the interaction results in checkpoint defects consistent with its importance in checkpoint activation [98].

One critical target of ATM signaling is MRN itself [44,99-105]. ATM mediates MRN phosphorylation and affects MRN localization, protein-protein interactions, and DNA repair function. ATM-dependent NBS1 phosphorylation is important for proper ATM targeting of SMC1 and CHK2, intra-S phase checkpoint activation, and radioresistance [105-109]. RAD50 S635 phosphorylation dispensable for MRN complex formation and ATM activation but not ATM activity towards SMC1, radioresistance, DSB repair, and S phase checkpoint activation [110]. Though MRE11 is also an ATM substrate, the functional significance of this relationship has not yet been determined.

ATM targeting of CTIP modulates DNA repair. CTIP participates in and has been proposed to modulate choice between HDR and A-EJ [111-114]. CTIP phosphorylation, levels, and complex formation with MRN and BRCA1 are controlled by CDK activity in a cell cycle-dependent manner (Figure 4) [115]. Following DNA damage in S or G_2 phases, CTIP is phosphorylated in an ATM-dependent manner. Hyperphosphorylated CTIP promotes MRN-mediated DNA resection, BLM and EXO1 recruitment, checkpoint signaling, and homologous recombination [111,115]. Resected DNA is loaded with replication protein A (RPA). RPA-ssDNA recruits ATR along with its interacting protein ATRIP [40,41]. In this context ATR is activated. A critical target of ATR is checkpoint kinase (CHK) 1 [45,48,116,117]. ATR-mediated CHK1 S345 phosphorylation is required for mitotic catastrophe avoidance and cellular viability. In fact, CHK1 S345A is unable to support cellular proliferation [117].

Figure 4: DNA resection and repair is modulated by cell cycle- and ATM-controlled CTIP modification

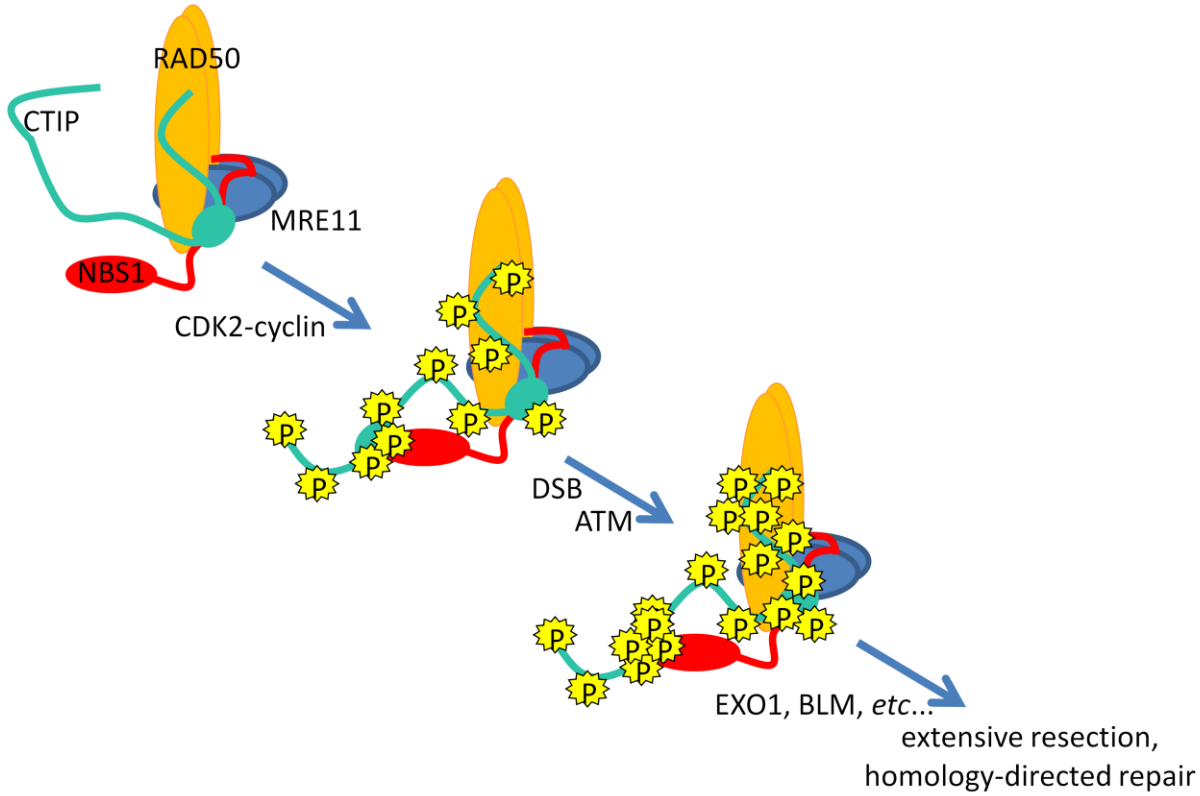

Condensed chromatin presents a major impediment to DNA repair. ATM acts to alleviate this issue through phosphorylation of the transcriptional corepressor KAP1 [118]. Under unstressed conditions, KAP1 activity promotes heterochromatin formation through autoSUMOylation and recruitment of nucleosome deacetylases, methylases, and remodelers. ATM-dependent KAP1 S824 phosphorylation results in abrogation of KAP1-chromatin remodeler CHD3 interaction and chromatin relaxation [119].

MRE11/RAD50/NBS1 confirmation in DSB detection, signaling, and effector responses

An integrated model of MRN as a molecular clamp has been proposed (Figure 5) [67,73,120-122]. In it, MRN alternates between extended and compact states depending upon nucleotide and DNA binding status. The open configuration consists of $M_2R_2N_2$ splayed such that DNA binding and nuclease sites are unobstructed, RAD50 coiled-coils are lax, and homodimerization is

mediated through MRE11 phosphodiesterase domains and intracomplex Zn^{2+} hook interactions. MRN of this configuration could bind DNA ends with large covalent adducts, e.g. SPO11 or topoisomerase II. Recognition and processing of a DSB or DNA hairpin and ATP binding together promote a more compact $M_2R_2N_2$ catalytic head and tighter DNA binding. RAD50 coiled-coil domain rigidity is increased, and RAD50 Zn^{2+} hooks make intercomplex interactions to tether DSBs over large distances. In this closed configuration, MRE11 is sterically hindered from binding dsDNA, and therefore, its dsDNA exonuclease activity is stymied. On the other hand, MRE11 retains binding and endonuclease activities towards ssDNA and hairpins. Iterative ATP hydrolysis results in partial melting of dsDNA and hairpin opening. Finally, the closed form promotes and is promoted by tighter NBS1 binding. This configuration thereby promotes MRN-mediated ATM activation and activity.

Figure 5: An integrated model of MRE11/RAD50/NBS1 structure-function relationships

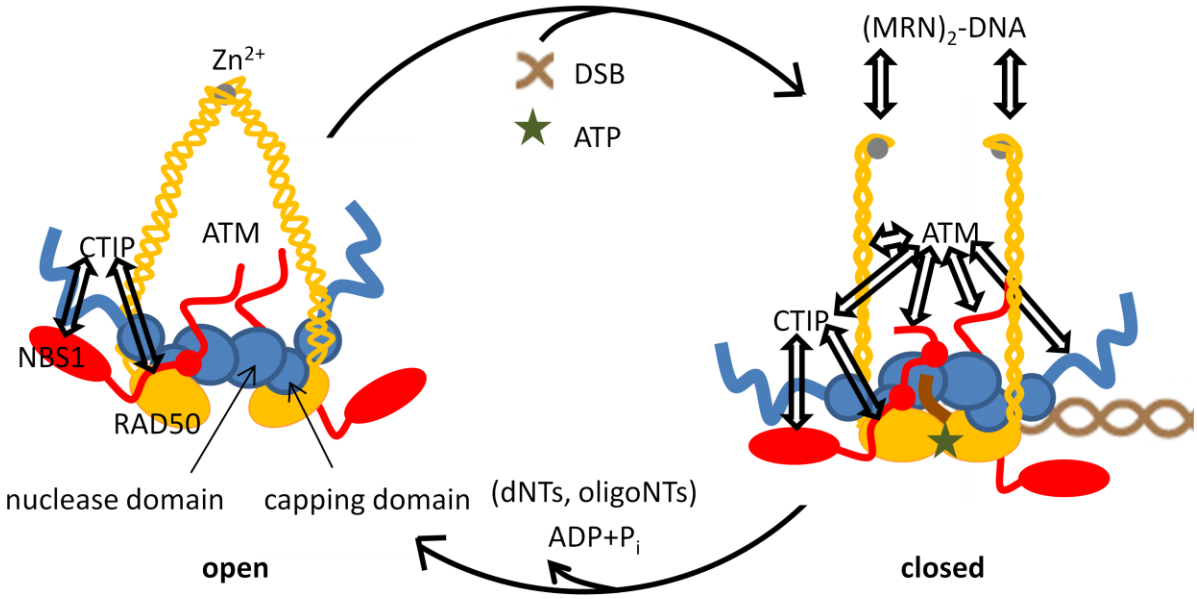

1.4: MRE11/RAD50/NBS1 and ATM dysfunction in human disease

Human genetic disease

Lesions to MRE11 or its partners have been associated with human genetic disease (Tables 1 and 2). Biallelic hypomorphic or null mutations in *ATM* result in ataxia-telangiectasia (AT; MIM 208900) [123]. AT is characterized by progressive cerebellar ataxia, oculocutaneous telangiectasia, immunodeficiency, radiation hypersensitivity, sterility, and marked predisposition to malignancy, especially lymphoreticular neoplasia. Inheritance of two hypomorphic *NBN* (*NBS1*) alleles causes Nijmegen breakage syndrome (NBS; MIM 251260) [124]. Like AT, NBS includes immunodeficiency, radiation hypersensitivity, and a marked cancer predisposition. NBS is distinguishable from AT by the lack of ataxia and telangiectasia and by the presence of microcephaly and growth retardation. Also notable is that the predisposition to malignancy is more marked in NBS; NBS patients have a lower age of incidence and a higher lifetime prevalence of cancer.

Table 1: Human genetic diseases associated with MRE11 partners

disorder	ataxia telangiectasia (AT)	Nijmegen breakage syndrome (NBS)	Nijmegen breakage syndrome-like disorder (NBSLD)
mutated gene	*ATM*	*NBN (NBS1)*	*RAD50*
cerebellar ataxia	+	-	+
microcephaly	-	+	+
telangiectasia	+	-	nr
immunodeficiency	+	+	-
malignancy	+	+	-
MRE11 protein	wild-type	wild-type	wild-type
MRE11/RAD50/NBS1 levels*	++++/++++/++++	++++/++++/+	+++/+/+
defective MRE11 IRIF formation	+	+	+
deficiency in ATM-dep events	+	+	+
spontaneous chromosomal aberrations	+	+	+
cellular IR hypersensitivity	+	+	+

nr=not reported

*: +=very low, ++=low, +++=moderate, ++++=normal, +++++=high

Table 2: *MRE11A* mutation-associated human genetic diseases

disorder	ATLD1-2, 19-20	ATLD3-4	ATLD5-6	ATLD7-16	ATLD17-18	NBSLSM1	NBSLSM2
cerebellar ataxia	+	+	+	+	+	-	+
microcephaly	-	-	-	±	-	+	+
telangiectasia	-	-	-	-	-	nr	nr
immunodeficiency	-	-	-	-	-	-	-
malignancy	-	-	-	-	+	-	-
MRE11 protein	R633X	N117S, (R571X)	T481K, (R571X)	W210C	W243R, (Δ340-366)	wild-type	wild-type, D113G
MRE11/RAD50/NBS1 levels*	+/+/+	++/++/+	++/++/++	+++++/+++++/+	++/++/+	+/+/++	+/+/++
defective MRE11 IRIF formation	+	+	+	+	nr	+	+
deficiency in ATM-dep events	+	+	+	+	+	+	+
spontaneous chromosomal aberrations	+	+	-	-	+	nr	nr
cellular IR hypersensitivity	+	+	+	+	nr	+	+

ATLD=ataxia telangiectasia-like disorder, NBSLSM=Nijmegen breakage syndrome-like severe microcephaly
nr=not reported
*: +=very low, ++=low, +++=moderate, ++++=normal, +++++=high

Autosomal recessive syndromes due to mutation of *RAD50* or *MRE11A* (*MRE11*) appear to be much rarer and were more recently discovered than those caused by *ATM* or *NBN* mutation; therefore, the former are mostly thought of in terms of their likeness to AT or NBS. Hypomorphic *RAD50* mutation has been associated with autosomal recessive NBS-like disorder (NBSLD; MIM 613078) [125]. NBSLD resembled NBS in terms of microcephaly and growth retardation. Unlike NBS, NBSLD was not associated with immunodeficiency or lymphoid malignancy, and it included uncoordinated movements and nonprogressive ataxia. Biallelic hypomorphic *MRE11A* mutation has been associated with NBS-like severe microcephaly (NBSLSM) though it has been more commonly associated with ataxia telangiectasia-like disorder (ATLD; MIM 604391) [126-132]. The former was characterized by severe microcephaly, developmental delay, and lack of coordination or nonprogressive ataxia without obvious predisposition to malignancy or immunodeficiency. ATLD is characterized by cerebellar ataxia and cellular genomic instability similar to but milder than that seen in classic AT. Neither immunodeficiency nor telangiectasia have been associated with ATLD.

These diseases are alike in that they show neurologic phenotypes though the phenotypes appear to vary from those representing developmental defects - exemplified by microcephaly, for instance - to those representing neurodegeneration - e.g. progressive cerebellar ataxia. Because HR is required for cellular proliferation and stem cell function, the developmental defects could

arise due to decreased HR efficiency [81,133-135]. On the other hand, the neurodegeneration could be due to decreased capacity to deal with the DNA damage common to terminally-differentiated neurons. Neurons have a high rate of mitochondrial respiration and therefore possess high levels of ROS [136]. As a result, neurons experience a high rate of oxidative DNA damage. Oxidative lesions often block transcription, upon which neurons rely heavily. Hence, neurons without the capacity to efficiently deal with these lesions would be expected to experience a substantial loss of function due to inability to sustain the necessary rate of transcription. Moreover, the limited regenerative capacity of adult central nervous system neurons means there is little ability to replace underperforming neurons. Accumulation of ROS-associated DNA lesions is associated with common neurodegeneration phenotypes, including Alzheimer's, Huntington's, and Parkinson's diseases [137]. ATM plays a role in the cellular oxidative stress response [138], and ATLD patient cerebella have been found to accumulate oxidized DNA species [139]. Hence, defective responses to ROS-induced DNA damage could contribute to the AT and ATLD neurodegeneration phenotypes. On top of increased ROS-related lesions, terminally-differentiated neurons are in G_0. With no sister chromatids available, they have to rely on lower-fidelity repair of DSBs by C-NHEJ or A-EJ [81]. Because MRN and ATM promote these processes, their deficiency could result in decreased ability of neurons to properly repair DSBs. Hence, defective DSB repair could also contribute to the neurodegeneration phenotype seen in AT and ATLD patients.

AT, NBS, ATLD, NBSLD, and NBSLSM are also all associated with a cellular genomic instability phenotype. This was typically exemplified by deficiency in ATM signaling, cell cycle checkpoint dysfunction, cellular radiation hypersensitivity, and spontaneous translocations of chromosomes 7 and 14 in circulating lymphocytes [125,126,132,140,141]. Lack of ATM or NBS1 especially appears to result in impaired NHEJ-mediated antigen receptor rearrangement [135,142]. The decrease in productive rearrangement efficiency results in decreased circulating lymphocytes, agammaglobulinemia, and immunodeficiency. Inefficient DSB repair also results in DSB persistence and misrepair. This misrepair accounts for the high levels of circulating lymphocytes with spontaneous translocations involving antigen receptor loci and predisposition to lymphomagenesis. Predisposition to infection and malignancy account for substantial disease-associated morbidity and mortality.

Cancer

Genomic instability is a characteristic of cancer and its development [19,56]. Most carcinogens contribute to carcinogenesis through inducing DNA mutation. Such mutations can contribute to tumor suppressor inactivation and proto-oncogene activation. Oncogenic replication stress can result in continuous genomic instability. During cancer development, DDR is selected against resulting in DDR defects and increased rates of mutation. In advanced cancers, cycles of hypoxia-normoxia may cause DNA oxidation.

Efficient DDR is crucial to prevention of tumorigenesis. DDR is often upregulated during the early stages of oncogenesis [143], consistent with its role in tumor suppression. Enhanced DDR has been shown to protect against tumorigenesis in certain contexts [144]. On the other hand, inherited DDR defects can contribute to mutator phenotypes and may allow continued proliferation despite accumulation of DNA damage. Inherited perturbations in the DSBR machinery often manifest as autosomal dominant familial cancer syndromes. Lesions to the tumor suppressors *BRCA1*, *BRCA2*, or their partners are responsible for familial breast cancer syndromes [145-147]. Moreover, inheritance of a single *ATM* mutation appears to predispose to breast cancer, and *NBN* mutation carriers are malignancy prone [148-156].

Somatic disruptions of DSBR genes also play roles in sporadic malignancies. Biallelic somatic *ATM* mutations are common in certain lymphomas and leukemias [157]. Somatic disruptions of *BRCA1/2* and their partners are even more common in tumors than their germline defects [158].

1.5: Insights from murine models of MRE11/RAD50/NBS1 or ATM dysfunction

Mice lacking any member of the MRN complex are inviable [133,134,159,160]. Conditional allele deletion of any of the corresponding genes in cultured cells or *in vivo* proliferating tissues results in dramatic genomic instability and cell death [133,161,162]. These observations are consistent with the view that MRN is required to resolve DNA replication-associated breaks via homology-directed recombination. It should be noted that human genetic diseases have been associated with *MRE11A*, *RAD50*, or *NBN* hypomorphism and not nullizygosity [124-132,163,164]. Hence, nullizygosity of any of these complex components is expected to be

embryonic lethal in humans, and the most appropriate murine models of these disorders are those with *Mre11a*, *Rad50*, or *Nbn* hypomorphism.

Mice expressing hypomorphic *Mre11a* alleles have revealed striking phenotypes. *Mre11a*$^{ATLD1/ATLD1}$ mice expressed murinized versions of the first ATLD allele identified [126,165]. ATLD1 lacks the C-terminal 76 amino acid residues including the CDK2 interaction motif [69]. These mice appeared to reiterate the patient phenotype. They were viable and had no predisposition to lymphomagenesis. *Mre11a*$^{ATLD1/ATLD1}$ cells exhibited DSBR signaling defects - including reduced ATM signaling and checkpoint deficiencies, radiation hypersensitivity, and genomic instability. Though M(ATLD1)RN complex stability appeared intact, complex levels were very low. Still unknown is whether the cellular phenotypes were due to low levels of MRN complex or more directly due to the lack of MRE11 C-terminus. The lack of lymphomagenesis despite reduced NBS1 and ATM function suggests loss of some MRE11 function requisite for oncogenesis. Whether the requirement is for higher MRN levels and non-C-terminus functions or C-terminus-specific functions remains an open question.

A nuclease-dead *Mre11a* allele, *Mre11a*^{H129N}, has also been knocked in [76]. MRE11 H129N supported normal levels of the MRN complex, ATM activation, and G_2/M checkpoint activation but failed to rescue embryonic lethality, cellular proliferation, radiation and replication stress hypersensitivity, homology-directed repair, and genomic stability. These findings show that nuclease function is essential for cellular proliferation during development but dispensable for ATM activation.

Mre11a$^{RK/RK}$ mice - in which the MRE11 glycine-arginine-rich domain arginines have been changed to lysines - exhibited radiation hypersensitivity. MRE11 RK appeared defective in MRE11 DSB localization, DNA binding, exonuclease activity, and mediation of ATR activity, cell cycle checkpoint function, and chromosomal stability [65,166-168]. However, once again the MRE11 mutant levels were sub-physiologic. In this case, *Mre11a*$^{RK/RK}$ cells had MRE11 RK levels 50% of physiologic MRE11 levels. Hence, the MRE11 RK-associated phenotypes could potentially be attributed to low cellular MRE11 RK levels and/or some MRE11 RK-specific dysfunction.

Mice have also been engineered to express hypomorphic *Nbn*. The predominant *NBN* mutation is c.657Δ5 [124,169]. Internal ribosomal entry is required to produce a hypomorphic p70 product with N-terminal truncation. $Nbn^{\Delta B/\Delta B}$, $Nbn^{m/m}$, and $Nbn^{-/-}$+$NBN^{657\Delta 5}$ mice were created to mimic this truncation [170-172]. Each mutant is associated with loss of the N-terminal FHA domain. Though $Nbn^{\Delta B/\Delta B}$ mice only reiterated the cellular phenotypes (radiation hypersensitivity, intra-S and G_2/M checkpoint dysfunction, and IR-induced chromosomal instability) and subfertility, $Nbn^{m/m}$ and $Nbn^{-/-}$+$NBN^{657\Delta 5}$ mice also reflected other patient phenotypes (including growth retardation, immunodeficiency, decreased lymphocyte maturation, increased spontaneous chromosomal translocations, and – for $Nbn^{m/m}$ mice only –predisposition to lymphomagenesis). $Nbn^{m/m}$ cells had intact DSB-induced ATM activation, but DSB-induced ATM activity towards other targets, including CHK2, was diminished in $Nbn^{m/m}$ and $Nbn^{-/-}$+$NBN^{657\Delta 5}$ cells. This phenotype was partially phenocopied in cells expressing another NBS patient allele, NBN^{H45A}, which disrupted a highly conserved NBS1 FHA domain residue [172,173]. These results are consistent with the NBS1 N-terminus – and the FHA domain in particular - being dispensable for ATM activation but essential for appropriate ATM targeting.

Lack of the NBS1 ATM binding motif in $Nbn^{\Delta C/\Delta C}$ and Nbn^{tr735} mice resulted in mild phenotypes [173,174]. $Nbn^{\Delta C/\Delta C}$ and Nbn^{tr735} cells did not have gross defects in DSB-induced ATM activation or ATM activity towards CHK2. Moreover, no change in MRN levels, subcellular localization, or localization to DSBs was detected. However, thymocytes were defective in IR-induced apoptosis, a very mild intra-S phase defect was detected, and ATM-dependent SMC1 and BID phosphorylation was impaired. These results suggest the NBS1 C-terminal ATM interaction motif is dispensable for ATM activation but necessary for appropriate ATM-mediated DSBR.

AT differs from ATLD, NBSLSM, NBLD, and NBS in that it can result from *ATM* nullizygosity as well as hypomorphism. The majority of reported AT cases have been associated with two *ATM* frameshift, nonsense, splice site, or large gene deletion mutations that resulted in loss of detectable protein [163,164]. Other patients had missense mutations, in-frame deletions, or aberrant splicing and detectable ATM by immunoblot. $Atm^{-/-}$ mice largely reiterated the classic AT patient phenotype, including growth retardation, infertility, impaired lymphocyte development, dramatic lymphoma predisposition, and cellular genomic instability [175-177]. In

contrast to the patient phenotype, no cerebellar ataxia was evident. Mice expressing the murinized AT patient allele $Atm^{\Delta SRI}$ had a somewhat milder phenotype than nullizygous mice [178]. Notably, though $Atm^{\Delta SRI}$ mice were also cancer-predisposed, they outlived their nullizygous counterparts. The cancers to which the mice succumbed varied by genotype, too: While nullizygous mice uniformly died of thymic lymphoma, $Atm^{\Delta SRI}$ mice developed a variety of malignancies.

In striking contrast to the viability seen in AT mouse models, ATM kinase dead mice are inviable [179]. Murine cells expressing kinase dead ATM displayed increased spontaneous genomic instability and decreased HR efficiency relative to $Atm^{-/-}$ cells. Hence, kinase dead ATM appears to actually interfere with HR and maintenance of genomic integrity.

As is seen in humans, mice with heterozygosity in DSB repair components are cancer predisposed. Mice with *Nbn* heterozygosity or hypomorphism are predisposed to oncogenesis [171,180]. Mice carrying one hypomorphic *Atm* allele are cancer-predisposed [181] as are $Ctip^{+/-}$ mice [182]. These results support the importance of DSB repair machinery component gene dosage in tumor suppression.

1.6: *MRE11A* mutation and oncogenesis

Cancer-associated DSBR alterations can be exploited for prognostic and therapeutic purposes. For example, higher tumor MRN complex levels have been associated with better response to radiotherapy and better prognosis [183-186]. Hence, knowledge of tumor MRN levels could inform prognostication and treatment choice. Furthermore, cancer-specific DSBR alterations can be used for development of therapeutic targeting strategies; this point is well-illustrated by the success of PARP inhibitors against tumors with BRCA1 or BRCA2 deficiency [187,188].

Despite the importance of the DSBR in cancer predisposition, prognostication, treatment choice, and therapeutic development, the role of *MRE11A* mutations in carcinogenesis remains poorly understood. MRE11 participates in the activation of several tumor suppressors and is frequently downregulated in malignancies [186,189-192]; however, an abundance of evidence suggests MRE11 is not a simple tumor suppressor. When MRE11A is altered in malignancies, a wild-type

allele usually remains intact. ATLD is assumed to be a cancer-prone syndrome; however, cancer has only been associated with a small subset of reported ATLD patients [126-130]. Moreover, *Mre11a*$^{ATLD1/ATLD1}$ mice are not predisposed to the development of lymphoma - the malignancy to which AT and NBS patients are most markedly predisposed [165]. Organism viability and normal cellular proliferation require MRE11 nuclease activity [76], suggesting MRE11 may be required for carcinogenesis as well. Additionally, many human genetic diseases resulting from hypomorphic mutations in the DSBR machinery do not appear to feature cancer predisposition. *RAD50, ATR,* or *CTIP (RBBP8)* mutations have been associated with the autosomal recessive NBS-like disorder (MIM 613078) [125], Seckel syndrome (MIM 210600) [193], or Jawad syndrome (MIM 251255) [125,194], yet none of these syndromes have been linked to gross cancer predisposition.

We set out to help clarify the role of *MRE11A* mutation in carcinogenesis. To this end, the major impacts of previously reported *MRE11A* mutations were sought. A few mutants were found to have distinct deficits in apical kinase activation. Because of the centrality of MRN complex stability to many well-recognized MRE11 functions, including apical kinase activation, mutants' abilities to complex were also assessed. For two mutants, MRN complex instability could explain the signaling defects observed. These findings provide new insight into MRN function and human disease pathogenesis and treatment.

CHAPTER 2: RESULTS

2.1: Meta-analysis of disease-associated *MRE11A* mutations

Several categories of *MRE11A* mutation were uncovered. Most common were loss of nucleotides from the accessory splice signal upstream of exon 5 [191,192,195-202]. Shortening of the poly-T tract in microsatellite instable cells lines and primary tumor cells was linked to exon 5 skipping and decreased MRE11 expression [191]. A few other mutations were associated with aberrant *MRE11A* splicing [129,132]. One such mutation, c.338A>G, was also associated with exon 5 skipping and a small amount of full length transcript [132]. The resulting mRNAs potentially encoded F106QfsX10 or D113G, respectively. Exon 7 was reported to be skipped more frequently in the context of point mutations at the exon 7-intron 7 border – c.658A>C and c.659+1G>A [132]. The resulting mRNA potentially encoded MRE11 S183VfsX31 though none of this species was detected. C.1098+5G>A was reported in an allele that produced *MRE11A* mRNA lacking exon 10 [129]. This loss of 81 bp maintained downstream codons in frame. Hence, the mRNA potentially encoded MRE11 Δ340-366 though this species did not appear to have been detected. In rare instances, *MRE11A* was amplified [203]. More commonly, *MRE11A* was deleted [186,204]. *MRE11A* missense and nonsense mutations were not obviously clustered (Figure 6) [129,130,205-210]. Mutations were distributed both within the N-terminal phosphodiesterase domain and the C-terminal region.

MRE11A mutations arose in a variety of contexts. Twenty ATLD patients have been reported thus far who inherited some combination of missense and nonsense mutations. A couple of these mutants, W243R and R633X, along with a few additional mutants were associated with familial cancer syndromes when inherited along with a wild-type allele. Several somatic missense and nonsense mutations were found in spontaneous malignancies. Microsatellite instable cancer cells were found to have *MRE11A* exon 5 skipping and reduced MRE11 levels. Two NBS-like severe microcephaly patients were each found to have inherited two miss-splicing alleles.

Figure 6: MRE11 mutant meta-analysis results

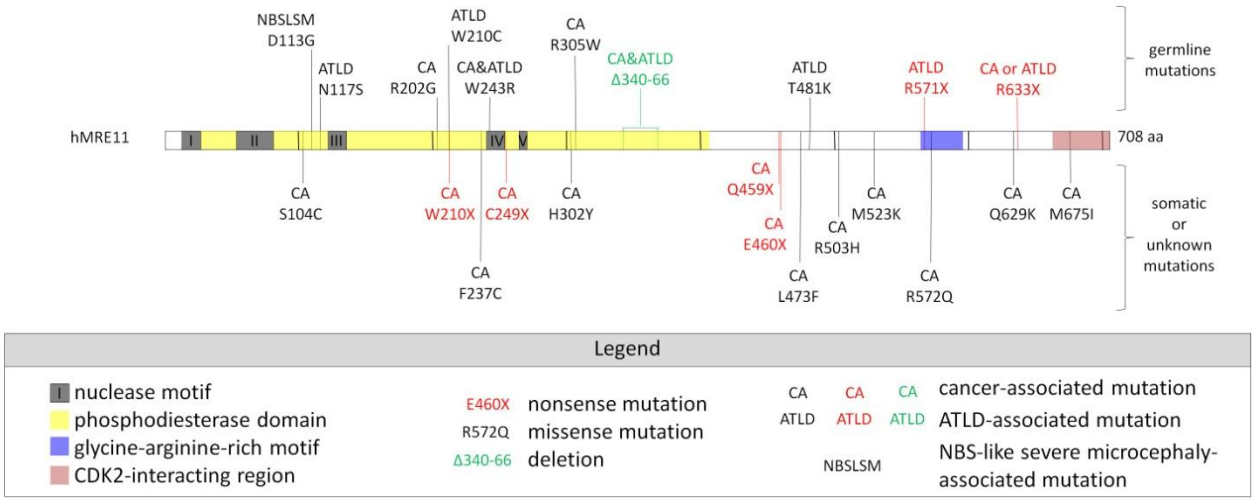

2.2: MRE11 mutant selection

We sought to determine how select cancer-associated *MRE11A* mutations (Figure 7A) impacted MRE11 function [129,205,207]. Alleles encoding ataxia-telangiectasia-like disorder 17/18 (ATLD17) and an alternative splice mutant (ASM) were found in two brothers with ATLD who succumbed to pulmonary adenocarcinoma at the ages of 16 and 9 years [129]. These two mutants were interesting for several reasons. Until report of these brothers, no association between ATLD and cancer had been reported. Also, the young age of incidence of pulmonary adenocarcinoma – a disease of old age [211] – in carriers of both mutations suggests a marked genetic cancer predisposition. Furthermore, the substitution in ATLD17 occurred at a highly conserved residue – W243 – near motif IV of the phosphodiesterase domain (Figure 7B). This motif contains Mn^{2+}-coordinating residues important for MRE11 folding and nuclease activity [59,73]. Hence, W243R might plausibly affect MRE11 folding and nuclease function. The other *MRE11A* allele of these brothers contained an intronic mutation, c.1098+5G>A, and encoded mRNA lacking exon 10. This mRNA could potentially give rise to a protein lacking 27 amino acid residues. Codons downstream of the deletion would be read in frame. The deleted residues reside in the

capping motif of the phosphodiesterase domain and include several conserved broadly amongst eukarya and even a few conserved between eukarya and prokarya.

Mutational analysis of *MRE11A* in unselected primary tumors revealed a mutation encoding MRE11 R572Q (GRM) [205]. The mutation was identified in a heterozygous lymphoma. R572 lies in the disordered C-terminus of MRE11 [59]; hence, no structural information is available for the residue. Nonetheless, R572 is in the MRE11 glycine-arginine-rich (GAR) motif, elements of which are conserved amongst mammals, birds, amphibians, insects, nematodes, and plants. Studies of MRE11 RK suggest R572Q could affect MRE11 nuclease activity, apical kinase activity, checkpoint activation, and genomic stability [65,166-168].

Ataxia-telangiectasia-like 1/2 (ATLD1) was first identified in an ATLD-afflicted kindred [126]. *MRE11A*$^{ATLD1/ATLD1}$ patients and *Mre11a*$^{ATLD1/ATLD1}$ mice exhibited the cellular hallmarks of cancer though they did not appear to be cancer predisposed [126,165]. The lack of malignancy could be a consequence of very low cellular MRN levels. In contrast with *MRE11A*^{ATLD1} homozygosity, *MRE11A*^{ATLD1} heterozygosity has been linked with cancer predisposition [207]. We sought to determine the functional status of ATLD1 in order to clarify its role in carcinogenesis and to further delineate the role of the MRE11 C-terminus in DSBR signaling.

Figure 7: An overview of the mutants discussed

(A) A table summarizing the name, nickname, amino acid change, and clinical context for each mutant. (B) A *Hs*MRE11 stick diagram with pertinent domains and motifs. Note that the phosphodiesterase domain includes both the nuclease (or catalytic) domain and the capping domain. Amino acid changes are labeled along with mutant aliases and associated human diseases. Alignments of the residues surrounding the mutant sites are also shown.

A

mutant name	alias	amino acid change	somatic or germline	zygosity	ataxia telangiectasia-like disorder-associated	cancer-associated
ataxia telangiectasia-like disorder 17/18	ATLD17	W243R	germline	compound heterozygous	yes	pulmonary adenocarcinoma
alternative splice mutant	ASM	Δ340-366	germline	compound heterozygous	yes	pulmonary adenocarcinoma
glycine-arginine-rich motif mutant	GRM	R572Q	unknown	heterozygous	no	lymphoma
ataxia telangiectasia-like disorder 1/2	ATLD1	R633X	germline	homozygous	yes	no
			germline	heterozygous	no	breast carcinoma

B

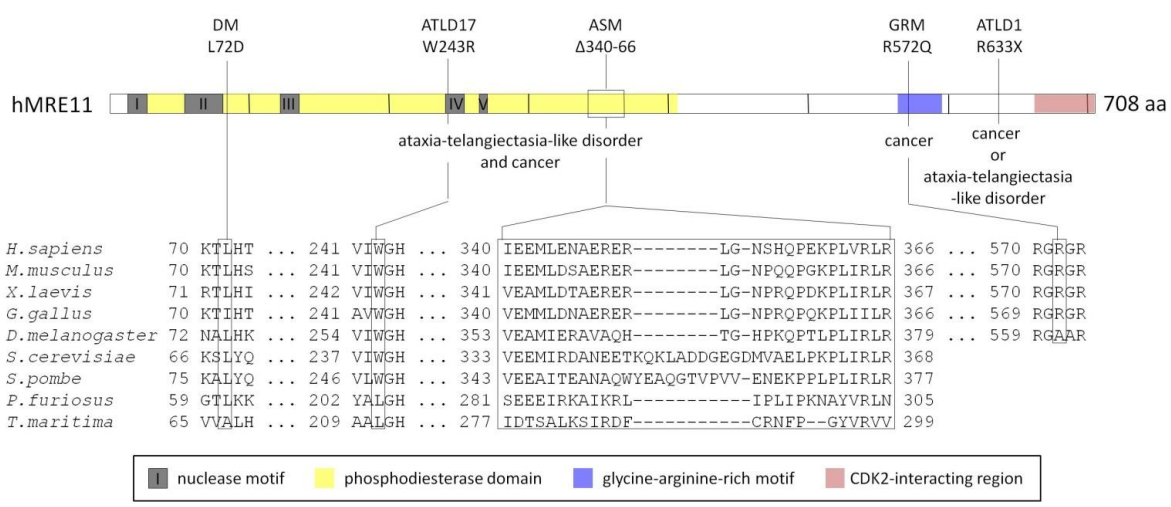

2.3: Mutant-expressing MEF creation and validation

SV40 large T antigen immortalized *Mre11a*$^{cond/\Delta}$ murine embryonic fibroblasts (MEFs) [76] were transfected with pEF6-*Mre11a* constructs encoding mutants of interest, clones were isolated, and the remaining endogenous allele was deleted by adeno-cre treatment to yield mutant-expressing MEFs. Mutant-expressing clones with at least physiologic levels of MRE11

were deemed desirable to avoid low MRE11 levels as a possible confounding variable in characterization. Additionally, clones that allowed efficient deletion of *Mre11a*^{cond} were desired.

To determine whether clones were maintaining mutant levels to at least physiologic MRE11 levels during experiments, whole cell lysates were obtained before and after each experimental time period (Figure 8A). To probe for MRE11, an antibody recognizing the residues around *Hs*MRE11 K496 was used. This region of the protein was not mutated in any mutants; hence, we had no *a priori* reason to think that antibody-MRE11 affinity would vary between wild-type MRE11 and any of the mutants. Each MRE11-expressing clone chosen for characterization possessed at least physiologic MRE11 levels (Figure 8B). The loss of a wild-type MRE11 band in empty-vector controls and ASM and ATLD1 clones was consistent with efficient deletion of the remaining endogenous *Mre11a*^{cond}. However, for clones with missense mutants, the MRE11 type remained undetermined by MRE11 immunoblot alone. Untagged proteins were expressed exogenously in order to avoid disruption of any MRE11-protein interactions [69]. As such, MRE11 type in these mutants was monitored indirectly by determining *Mre11a* mRNA type. An RT-PCR strategy was designed to amplify only *Mre11a* mRNA encoding functional protein (Figure 8C). Bands were only detected with the use of reverse transcriptase, consistent with these bands representing the amplification of *Mre11a* mRNA rather than pEF6-*Mre11a* DNA. Sanger sequencing of cDNA from ATLD17-, ASM-, and GRM-expressing clones revealed little wild-type species (Figure 8D-F) consistent with mutant MRE11 being the predominant MRE11 type present in the cells during experimentation.

Figure 8: Validation of MEF mutant expression

(A) The peri-experimental timeline. (B) Physiologic MRE11 levels are represented to the far left. Peri-experimental MRE11 levels are shown for each clone. Empty-vector control and ASM- or ATLD1-expressing clone lysates had wild-type MRE11 bands of ≥90% reduced intensity. In most cases, no wild-type MRE11 was detected by immunoblot of these cell lysates. The observations are consistent with efficient deletion of *Mre11a*^{cond} and loss of endogenously-produced MRE11 prior to experimentation. Each MRE11-expressing cell line possessed at least physiologic levels of MRE11 at P1 and P2. (C) The RT-PCR strategy to type *Mre11a* mRNA of MRE11-expressing clones is shown (above) along with RT-PCR results (below). Bands of the expected sizes were detected for each clone (upper panel). No bands were detected in the absence of reverse transcriptase (lower panel). (D-F) Sanger sequencing of *Mre11a* cDNA from ATLD17 (D)-, ASM (E)-, or GRM (F)- expressing clones revealed little wild-type *Mre11a*.

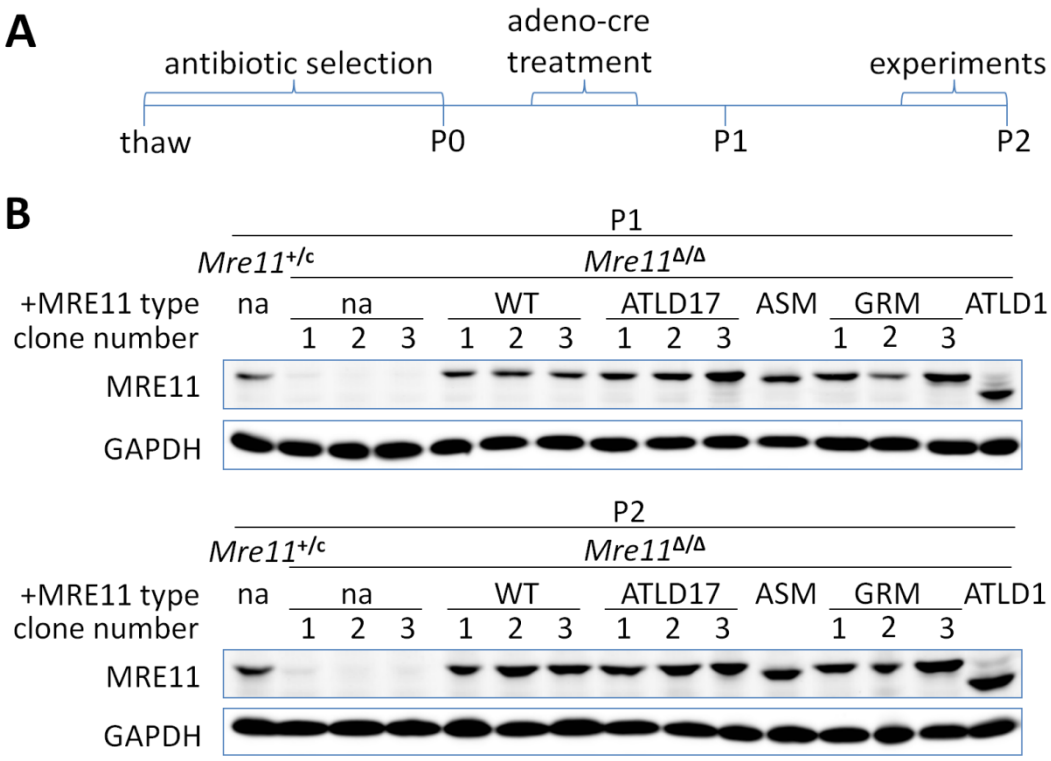

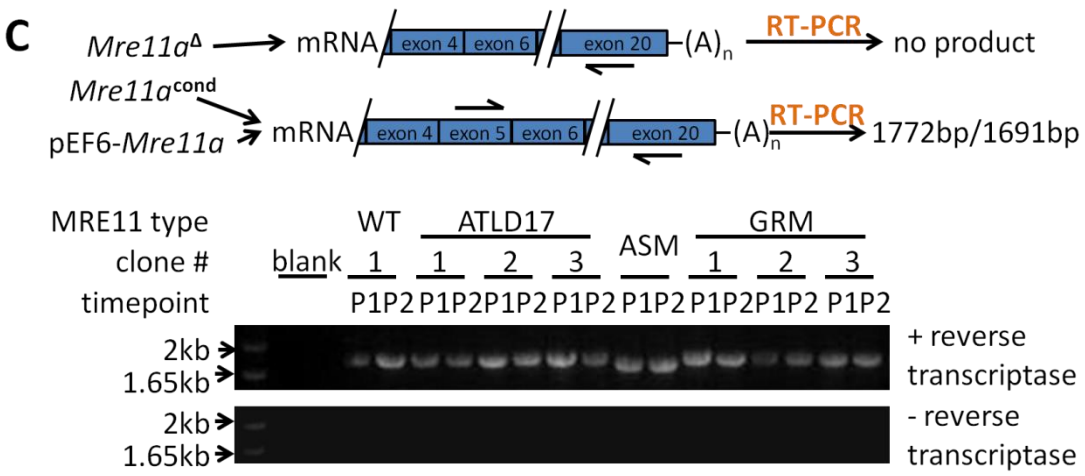
C
Mre11aΔ
mRNA
exon 4
exon 6
exon 20
(A)n
RT-PCR
no product
Mre11acond
pEF6-Mre11a
mRNA
exon 4
exon 5
exon 6
exon 20
(A)n
RT-PCR
1772bp/1691bp
MRE11 type
WT
ATLD17
ASM
GRM
clone #
blank
1
1
2
3
1
1
2
3
timepoint
P1P2 P1P2P1P2 P1P2 P1P2 P1P2P1P2 P1P2
2kb
1.65kb
+ reverse transcriptase
2kb
1.65kb
- reverse transcriptase

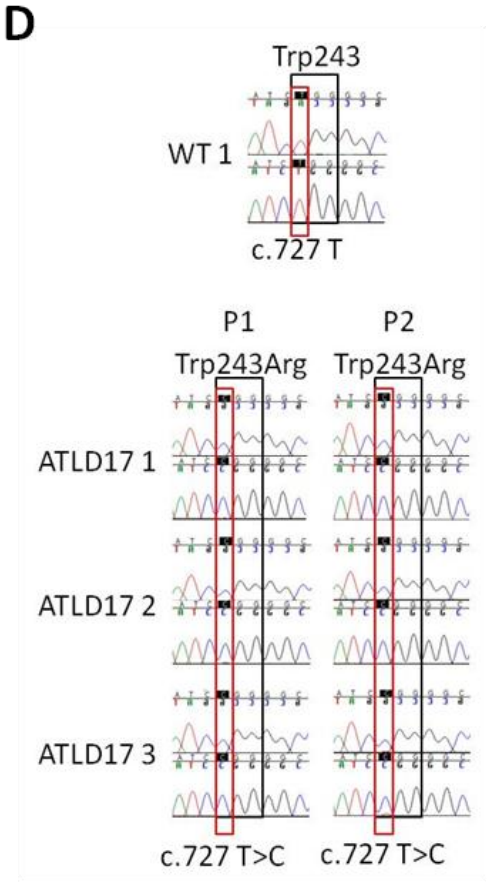
D
Trp243
WT 1
c.727 T
P1
P2
Trp243Arg
Trp243Arg
ATLD17 1
ATLD17 2
ATLD17 3
c.727 T>C
c.727 T>C

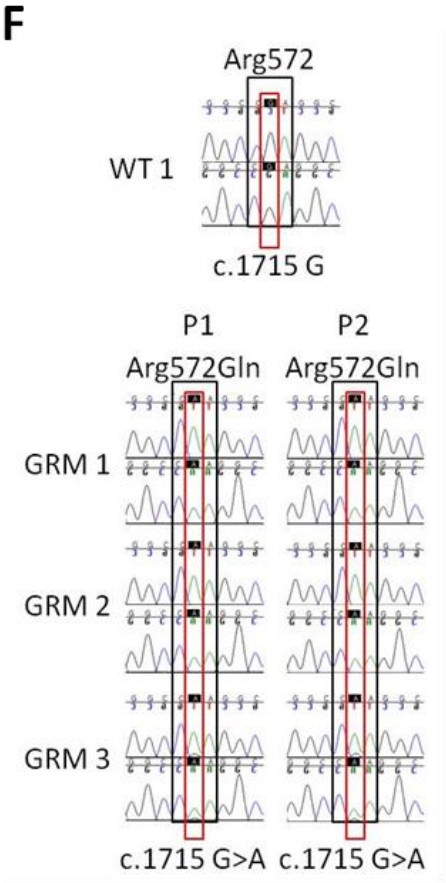
F
Arg572
WT 1
c.1715 G
P1
P2
Arg572Gln
Arg572Gln
GRM 1
GRM 2
GRM 3
c.1715 G>A
c.1715 G>A

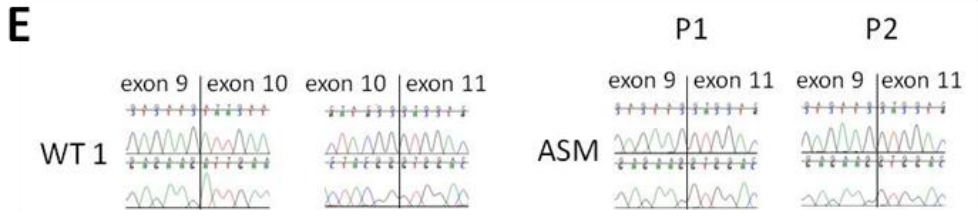
E
exon 9
exon 10
exon 10
exon 11
WT 1
P1
P2
exon 9
exon 11
exon 9
exon 11
ASM

2.4: Apical kinase activation and activity

We chose to monitor MRN-mediated DSB-induced ATM activation and activity by measuring ionizing radiation (IR)-induced ATM S1987 and KAP1 S824 phosphorylation [92,212]. To determine the ability of each MRE11 mutant to facilitate ATR activity, IR-induced pCHK1 S345 was measured [45].

Controls showed robust IR-induced pKAP1 S824 and pCHK1 S345 induction in the presence of wild-type MRE11 (Figure 9A). On the other hand, only weak induction was observed in the absence of MRE11 or ATM (Figure 9A and 9B), consistent with IR-induced KAP1 S824 and CHK1 S345 phosphorylation being both MRE11- and ATM-dependent.

ATLD17-expressing cells showed deficiencies in pATM and pKAP1 but not pCHK1 induction following IR treatment (Figure 9C and 9D). Hence, despite an upstream defect in ATM activation, ATLD17 appears competent enough in facilitating ATM activity to complement IR-induced ATR activity towards CHK1 S345. Induction of pKAP1 and pCHK1 were substantially abrogated in ASM cells. These findings are consistent with ASM being grossly defective in facilitating apical kinase activity (Figure 9D).

GRM appeared to complement ATM activation and activity (Figure 9E and 9F). MRE11 RK studies left open the possibility that the more subtle nature of the alteration in GRM might allow GRM to complement ATR activity [65]. In fact, GRM cells showed reduced CHK1 phosphorylation post-IR. Therefore, even a subtle disruption of the GAR motif is sufficient to compromise ATR activity. Expression of ATLD1 to physiologic levels complemented both ATM and ATR activities (Figure 9F and [69]). Quantitation of pKAP1 and pCHK1 induction is also shown (Figure 9G through 9J).

Dose-response and time-course studies were consistent with our findings 30 minutes after 10 Gy of IR. In ATLD17-expressing cells, decreased pKAP1 induction was observed following IR doses ranging from 0.5 Gy to 10 Gy and following recovery times from 6 minutes to 8 hours (Figure 10A-10C). These cells also had decreased pATM but not pCHK1 30 minutes to 8 hours post-IR compared to wild-type MRE11-expressing cells. Cells with ASM had reduced pKAP1

and pCHK1 throughout this time (Figure 10D). GRM-expressing cells complemented pATM and pKAP1 but had reduced pCHK1 levels during this time period (Figure 10E).

Figure 9: Ionizing radiation-induced apical kinase activation and activity

The indicated MEF clones were either left untreated or treated with 10 Gy IR and allowed to recover for 30 minutes. Whole cell lysates were immunoblotted for the proteins shown. GAPDH is a loading control. (A-F) Immunoblots are representative of at least three independent experiments. (A) Comparison of empty-vector and wild-type controls. Whereas only weak pKAP or pCHK1 induction was observed in empty-vector controls, these species were robustly induced in cells with wild-type MRE11. The extent of induction was similar across the range of wild-type MRE11 levels seen. (B) Induction of these phosphoproteins was ATM-dependent. (C,D) Induction of pATM and pKAP1, but not pCHK1, was partially abrogated in ATLD17-expressing clones. (D)ASM-expressing cells showed dramatic defects in pKAP1 and pCHK1 induction. (E,F) GRM expression largely complemented pATM and pKAP1 induction; however, GRM complemented pCHK1 induction to a much lesser extent. (F) Cells expressing ATLD1 displayed wild-type levels of pKAP1 and pCHK1 induction. (G-J) Quantitation of pKAP S824 and pCHK S345 induction by cell line (G, I) or cell type (H, J). After accounting for protein loading, induction was normalized to the weighted mean induction of the wild-type lines. Each bar represents at least three independent experiments. Error bars represent standard error of the mean.

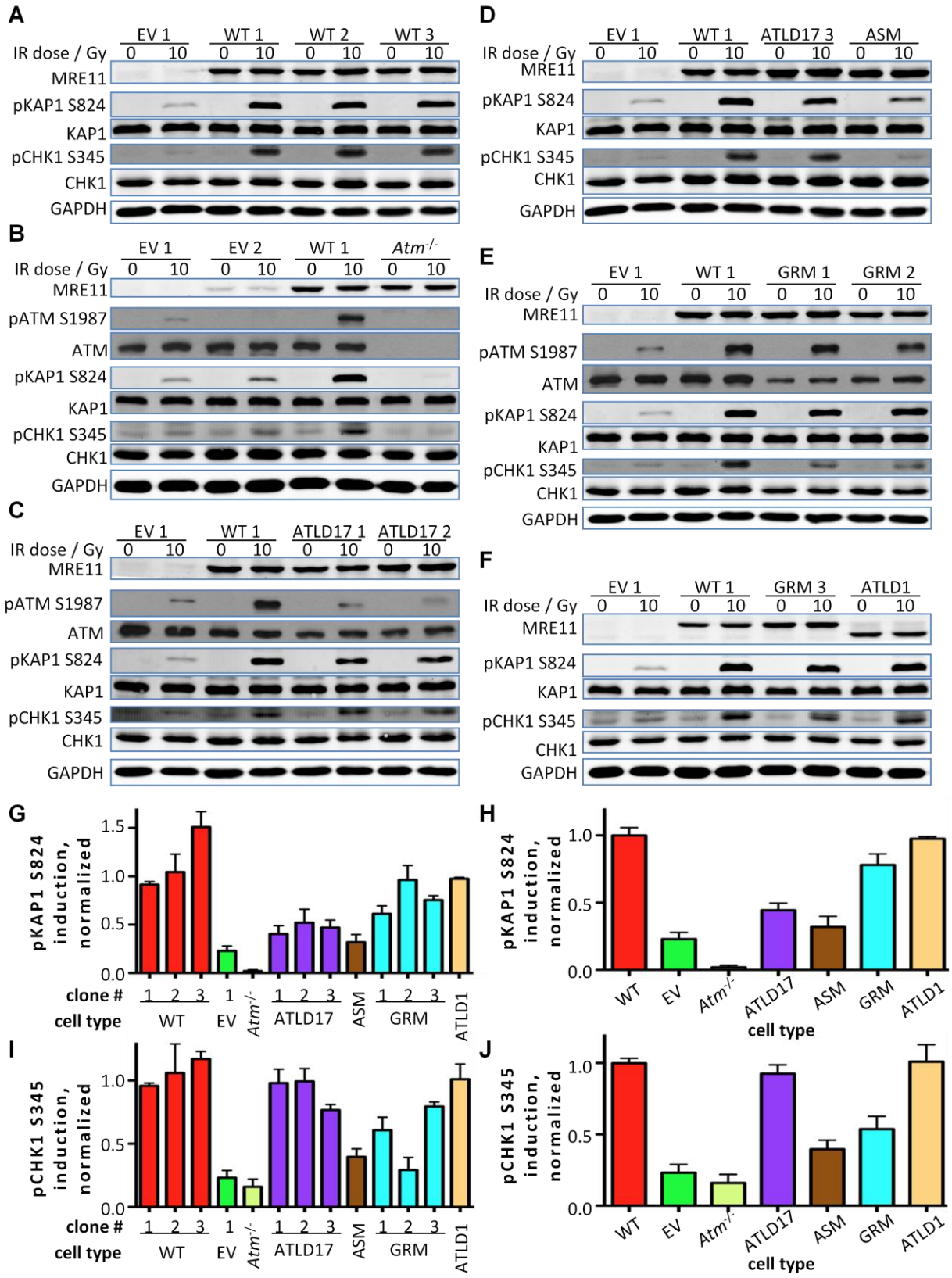
A
EV 1
WT 1
WT 2
WT 3
IR dose / Gy
0 10 0 10 0 10 0 10
MRE11
pKAP1 S824
KAP1
pCHK1 S345
CHK1
GAPDH
B
EV 1
EV 2
WT 1
Atm-/-
IR dose / Gy
0 10 0 10 0 10 0 10
MRE11
pATM S1987
ATM
pKAP1 S824
KAP1
pCHK1 S345
CHK1
GAPDH
C
EV 1
WT 1
ATLD17 1
ATLD17 2
IR dose / Gy
0 10 0 10 0 10 0 10
MRE11
pATM S1987
ATM
pKAP1 S824
KAP1
pCHK1 S345
CHK1
GAPDH
D
EV 1
WT 1
ATLD17 3
ASM
IR dose / Gy
0 10 0 10 0 10 0 10
MRE11
pKAP1 S824
KAP1
pCHK1 S345
CHK1
GAPDH
E
EV 1
WT 1
GRM 1
GRM 2
IR dose / Gy
0 10 0 10 0 10 0 10
MRE11
pATM S1987
ATM
pKAP1 S824
KAP1
pCHK1 S345
CHK1
GAPDH
F
EV 1
WT 1
GRM 3
ATLD1
IR dose / Gy
0 10 0 10 0 10 0 10
MRE11
pKAP1 S824
KAP1
pCHK1 S345
CHK1
GAPDH
G
pKAP1 S824 induction, normalized
1.5
1.0
0.5
0.0
clone #
1 2 3 1 1 2 3 1 2 3
cell type
WT EV Atm-/- ATLD17 ASM GRM ATLD1
H
pKAP1 S824 induction, normalized
1.0
0.5
0.0
WT EV Atm-/- ATLD17 ASM GRM ATLD1
cell type
I
pCHK1 S345 induction, normalized
1.0
0.5
0.0
clone #
1 2 3 1 1 2 3 1 2 3
cell type
WT EV Atm-/- ATLD17 ASM GRM ATLD1
J
pCHK1 S345 induction, normalized
1.0
0.5
0.0
WT EV Atm-/- ATLD17 ASM GRM ATLD1
cell type

Figure 10: Ionizing radiation-induced apical kinase activation and activity, dose-response and time-course studies

(A) ATLD17 expression failed to fully complement pKAP1 induction over a wide range of IR doses. (B) Early pKAP1 induction was not fully complemented by ATLD17 expression. (C) ATLD17 expression fully complemented pCHK1 but not pATM or pKAP1 levels 30 minutes to 8 hours post-IR. (D) ASM-associated defects in pKAP1 and pCHK1 induction persisted 30 minutes to 8 hours post-IR. (E) Over the duration of several hours post-IR, GRM complemented pATM and pKAP1 induction but failed to fully complement pCHK1 induction.

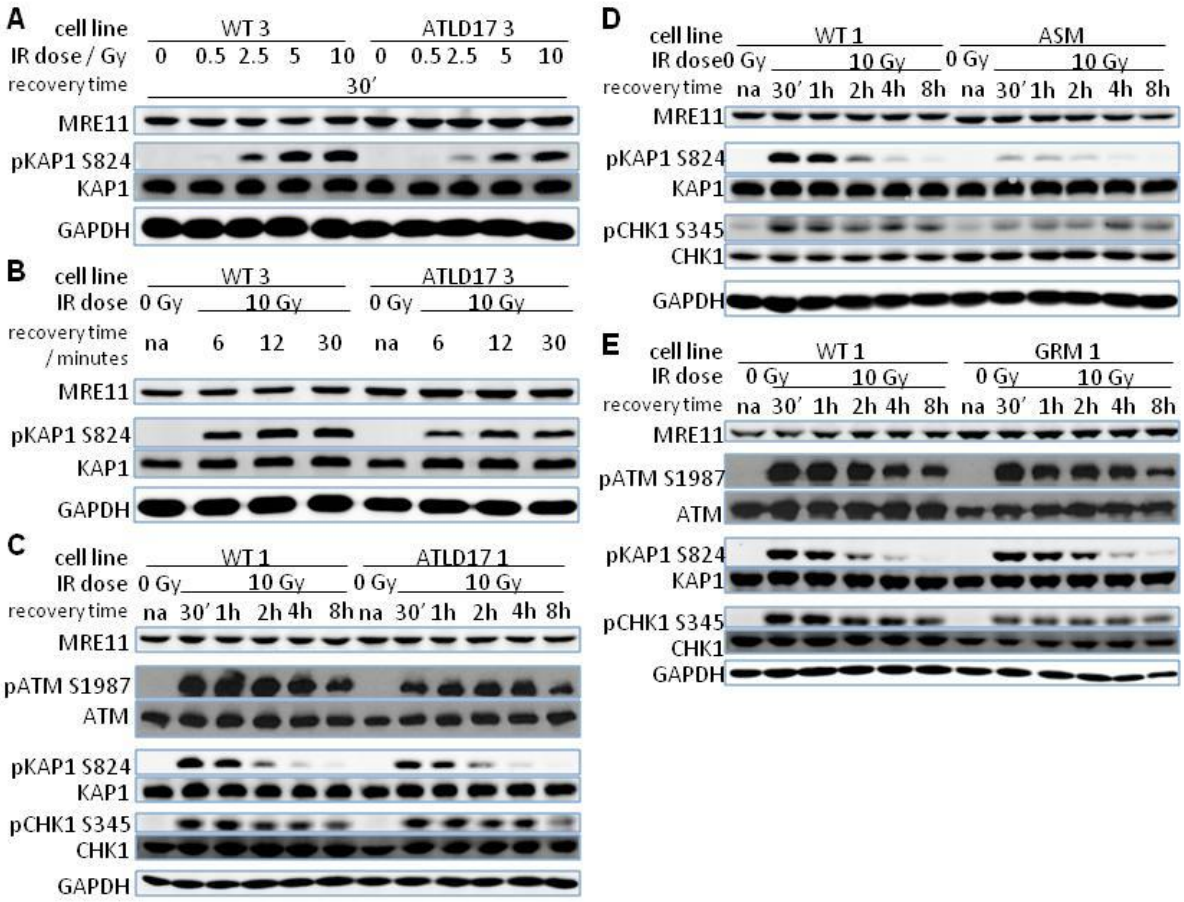

IR-induced early G_2/M checkpoint activation is MRN- and ATM-dependent [165,213]. We chose to measure the competency of this checkpoint in mutant-expressing cells. To do so, MEFs were mock-treated or treated with 10 Gy IR, and the percentages of cells positive for the mitosis-specific phospho-histone H3 S10 marker were compared [214]. A relatively high mitotic index post-IR was interpreted as a G_2/M checkpoint defect. Wild-type MRE11-expressing MEFs displayed a reduced mitotic index post-IR reflecting G_2/M checkpoint activation (Figure 11A and 11B). Relative to the wild-type control, significantly more MEFs lacking MRN or ATM were in mitosis after IR treatment, consistent with previous findings that the G_2/M checkpoint is mediated by both MRN and ATM.

Mutants defective in facilitating ATM activation would also be expected to fail to properly activate the G_2/M checkpoint. Such a defect was observed in ASM cells; *Atm*$^{-/-}$ and ASM cells had similar mitotic indexes post-IR. However, ATLD17, which exhibited relatively minor defects in facilitating apical kinase activation, was associated with decreased mitotic entry post-IR similar to what was seen for wild-type MRE11.

Mre11a$^{RK/RK}$ cells are G_2/M checkpoint defective post-IR, and these cells and GRM-expressing cells exhibit(ed) defects in ATR activity [65]. Thus, GRM was expected to be G_2/M checkpoint defective. However, GRM cells appeared checkpoint competent. The more subtle nature of the substitution in GRM compared to MRE11 RK potentially accounts for the discrepancy. Alternatively, phenotypic dissimilarities might reflect the differences in cellular protein levels, with *Mre11a*$^{RK/RK}$ cells having only about 50% of physiologic MRE11 levels.

ATLD1 was previously associated with defects in apical kinase activity and G_2/M checkpoint activation [165]. However, we found ATLD1 expression to result in wild-type levels of mitotic entry following IR treatment; therefore, we found no evidence of gross defect. This discrepancy likely reflects a difference in cellular ATLD1 levels. Our results showed no proof that the lack of a C-terminus hindered the ability of ATLD1 to facilitate apical kinase activity or G_2/M checkpoint function.

Figure 11: G_2/M checkpoint assay

MEFs were either mock treated or treated with 10 Gy IR and allowed to recover for an hour. Cells were stained for the mitosis-specific p-histone H3 S10 modification. Mitotic index was obtained by comparison of the percentage of pH3-positive IR-treated cells to that for mock-treated cells for each cell line. Results are shown by cell line (A) or cell type (B). A minimum of three independent experiments were performed for each cell line shown. Error bars represent standard error of the mean. At least 80% of wild-type-expressing MEFs that would otherwise be in mitosis were not in mitosis 1h post-IR, consistent with efficient IR-induced G_2/M checkpoint activation. In contrast, IR treatment reduced the proportion of MRE11- or ATM-deficient cells in mitosis to a much lesser extent, which suggests a G_2/M checkpoint defect. ATLD17-, GRM-, or ATLD1-expressing cells all appeared checkpoint proficient while ASM-expressing cells displayed a pronounced checkpoint defect.

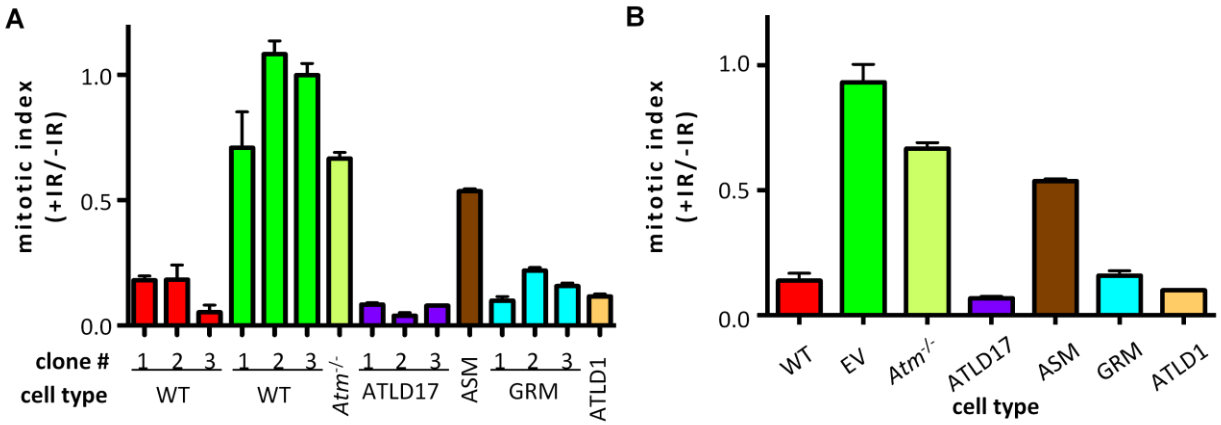

2.5: MRE11/RAD50/NBS1 complex stability

Mutant-associated defects in apical kinase activity could be a consequence of MRN complex disruption [40,41,215,216]. MRE11 plays a role in maintaining RAD50 and NBS1 levels. ATLD and NBS-like severe microcephaly patient cells as well as breast cancer tissue with reduced MRE11 levels have reduced RAD50 and NBS1 levels [126,127,129,131,132,189]. Additionally, disrupted MRN complex formation has been previously detected as abnormal ratios of the complex components; patients with MRE11 mutations that compromise MRE11-NBS1 interaction have reduced NBS1:MRE11 molar ratios [128,129,131]. We assessed cellular RAD50:MRE11 and NBS1:MRE11 molar ratios in order to determine whether they suggested any defect in MRN complex stability.

MRE11 depletion resulted in proportionally decreased RAD50 levels (Figure 12A and 12B). Expression of wild-type MRE11, ATLD17, ASM, GRM, or ATLD1 resulted in proportionally similar increases in RAD50 levels. A least-squares best fit for all MRE11 types yielded a line with an R^2=0.93. RAD50:ATLD17 and RAD50:ATLD1 molar ratios were consistent with those found in ATLD17 and ATLD1 patient cells [126,129]. These results suggest that each mutant can maintain RAD50 levels to a similar extent as wild-type MRE11. Whether these observations are due to MRE11-mediated RAD50 stabilization through MRN complex formation is not entirely clear.

Depletion of MRE11 also resulted in decreased NBS1 levels (Figures 12A and 12C). MEFs expressing either ATLD17 or ASM had reduced NBS1:MRE11 ratios suggestive of compromised ATLD17-NBS1 and ASM-NBS1 interaction. ATLD17 patient cells, which express the ATLD17 mutant, have reduced NBS1:MRE11 ratios [129], consistent with our findings for the ATLD17 mutant. In contrast, MEFs expressing GRM or ATLD1 had wild-type-like NBS1:MRE11 molar ratios. Therefore, MRN complex molar ratios failed to reveal any defect in GRM- or ATLD1-mediated complex formation. Consistent with these findings, ATLD1 patient cells have NBS1:MRE11 molar ratios at least those of wild-type cells [126]. The least squares fit for wild-type-like cell lines had a slope appreciably different from the best fit for ATLD17- or ASM-expressing lines.

Figure 12: MRE11/RAD50/NBS1 molar ratios

(A) MRN complex component levels in empty-vector controls and wild-type MRE11- or mutant-expressing MEF clones. Though ATLD17- and ASM-expressing cells had a wild-type-like RAD50:MRE11, NBS1:MRE11 was reduced in these cells. In contrast, both RAD50:MRE11 and NBS1:MRE11 were wild-type-like in GRM- and ATLD1-expressing cells. GAPDH was used as a loading control. (B-C) Quantitation of cellular MRN complex component levels. MRE11, RAD50 (B), and NBS1 (C) levels were normalized to those in wild-expressing clone 1 (WT 1) whole cell lysate after accounting for protein loading. Each data point represents a minimum of three measurements (range: 3-15, median: 5), and error bars represent standard error of the mean. (B) Each MRE11 type complemented RAD50 levels to a similar extent; the trendline shown with R^2 value represents the least-squares best fit for all cell types. (C) ATLD17 and ASM failed to complement NBS1 levels to the same extent as wild-type MRE11, GRM, or ATLD1; the trendlines shown with R^2 values represent the least-squares best fits for wild-type-like cell lines (EV, WT, GRM, and ATLD1) or non-wild-type-like clones (ATLD17 and ASM).

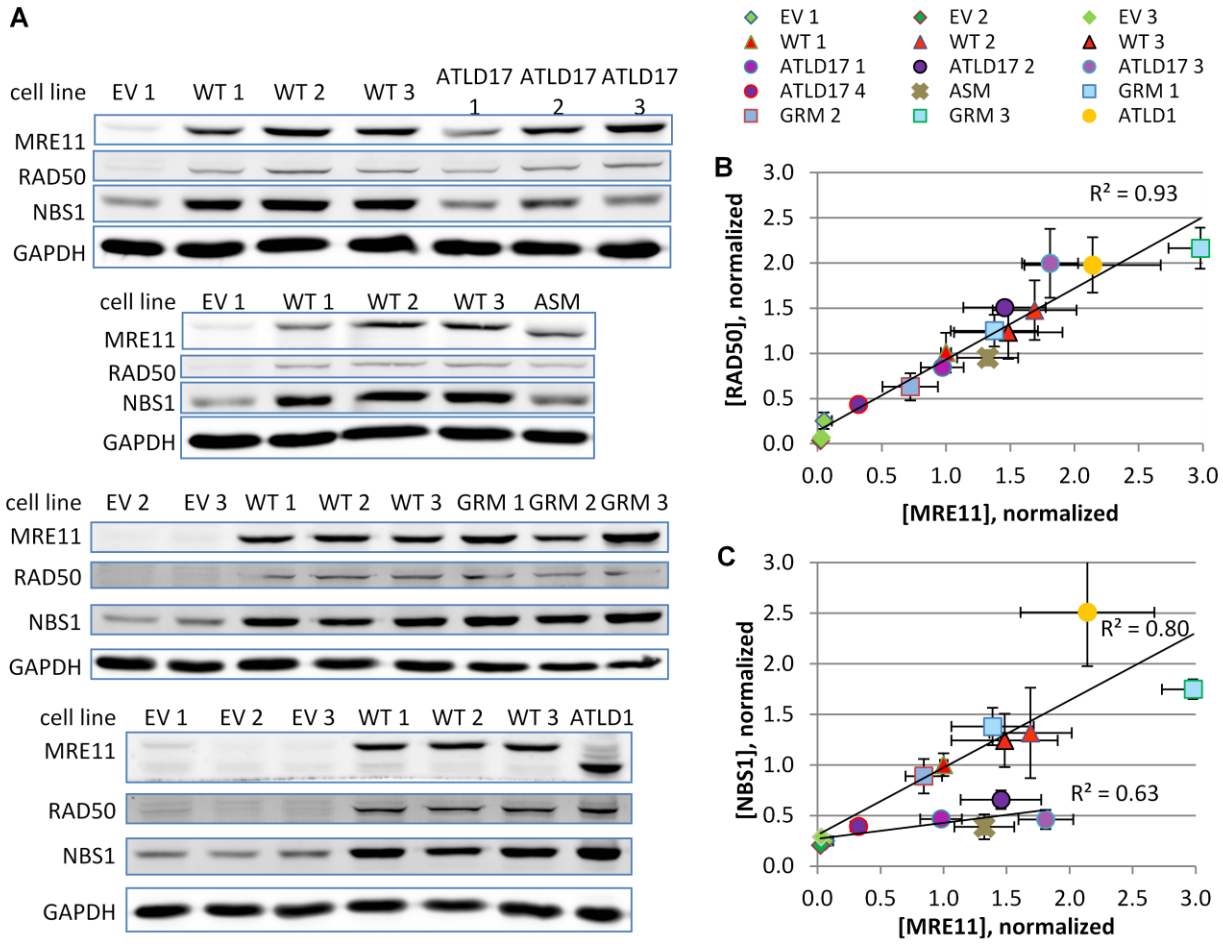

To further investigate whether the mutants affected MRN complex stability, co-immunoprecipitation of complex components was checked. Wild-type MRE11 pulled down and was pulled down by RAD50 and NBS1 (Figure 13). ATLD17 co-immunoprecipitated with RAD50 to a slightly lesser degree than wild-type MRE11. This defect was notably less than that observed with the analogous *S. pombe* mutant [217]. Co-IP of ATLD17 and NBS1 appeared substantially abrogated – similar to what was previously reported for *S.pombe* ATLD17 [217]. Similar outcomes were observed whether cells were untreated, treated with 10 Gy IR and allowed a 12 minute recovery, or treated with 10 Gy IR and allowed a 30 minute recovery (Figure 14). Because NBS1 makes contacts with both MRE11 and RAD50 [218], the defect in ATLD17-RAD50 co-IP may reflect both a lack of NBS1 to stabilize M(ATLD17)R and decreased ATLD17-NBS1 interaction. Therefore, these findings are consistent with disrupted M(ATLD17)RN complex stability though the low levels of NSB1 in ATLD17 cells confounded the interpretation of these results.

ASM displayed dramatically reduced co-IP with RAD50 and NBS1. As was the case for ATLD17, the low NBS1:MRE11 ratios in ASM-expressing cells confounded the interpretation of the ASM co-IP results; however, the observations are consistent with a substantial defect in M(ASM)RN complex stability. In contrast, GRM appeared just as capable as wild-type MRE11 of pulling down and being pulled down by RAD50 and NBS1. Hence, no defect in M(GRM)RN complex stability was evident by co-IP. Previous work has shown ATLD1 to stably complex by co-IP [69,165].

Figure 13: MRE11/RAD50/NBS1 co-immunoprecipitation

MRE11, RAD50, or NBS1 were pulled down, and immunoprecipitates were immunoblotted for each MRN complex component. GAPDH was used as a whole cell lysate loading control. Results shown are representative of a minimum of three co-IPs. ATLD17 pulled down and was pulled down by RAD50 to a slightly lesser extent than was observed for wild-type MRE11. Additionally, in ATLD17-containing lysates, less NBS1 was pulled down by MRE11 or RAD50, and less MRE11 and RAD50 were pulled down by NBS1. The results for ASM were similar to those for ATLD17 except that the defect in MRE11-RAD50 co-immunoprecipitation was more pronounced. GRM appeared as capable as wild-type MRE11 to co-IP with RAD50 and NBS1.

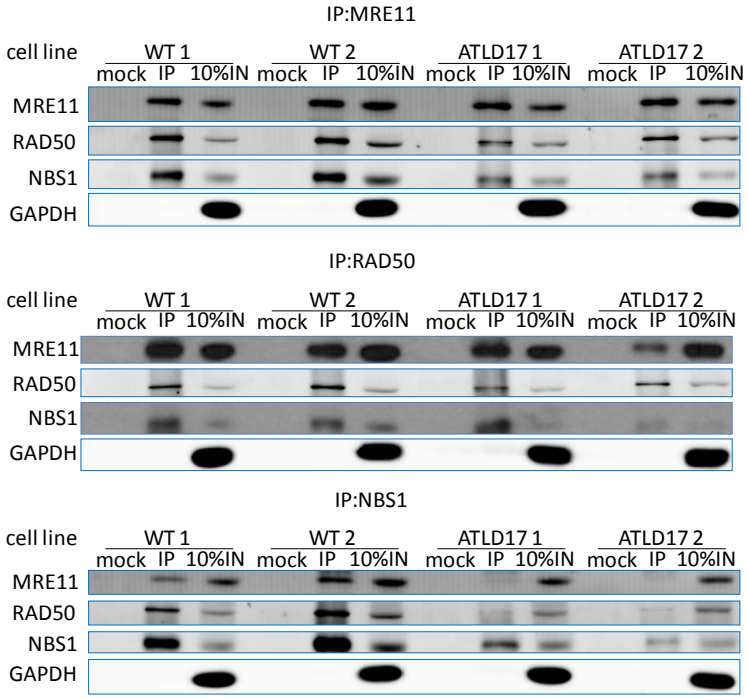

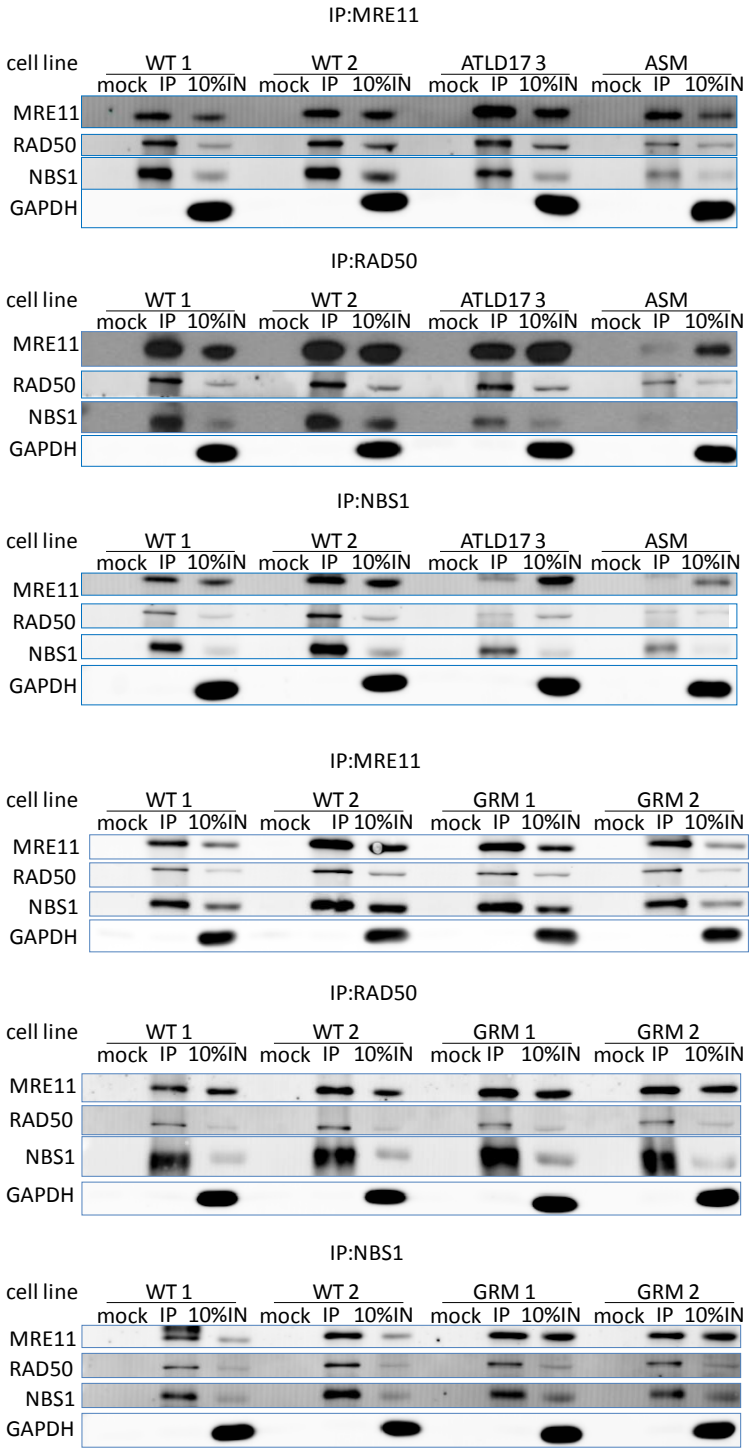
IP:MRE11
cell line
WT 1
WT 2
ATLD17 3
ASM
mock IP 10%IN
MRE11
RAD50
NBS1
GAPDH
IP:RAD50
IP:NBS1
IP:MRE11
GRM 1
GRM 2
IP:RAD50
IP:NBS1

Figure 14: M(ATLD17)RN co-immunoprecipitation did not change with ionizing radiation treatment.

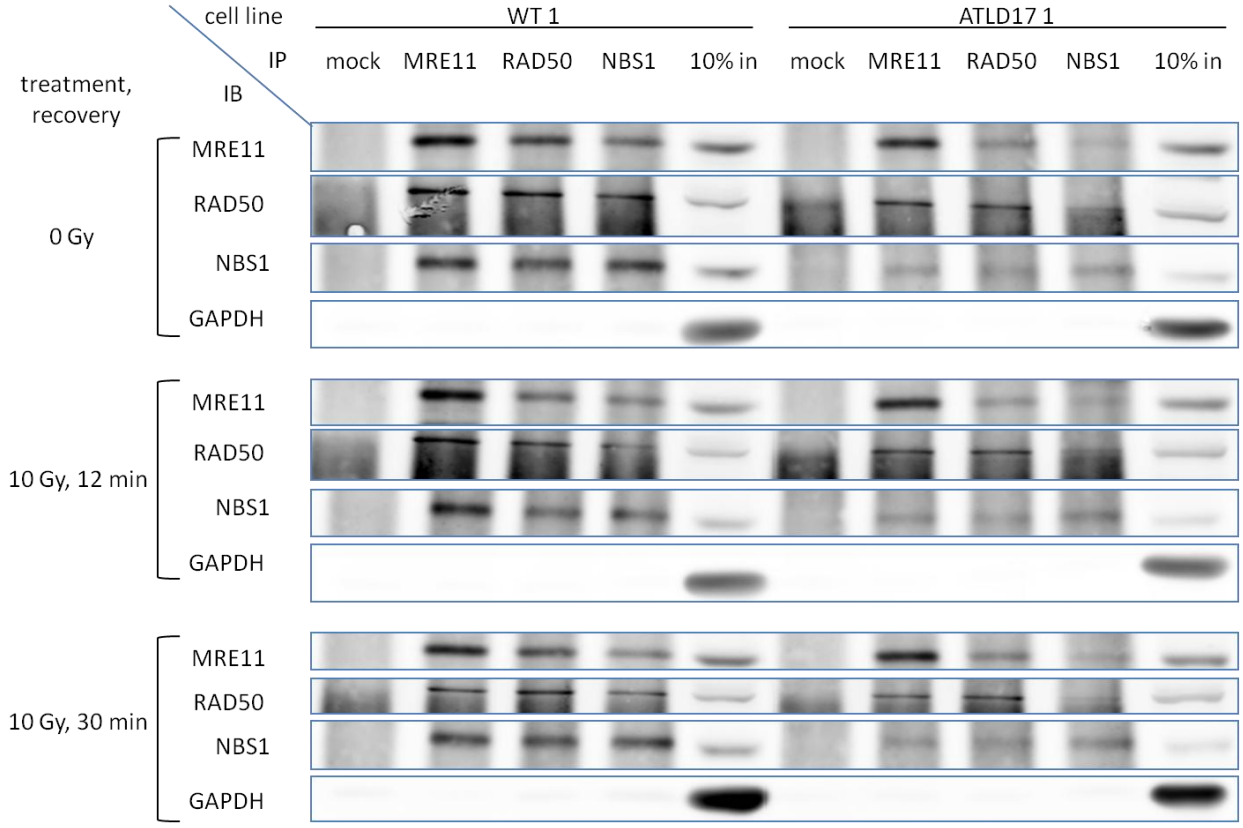

IP: MRE11

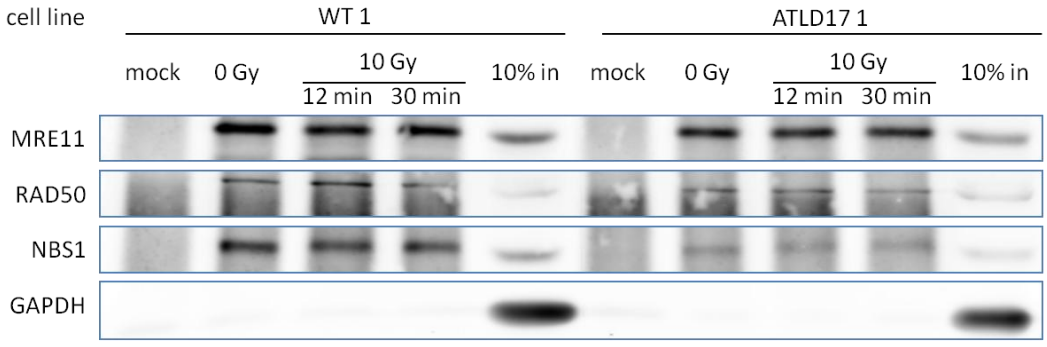

2.6: MRE11 homodimerization and MRE11-NBS1 direct interaction

Yeast two-hybrid was used to assess the abilities of each mutant to homodimerize. Yeast were cotransformed with vectors encoding bait (pGBK) and prey (pGAD) fusion proteins. Empty vectors were used as negative controls. Following cotransformation, yeast were grown on synthetic defined medium without leucine or tryptophan (SD-L-W) in order to select for yeast possessing the bait- and prey-encoding plasmids. Fusion protein interaction resulted in α-galactosidase expression, which in turn, could be used to quantitate homodimerization (Figure 15A). ATLD17 homodimerization was reduced compared to that for wild-type MRE11. ASM homodimerization was not detected. No defects in GRM or ATLD1 homodimerization were apparent. Homodimerization was also assayed by colony growth (Figure 15B). During the final round of plating, yeast clones were plated onto SD-L-W without histidine or adenine (SD-L-W-H-ade) in order to test for fusion protein interaction and onto SD-L-W for a loading control. As was seen previously [69], no autoactivation was detected with MRE11 fusion proteins, and yeast with MRE11 in both the bait and prey showed robust growth consistent with MRE11 homodimerization. Wild-type MRE11, GRM, and ATLD1 homodimerized to similar extents whereas ASM showed no evidence of homodimerization, and ATLD17 homodimerization was intermediate.

A-galactosidase assay was also used to assess direct interaction between MRE11 mutants and NBS1 (Figure 15C). Autoactivation was minimal. Wild-type MRE11, GRM, and ATLD1 directly interacted with NBS1 to similar extents. A gross defect in NBS1 interaction was seen for ATLD17 whereas ASM-NBS1 interaction was not detected. Similar results were found by colony growth assay (Figure 15D). Wild-type MRE11 fusion proteins and ASM fusion proteins were of similar levels (Figure 16A-16C); hence, ASM fusion protein instability could not explain the results. Full colony growth assay plates are shown (Figure 16D and 16E).

Figure 15: MRE11 homodimerization and direct interaction between MRE11 and NBS1

Yeast two-hybrid analysis was performed using pGBK and pGAD – encoding the bait and prey, respectively. Empty vectors were negative controls. Plasmids were selected for by culturing in the absence of leucine and tryptophan (SD-L-W). (A) MRE11 homodimerization by Y2H colorimetric assay. Bait-prey interaction resulted in α-galactosidase expression. A-galactosidase activity was visualized as conversion of p-nitrophenyl-α-D-galactopyranoside (colorless) to p-nitrophenoxide (yellow, λ_{max}=410nm). Bait-prey combinations are shown below each bar. Each bar represents at least three clones per combination with at least three measurements per clone. Error bars represent standard error of the mean. Wild-type MRE11, GRM, and ATLD1 showed similar amounts of homodimerization. ATLD17 homodimerized less than wild-type MRE11, and ASM interaction appeared similar to that of empty vector controls. (B) MRE11 homodimerization by Y2H colony growth assay. Bait and prey proteins are indicated on the left. Ten-fold serial dilution series are shown on interaction test plates (SD-L-W-H-ade, center) and loading control plates (SD-L-W, right). Results are representative of those for at least three clones per bait-prey combination. ATLD17 homodimerization was slightly abrogated. No ASM homodimerization was detected. No defects in GRM or ATLD1 homodimerization were apparent. (C) MRE11-NBS1 interaction by Y2H colorimetry. Similar to panel A in setup. ATLD17 showed a 54% reduction in NBS1 interaction compared to wild-type MRE11. ASM did not appear to interact with NBS1. GRM and ATLD1 interacted with NBS1 to the same extent as wild-type MRE11. (D) Bait and prey proteins (left), interaction test plates (center), and loading control plates (right) are shown as in panel B. The interaction of ATLD17 with NBS1 was slightly but consistently abrogated. ASM-NBS1 interaction was not appreciated. No defects were detected in GRM or ATLD1 interaction with NBS1.

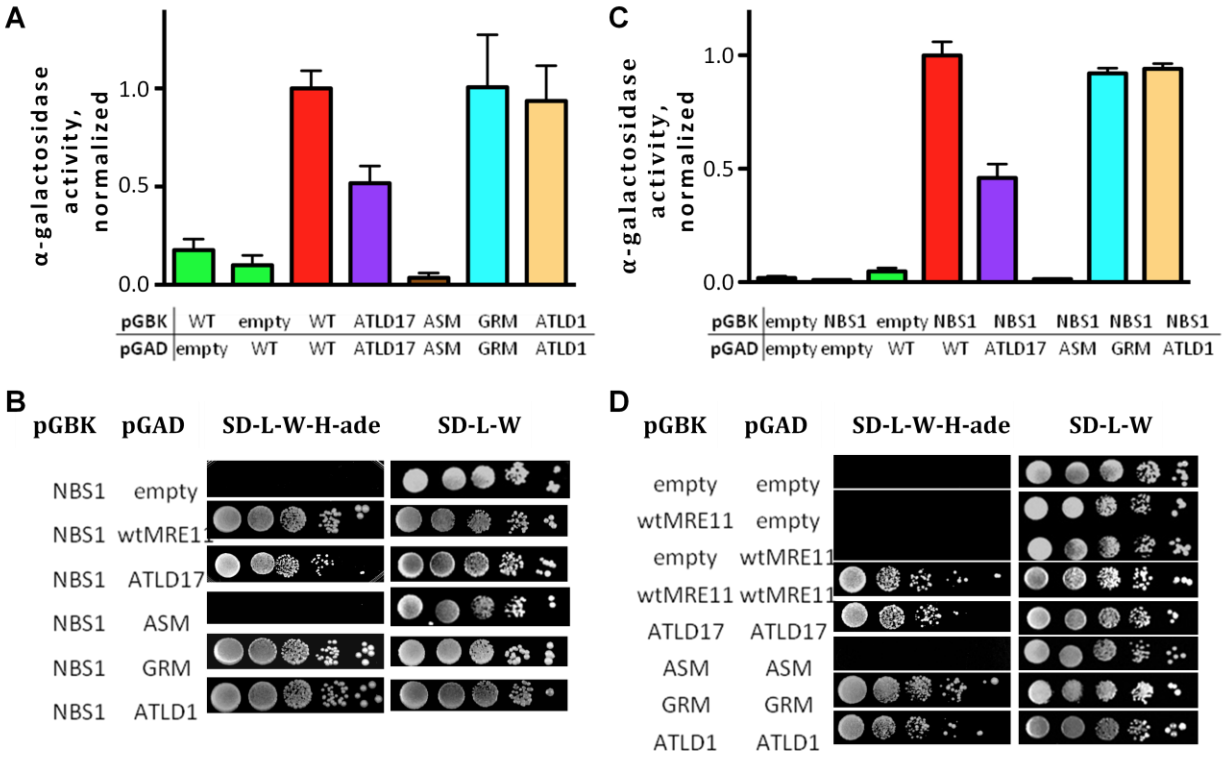

Figure 16: MRE11 homodimerization and direct interaction with NBS1 by yeast two-hybrid, supplemental

(A) ASM fusion protein levels were similar to wild-type fusion protein levels. Bait and prey were fused to a MYC-tag or HA-tag, respectively. Tubulin was used as a loading control. (B) and (C) Quantitation of bait and prey levels. Fusion protein levels are presented relative to wild-type MRE11 fusion protein levels after accounting for loading. Error bars represent the standard error of the mean for three clones per bait-prey combination. (D) MRE11 homodimerization showing full plates except for where a row or two were cropped out. (E) MRE11-NBS1 interaction showing full plates except for where a row or two were cropped out.

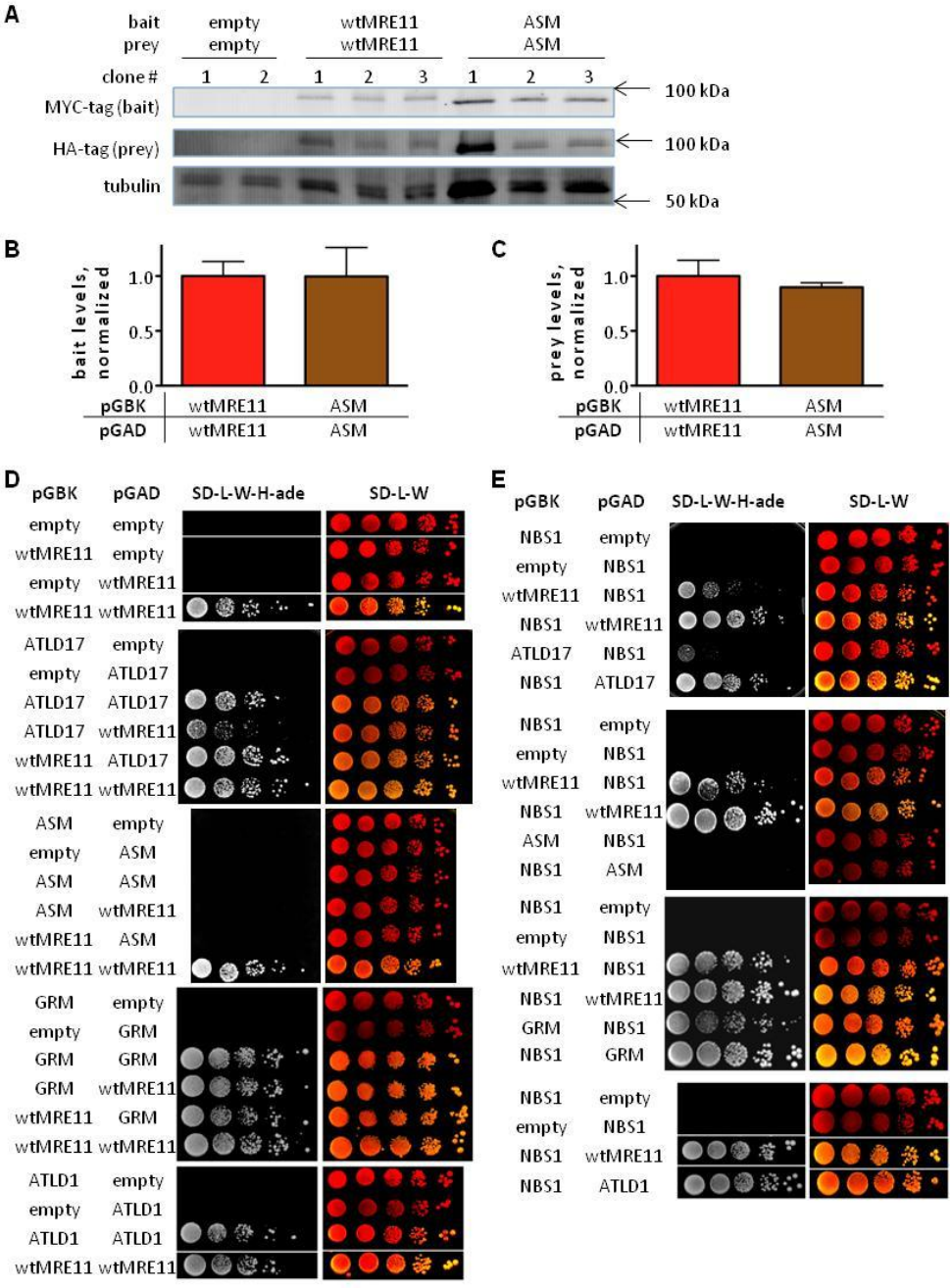

2.7: Dimerization mutant

We wished to determine the extent to which decreased MRE11-NBS1 interaction could be caused by disruption of the NBS1 binding site across the MRE11 homodimer interface. To ablate this binding site, an MRE11 homodimerization mutant (DM) was made. MRE11 L72 is a highly conserved residue – being an aliphatic hydrophobic residue in eukarya and prokarya (Figure 17A) – located at the MRE11 homodimer interface where loop α2-β3 packs against helix H2 of the opposite protomer [59]. Along with the latching loops, this residue participates in formation of a hydrophobic pocket (Figure 17B). MRE11 L72D was designed to perturb this hydrophobic pocket and thereby disrupt MRE11 homodimerization and NBS1 binding across the latching loops.

Yeast two-hybrid was used as before to assess DM homodimerization and direct interaction with NBS1 (Figure 17C-F). DM homodimerization was substantially impaired. Hence, MRE11 L72D is the first mammalian homodimerization mutant described. DM interaction with NBS1 was also impaired. These results are consistent with L72D disrupting NBS1 binding across the latching loops.

Notably, DM showed a similar degree of NBS1 binding deficiency as ATLD17. These results are consistent with ablation of the same NBS1 binding site on DM and ATLD17. The mutant residue in ATLD17, W243, is highly conserved and is near Mn^{2+}-coordinating residues important for MRE11 folding [59,73]. Hence, W243R might result in local misfolding and thereby disrupt the latching loop-mediated homodimerization and NBS1 binding. The other NBS1 binding sites could remain intact in this scenario explaining why NBS1 binding is only partially disrupted. This disruption of ATLD17-NBS1 interaction, in turn, could cause ATLD17 to be defective in facilitating ATM activation and activity.

Results are summarized in Tables 3 and 4.

Figure 17: Dimerization mutant

(A) MRE11 stick diagram and alignment showing L72, the residue changed in the DM. (B) *Hs*MRE11 phosphodiesterase domain dimer showing L72 (pink), W243 (violet), and residues 340-366 (mocha). One MRE11 protomer is depicted as light gray while the other is light blue. Note that the latching loops in these structures were mostly disordered and therefore are not shown. The two images shown are rotated ~90° about the long axis of M_2 from each other. (C) DM homodimerization was similar to background by yeast two-hybrid colorimetric assay. (D) Y2H colony growth assay revealed substantially abrogated DM homodimerization. (E) Direct interaction between DM and NBS1 was reduced by 59% compared to wild-type by α-galactosidase assay. (F) DM-NBS1 interaction was slightly but reproducibly reduced by Y2H colony growth assay.

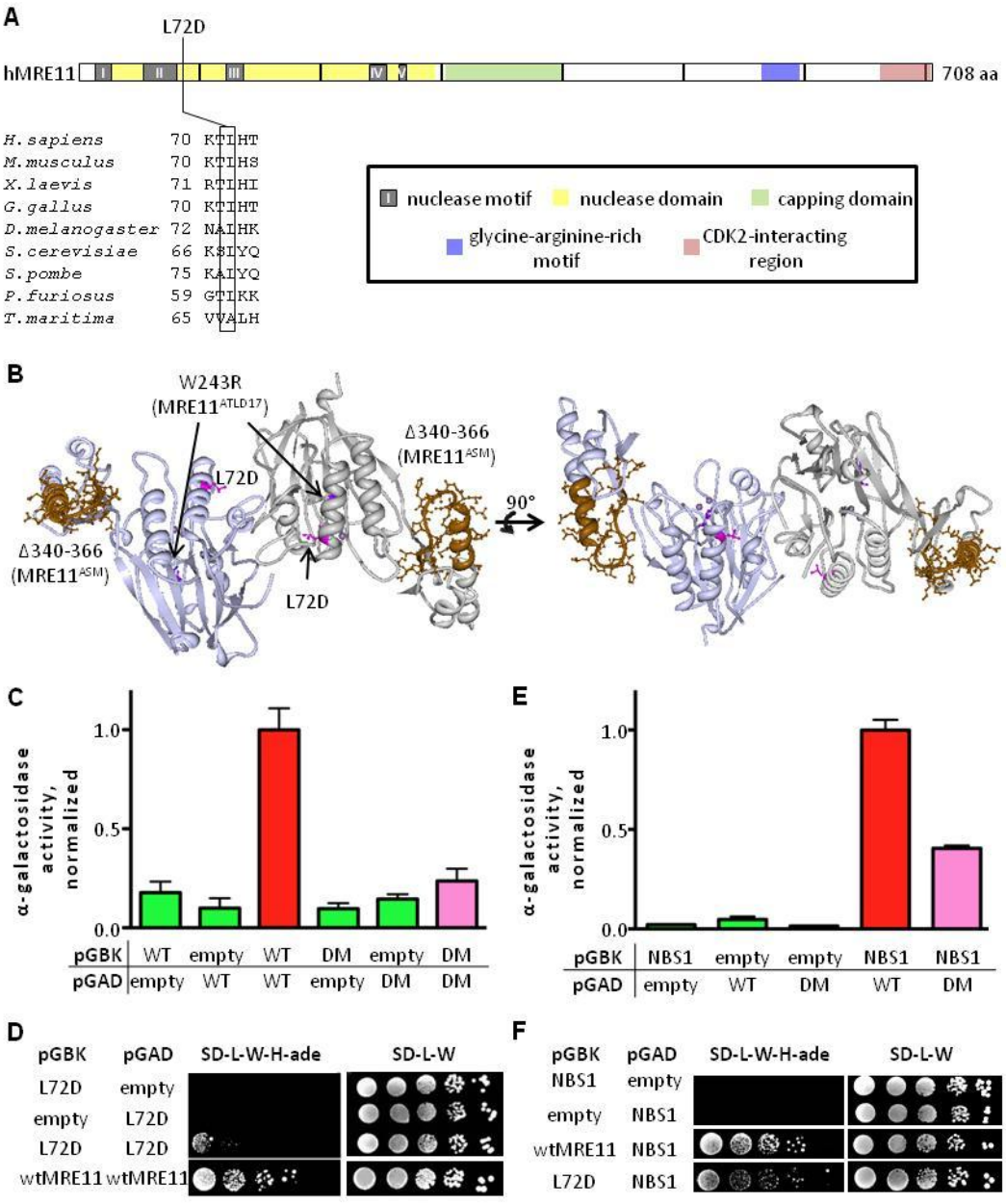

Table 3: A summary of kinase activity findings

			mutant			
		assay	ATLD17	ASM	GRM	ATLD1
ATM activity		pATM induction	+	ND	++++	ND
		pKAP1 induction	+	<+	+++	++++
		G2/M checkpoint	++++	++	++++	++++
	ATR activity	pCHK1 induction	++++	+	+	++++

symbol	+	++	+++	++++	ND
% of wild-type	[12.5%,37.5%)	[37.5%,62.5%)	[62.5%,87.5%)	[87.5%,112.5%)	not determined

Table 4: A summary of MRE11/RAD50/NBS1 complex integrity results

		mutant				
	method	DM	ATLD17	ASM	GRM	ATLD1
homodimerization	Y2H	<+	++	<+	++++	++++
RAD50 interaction	molar ratios	ND	++++	++++	++++	++++
	coIP	ND	+++	++	++++	ND
NBS1 interaction	molar ratios	ND	++	++	++++	++++
	Y2H	++	++	<+	++++	++++
	coIP	ND	≥++	≥++	++++	ND

symbol	+	++	+++	++++	ND
% of wild-type	[12.5%,37.5%)	[37.5%,62.5%)	[62.5%,87.5%)	[87.5%,112.5%)	not determined

CHAPTER 3: DISCUSSION

3.1: Roles of mutants in carcinogenesis

Here we have shown ATLD17, ASM, and GRM - even when expressed to physiologic MRE11 levels - to exhibit defects in facilitating IR-induced apical kinase activity (Figure 18A-C). For ATLD17 and ASM, the defects appeared to reflect varying degrees of abrogation of MRN complex stability. In contrast, though ATLD1 was previously associated with defects in apical kinase activity [165], ATLD1 expression to physiologic MRE11 levels complemented apical kinase activity. This characterization is the first of any kind for ASM, GRM, or a mammalian MRE11 homodimerization mutant. In addition, we were the first to describe ATLD17 in the context of physiologic MRE11 levels. Finally, no prior reports had been made regarding the effects of ATLD1 expressed to physiologic MRE11 levels on ATR activity or cell cycle checkpoint function.

Though ATLD17 patient cell lines displayed defects in IR-induced ATM activation, they also possessed reduced MRE11 levels [132]. Hence, our study is the first to show ATM activity defects in ATLD17-expressing mammalian cells to be due to ATLD17 hypomorphism *per se*. *S. pombe* were engineered to express *Sp*Mre11 W248R, a mutant analogous to ATLD17 [217]. This mutant was not found to be defective in facilitating the activity of Tel1, the *S.pombe* ATM orthologue, but it did have a defect in facilitating Chk1 phosphorylation. These findings in *S.pombe* were counterintuitive because authors of the same study found dramatic disruption of *Sp*M(ATLD17)RN complex stability and decreased cellular complex component levels, and in mammals, ATM activation is known to rely upon intact MRN [215]. Evolutionary divergence in MRN function could explain the discrepancies between yeast and mammalian ATLD17 findings.

Figure 18: Model depicting ionizing radiation-induced apical kinase activity in mutant-expressing cells

Schematics are shown for cells expressing ATLD17 (A), ASM (B), or GRM (C). Thick arrows represent normal flux whereas thin arrows represent suspected deficiency.

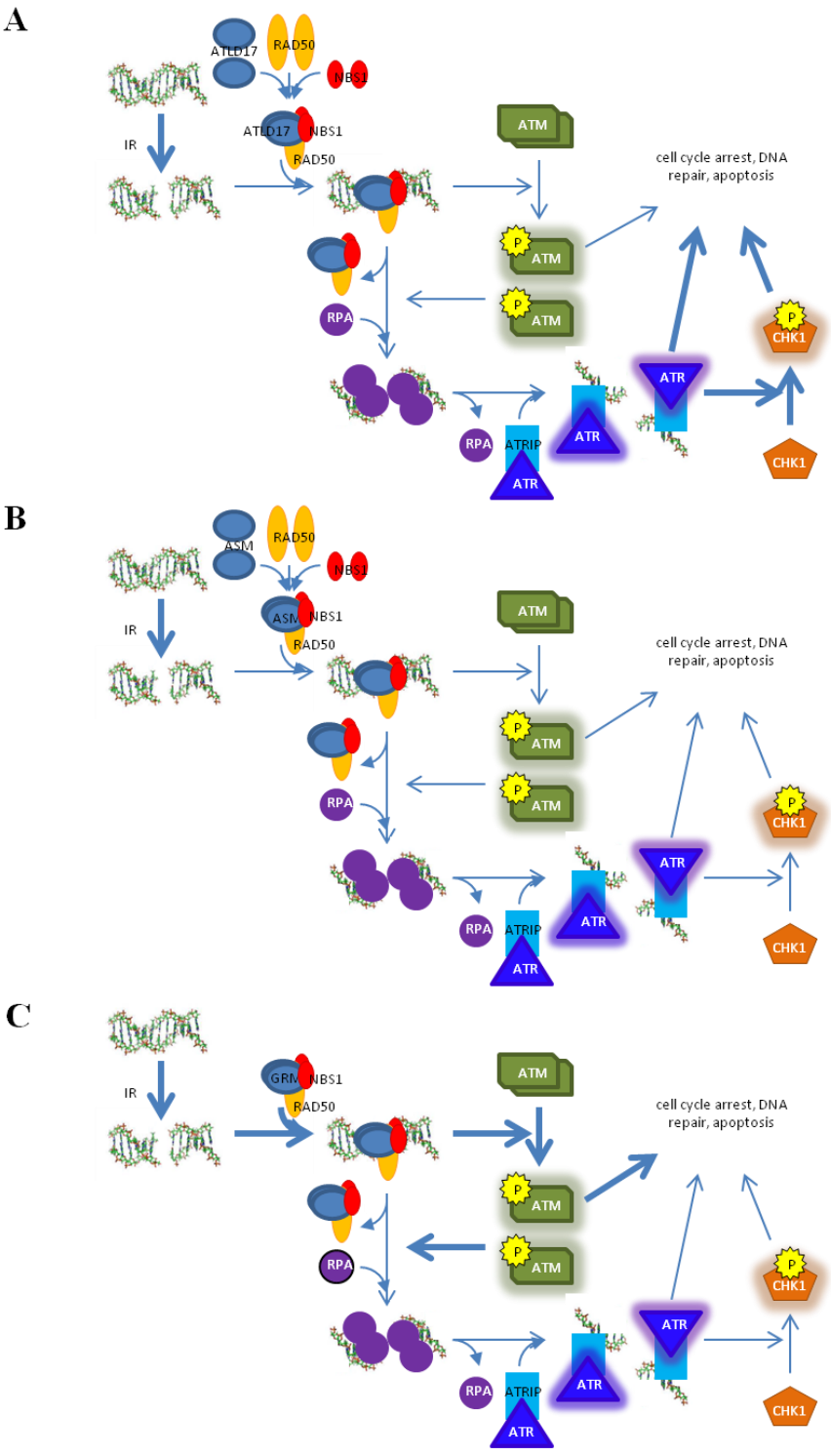

Due to the decreased NBS1 levels in ATLD17 cells and disrupted ATLD17-NBS1 interaction, ATLD17 is likely more cytoplasmic than wild-type MRE11. However, because some ATM-dependent events were observed and events downstream of DNA resection did not appear deficient, enough ATLD17 seemed to get to the nucleus to exert its functions on DNA resection and ATR activation. The result was cells that appeared to have suboptimal DSBR yet could possibly avoid mitotic catastrophe by G_2/M checkpoint activation following DNA damage. Further study of ATLD17 subcellular distribution is merited to discern this mechanism more accurately.

Whether ATLD17 is effective in aiding homologous recombination (HR) or alternative end-joining (A-EJ) remains to be seen. If ATLD17 alters the balance of pathway choice, it could have myriad effects. Error-prone A-EJ has been associated with both tumor-promoting translocations and tumor-maintaining DNA repair [187,188,219-226]. Hence, a tipping of the balance in favor of A-EJ could enable a mutator phenotype in which DSB repair proceeds efficiently enough to allow for continued proliferation. A-EJ inhibitors, such as PARP inhibitors, could prove to be synthetic lethal to such malignancies. On the other hand, tipping the balance in favor of HR would necessitate a distinct set of therapeutic choices and targeting strategies. Regardless of ATLD17's effects on pathway choice, one potential chemopreventative or chemotherapeutic strategy would be to design small molecules that stabilize MRE11-NBS1 interaction to overcome ATLD17's defect.

Though we did not formally measure protein stability, our observations are consistent with ASM being an unstable protein. Despite our attempts to drive expression of each mutant to physiologic MRE11 levels, we had lower yield in obtaining MEFs expressing ASM to at least physiologic MRE11 levels than we had with any other mutant discussed presently (data not shown). Additionally, those clones that did appear to express ASM did so at lower levels and for substantially fewer passages under selection compared to cells expressing other mutants (data not shown). Notably, other investigators have describe cells and tissues of patients with an *MRE11A* allele encoding $MRE11A^{ASM}$ mRNA, and they showed no evidence that they detected ASM protein [129,139]. All together, these results suggest that ASM is misfolded, unstable, and/or dysfunctional to the extent that it contributes little to MRE11 function.

Because ASM was not detected in *MRE11A*$^{ATLD17/ASM}$ patient cells or tissues [129,139], ATLD17 likely predominates in these patients' cells. ATLD17 failed to completely complement NBS1 levels, to complex with NBS1 optimally, and to efficiently facilitate ATM activation. Hence, ATLD17 appeared to impose NBS1 dysfunction, which could explain why ATLD17 patients exhibited an NBS phenotype, namely cancer predisposition. This notion is supported by the observation that some ATLD patients with a mutant defective in NBS1 interaction, MRE11 W210C, were microcephalic, another phenotype typically associated with NBS and not ATLD [128].

Unlike ATLD17 and ASM, GRM appeared to form stable MRN complexes and capable of facilitating ATM activation and activity similarly to wild-type MRE11. However, GRM did display a defect in facilitating ATR activity. This could reflect a defect in any one of several steps in DNA end processing: MRN DNA binding, MRE11 nuclease activity, CTIP/BRCA1 recruitment, recruitment of other nucleases, *etc*…. An MRE11 mutant in which nine glycine-arginine-rich motif arginine residues have been changed to lysine residues, MRE11 RK, was also defective in ATR activity following IR treatment [65]. In addition, MRE11 RK was found to be defective in DNA binding and exonuclease function, which were proposed to result in defective end-processing and ATR loading and activity. GRM could be qualitatively similar in its defects though, given the more subtle nature of amino acid residue substitution in GRM, the defects would be expected to be more subtle.

Given MRE11 RK DNA binding and exonuclease defects, R572Q could cause a defect in end processing. The lymphoma in which GRM was found was only heterozygous mutant [205]. Therefore, if GRM contributed to lymphomagenesis, it could have been through reduced MRE11 function and/or dominant-negative effects. The former possibility is supported by the observation that ATLD1 heterozygosity, which is associated with ~50% of physiologic MRE11 levels, has also been associated with malignancy [207]. A counter argument can be made based on the observation that *Mre11a*$^{+/\Delta}$ mice do not appear to be cancer predisposed. A dominant negative effect of GRM is easy to imagine. GRM was able to interact well with wild-type MRE11. Moreover, even the more severe MRE11 RK mutant was able to localize to DNA damage, suggesting that GRM might as well [65]. In sum, this data suggests that GRM could complex with wild-type MRE11 and localize to sites of DNA damage where GRM then might disrupt

DNA end processing. Defective end processing could favor lower-fidelity A-EJ pathways, which require less end processing than HR. Another interesting possibility is that R572Q disrupts MRE11 interaction with the mismatch repair protein mutL homolog (MLH) 1. R572 lies within the MRE11 452-632 motif, which was identified as being important for this interaction [227]. Disruption of MRE11-MLH1 interaction has been linked to defective mismatch repair [228,229]. Also, R572 lies in the C-terminal uncrystallized portion of MRE11. Recent work shows that the C-terminal-most 76 amino acid residues interact with CDK2, and other MRE11 residues might modulate MRE11-CDK2 interaction [69]. Alteration of this interaction in such a way that CDK2 interaction is enhanced could conceivably contribute to aberrant proliferation.

The MRN/CTIP/BRCA1 complex is important for cell cycle-dependent regulation of DNA resection and HR [69,115]. Central to the regulation of this complex is CDK-mediated CTIP phosphorylation during the S and G2 phases of the cell cycle. In the presence of DSBs, ATM mediates further CTIP phosphorylation. Only upon CDK- and ATM-mediated phosphorylation does CTIP properly promote DNA resection and HR. Hence, mutant-associated alteration of CDK or ATM activity could disrupt this complex and thereby alter DSB repair pathway choice. In fact, most of the mutants discussed presently appear(ed) to affect one of these activities. ATLD1 fails to enable CDK2-mediated CTIP phosphorylation, which has been shown to result in MRN/CTIP/BRCA1 complex disruption [69]; ATLD17 and ASM were each defective in IR-induced ATM activity. Though still speculative, GRM could plausibly be defective in enabling CDK2 activity towards CTIP as ATLD1 is. Indeed, MRN/CTIP/BRCA1 complex disruption is potentially a mechanism by which several cancer-associated *MRE11A* mutations contribute to carcinogenesis. Further study of these mutants' effects on CTIP phosphorylation, HR efficiency, and DSB repair pathway choice is requisite to better understanding of how these mutants might mediate oncogenesis.

Cancer-associated *MRE11A* mutations could alter MRE11 interaction with still other MRE11 interactors. An unbiased screen of MRE11 wild-type and mutant interactors could identify the full range of interactions disrupted by *MRE11A* mutation. Besides other well-recognized mediators of DSB repair, cell cycle machinery and mismatch repair proteins would be of special interest.

Our study has several limitations. Firstly, we used SV40 large T antigen immortalized cells; therefore, any mutant-associated defects in p53 activity were not appreciated [230-232]. Moreover, other mutant defects that are p53 function-dependent were not observable using this system. Secondly, we used murine embryonic fibroblasts rather than cells of the tissues which gave rise to patient malignancies. Therefore, tissue-specific splicing, DNA damage repair pathway choice, etc… could not be taken into account. Finally, we transduced our cells using an adenoviral vector. Adenoviral proteins have been shown to interfere with and degrade multiple DNA repair components, including MRN [233,234]. To minimize experimental artifacts due to adenoviral protein interference, we allowed several days between replication-defective adeno-cre treatment and our experiments. Nonetheless, it remains possible that adenoviral proteins still caused experimental artifacts. For these reasons and more, murine models could prove to be invaluable for further understanding of the roles of ATLD17, ASM, and GRM in oncogenesis. Ultimately, because MRN and ATM display differences in function between mice and humans [235,236], it would be beneficial to reproduce cell-based and *in vitro* studies using human cells and human proteins.

Nonetheless, our results suggest MRE11 mutants contribute to carcinogenesis through several distinct mechanisms. ATLD17, ASM, GRM, and ATLD1 each had unique effects on apical kinase activity and MRN complex stability. ATLD17 and GRM exhibited slight defects in facilitating apical kinase activity perhaps reflecting localized protein misfolding or defective DNA end processing, respectively. Despite the suboptimal DSBR, each of these mutants appeared to support proliferation and G_2/M checkpoint function. ASM, on the other hand, seemed grossly dysfunctional. Because GRM appeared competent in MRN complex formation and deficient in facilitating MRN-dependent events, GRM could exert a dominant negative effect on wild-type MRE11. Therefore, *MRE11A*$^{ATLD17/ASM}$ and *MRE11A*$^{+/GRM}$ cells could possess a mutator phenotype. In contrast, ATLD1 could broadly support apical kinase activation but is largely absent from *MRE11A*$^{ATLD1/ATLD1}$ cells. Thus, *MRE11A*^{ATLD1} carriers could be cancer-predisposed due to MRE11 haploinsufficiency.

3.2: Insights into structure-function relationships

Our findings are consistent with the MRE11 capping domain being important for nuclease domain folding and stability. Disruption of the capping domain by deletion of 27 amino acid residues in ASM was accompanied by disruption of every aspect of MRN complex formation and apical kinase activation tested. In unicellular organism MRE11 orthologues, the capping domain has DNA-, RAD50-, and NBS1-binding sites; however, the capping domain is not directly involved in MRE11 homodimerization [62,63,67,68,73]. Here, we found a capping domain deletion to affect homodimerization in the nuclease domain, even in the absence of RAD50 and NBS1. Therefore, the capping domain appears to be important for folding of the greater phosphodiesterase domain. Other investigators have described patient cells with an allele encoding *MRE11A*^{ASM} mRNA; however, they found no evidence of ASM protein [129,139]. Hence, the capping domain appears to be important for phosphodiesterase domain folding and protein stability.

Study of ATLD17 supported the notion that the MRE11 nuclease domain plays an important role in ATM activation and activity. MRE11 catalytic domain disruption has been shown to affect ATM activation independently of nuclease function [121]. Mirin is an MRE11 exonuclease and ATM activation inhibitor [237]. Treatment with mirin did not appear to differentially affect ATM activation by wild-type MRN or nuclease-deficient M(H129N)RN [121]. Moreover, MRE11 H129N was nuclease dead but still facilitated ATM activation while MRE11 D130V was deficient in both nuclease activity and ATM activation.

S.pombe Nbs1 binding has been shown to affect Mre11 homodimer conformation, DNA repair, and telomere maintenance [73]. This could serve as a means by which Nbs1 communicates information to Mre11 and thereby affects Mre11 function. By analogy, mammalian NBS1 could relay CTIP and MDC1 phosphorylation and binding status through modulation of MRE11 conformation. CTIP could thereby exert its influences on MRE11 nuclease activity. This communication would be expected to be bi-directional. MRE11 homodimer confirmation could reflect M_2R_2 DNA or RAD50 nucleotide binding status which could, in turn, be communicated to NBS1 via changes in latching loop conformation. Consistent with this idea, prokaryotic MR nucleotide binding status has been shown to influence protein conformation [63,67,68], and human RAD50 nucleotide binding status has been shown to influence MR NBS1 binding, MRN

DNA binding, and ATM activity [66,121]. Inability of MRE11 to communicate DSB sensing to NBS1 could result in defective ATM activation and activity. Alternatively, ATM makes multiple contacts on the MRN complex [91], so disruption of ATM-MRE11 interaction itself could affect ATM activity.

Our findings further understanding of the importance of arginine methylation in cellular processes. An ever-increasing number of proteins, including components of the pre-mRNA splicing, polyadenylation, transcription, signal transduction, and DNA damage response machinery, are being found to be subject to arginine methylation [238]. This modification often occurs around glycine residues. Clusters of glycines and arginines constitute glycine-arginine-rich (GAR) motifs, and such motifs are commonly found in nucleic acid binding proteins and are especially prone to arginine methylation. GAR motifs and their methylation have been shown to affect protein subcellular localization, nucleic acid binding, and protein function [65,166-168,239-244]. In the case of MRE11, GAR motif arginine methylation appears to influence MRE11 protein stability, subnuclear localization, DNA binding, and exonuclease activity [65,166,168]. MRE11 in which the GAR motif arginines have been replaced with lysines, MRE11 RK, exhibited decreased *in vitro* binding to dsDNA, ssDNA, and splayed-arm DNA and decreased *in vitro* exonuclease activity towards blunt-ended dsDNA in the context of RAD50 and NBS1 relative to wild-type MRE11. Replacement of the GAR motif arginines with alanines in MRE11 RA further reduced MRE11 exonuclease activity towards and binding of dsDNA. Deletion of MRE11 residues 498-615, which includes the MRE11 GAR motif, substantially abrogated MRE11 binding of and exonuclease activity on blunt-ended dsDNA. This region was intrinsically able to bind DNA in a manner which required methylation of the GAR motif. Moreover, MRE11 methylation was required for DNA damage-induced MRE11 movement from the nucleoplasm to chromatin, and MRE11 RK was defective in IR-induced CHK1 phosphorylation. All together, these results suggest that the MRE11 GAR motif is required for optimal MRE11 DNA binding and that disruption of the methylation or charge of the GAR motif, in turn, disrupts MRE11 localization to DSBs, DNA end resection, and checkpoint kinase activation. Our results are consistent with these conclusions and go further to suggest that even a subtle disruption of GAR motif methylation or charge is sufficient to affect these processes.

GAR motifs can be found in other proteins involved in maintenance of genomic stability, including p53 binding protein 1 (53BP1) and telomere repeat factor (TRF) 2. 53BP1 plays important roles in facilitating non-homologous end-joining and suppressing resection of DNA ends [241,245-247]. Substitutions of 53BP1 GAR motif arginines with lysines or alanines yielded 53BP1 RK or 53BP1 RA, respectively, and disrupted 53BP1 DNA binding *in vitro* [239,240]. Despite these DNA binding defects, the 53BP1 GAR motif is not essential for shelterin dysfunction-associated telomeric fusion; 53BP1 RK and 53BP1 ΔGAR mutants complemented shelterin dysfunction-associated telomeric fusion to 80% of wild-type levels whereas complete loss of 53BP1 reduced the frequency of such fusion events to less than 10% of wild-type levels [241,242]. The DNA binding defect of 53BP1 RK is not reflected by defects in 53BP1-facilitated class switch recombination either; 53BP1 RK was able to support 53BP1 functions in class switch recombination [245]. Indeed, though the 53BP1 GAR motif appeared important for DNA binding *in vitro*, it appears to be largely dispensable for 53BP1 function in promoting NHEJ and preventing CTIP-mediated DNA end resection.

TRF2 is a component of the telomeric repeat-binding shelterin complex crucial for protection of telomeres against aberrant DNA repair processes [248]. In contrast to the largely negative results observed for the 53BP1 GAR motif to date, TRF2 RK expression resulted in telomere deprotection and fusion [243]. The TRF2 GAR motif might be required for TRF2 interaction with telomere-repeat-encoding RNA (TERRA) and recruitment of the origin recognition complex (ORC) to telomeres [244]. This complex could facilitate timely replication of telomeres and help modulate telomeric chromatin compaction. Hence, subtle alterations of the TRF2 GAR motif like that seen for the MRE11 GAR motif in the GRM mutant could potentially affect telomere integrity, chromosomal stability, and cellular viability.

Unlike the other motifs studied, the CDK2 interacting motif was not required for stable MRN complex formation, apical kinase activity, or G_2/M checkpoint activation. Hence, MRE11-enabled CDK2 activity toward CTIP appeared dispensable for these functions. In contrast with our findings, the MRE11 C-terminus was required for ATM activity in biochemical assays [91]. It could be that the C-terminus is essential for directing ATM activity towards certain substrates. However, this requirement could be masked in cells by as yet unidentified compensatory mechanisms.

More broadly, our results point to the complexity and delicacy of protein complex regulation *in vivo*. Links between even subtle changes in essential proteins and human pathology should be carefully studied. Catalytic domain mutations might actually exert their pathogenic influences through alterations of protein-protein interactions. Kinase activation can be indirectly controlled via subtle conformational changes in protein sensors. Glycine-arginine-rich motifs are found on many proteins, methylated arginines on many more, and post-translational modifications abound in the proteome, and their control over protein function is evident here. Given the prevalence and centrality of protein environmental sensors, protein-protein communication through subtle conformational modulation, kinase regulation, and post-translational modification to life, the protein physiology and pathophysiology studied here may very well translate to elsewhere in the human proteome and mutatome. We hope our efforts inform future discernment of these fundamental processes.

CHAPTER 4: MATERIALS AND METHODS

DNA construct creation

Select *Mre11a* mutations were introduced into pEF6-Mm*Mre11a* using site-directed mutagenesis (Stratagene) or – for the alternative splice mutant – PCR amplification followed by ligation. These mutants were shuttled into pGBKT7 and pGADT7 (Clontech). Mm*Nbn* (GeneCopoeia) was TOPO PCR subcloned (Life Technologies) and shuttled into the Y2H vectors.

MEF engineering and culture

Mre11a$^{cond/\Delta}$ murine embryonic cell lines [76] were maintained using standard culture conditions. Cells were stably transfected with wild-type- or mutant-expressing pEF6-Mm*Mre11a* per manufacturer's instructions (Lipofectamine 2000, Life Technologies). Briefly, cells were grown to 50-90% confluency in six-well plates. Cells were treated with 10 µl lipofectamine 2000 transfection reagent and 2.5-10 µg pEF6-Mm*Mre11a* in 2.5 ml serum- and antibiotic-free medium per well. Twenty-four hours post-transfection, cells were split; they were seeded at 3200-200 cells per six-well plate well. Forty-eight hours post-transfection, the cells were treated with 5-10 µg/ml blasticidin. Blasticidin-containing medium was subsequently refreshed every two days. Four days post-transfection, it was decided whether the cells were seeded sparsely enough to allow for clonal isolation. Where that appeared to be the case, colonies were allowed to grow to confluency at which time they were picked using a pipette tip and seeded into a twenty-four-well plate well with blasticidin-containing medium.

Prior to each experiment, cells were grown under blasticidin selection for three days, split (seeded at a density of $5x10^5$ cells per 10 cm plate), allowed to recover for a day, treated with replication-defective adeno-cre (University of Michigan Vector Core; 3 µl adeno-cre and 5 ml

medium per 10 cm plate), allowed to recover for two days (in the presence of complete medium), split (seeded at a density of 5-7.5x10^5 cells per 10 cm plate), and allowed to recover for two-three days after which time experiments were performed. Where ionizing radiation treatment is indicated, slightly subconfluent cells were exposed to a ^{137}Cs source.

Mre11a RNA typing

5e5 cells per sample were pelleted, and RNA was isolated (AllPrep DNA/RNA Mini Kit, Qiagen). RNA concentration was determined by Nanodrop. RT-PCR was performed with the following specifications: forward primer: GCAATCTCAACATTTCCATTCC, reverse primer: GTTTCTTCTTGGGCAACTACTG; 200 ng RNA per reaction; Platinum Taq with or without Superscript III reverse transcriptase (Life Technologies) was used per manufacturer's protocol; PCR program: 55°C for 30 minutes, 94°C for 2 minutes, 94°C for 15 seconds, 59°C for 30 seconds, 68°C for 3.5 minutes, back to step 3 39 times, and 68°C for 7 minutes. Amplicons were run on an agarose gel or subjected to Sanger sequencing (sequencing primers: CAGTATTTAGTATCCACGGCAAC, CATCGTCATCATCCTCATCTG, GGAGAAGAGATCAACTTTGGG, and CTCTTCCTTGTCCACAAACTC).

Immunoblot

Cells were lysed in Laemmli buffer (BioRad; 200-300 µl 1:1 2x buffer:1x PBS per 10 cm plate) and heated at 100°C for 10 minutes. Protein concentrations were ascertained by BCA assay (Thermo Scientific). Beta-mercaptoethanol was then added to the samples to a final concentration of 2.5%. Proteins were resolved by SDS-PAGE (4% polyacrylamide stacking gels; 6% polyacrylamide separation gels were used if probing for pATM; otherwise, 8% polyacrylamide separation gels were fine), transferred (for 20-24 hours at 25V in 20% methanol-containing transfer buffer (National Diagnostics) or for 2-2.5 hours at 25V in 10% methanol-containing transfer buffer) to PVDF membranes (Immobilon), and blocked in 5% milk TBST (25 mM Tris-Cl, 150 mM NaCl, 0.05% tween-20, pH 7.6). Primary antibodies used were as follows: MRE11 (Cell Signaling 4895, 1:1000 in 5% BSA TBST for 16-20 hours), RAD50 (Bethyl A300-184A, 1:500 in 3% milk TBST for two days), NBS1 (Novus NB110-57272, 1:500 in 3% milk TBST for two days), pATM S1987 (Rockland 200-301-400, 1:500 in 3% milk TBST for 2-4 days), ATM (Cell Signaling 2873, 1:1000 in 5% BSA TBST for two days), pKAP1 (Bethyl

A300-767A, 1:2500 in 3% milk TBST for 1-2 days), KAP1 (Cell Signaling 4124, 1:1000 in 5% BSA TBST for 2 days), pCHK1 S345 (Cell Signaling 2341, 1:500 in 5% BSA TBST for two days), CHK1 (Cell Signaling 2360, 1:1000 in 3% milk TBST for two days), GAPDH (Abcam ab8245, 1:4000 in 5% milk TBST for 1.5 hours to overnight), HA-tag (Cell Signaling 2367, 1:1000 in 5% milk TBST overnight), MYC-tag (Cell Signaling 2278, 1:1000 in 5% BSA TBST overnight), and tubulin (Pierce MA1-80017, 1:1000 in TBST overnight). Either fluorophore (Li-Cor, 1:4000-1:2000 in 3-5% milk TBST for 1.5 hours to overnight)- or peroxidase (Jackson Immunolabs, 1:2000 in 3-5% milk TBST for 1.5 hours)-conjugated secondary antibodies were used. When called for, membranes were stripped for 30-60 minutes at room temperature (stripping buffer recipe: 60 ml 0.5M Tris-HCl pH 6.8, 3.5 ml of β-mercaptoethanol, 50 ml of 20% SDS, and 386.5 ml of ultrapure water), rinsed, and reblocked with 5% milk TBST prior to being reprobed. Quantitation was performed following the use of Li-Cor secondaries.

G2/M checkpoint

7.5e5 cells were plated per 10 cm dish, grown for 48 hours, treated with 10 Gy IR from a ^{137}Cs source or mock treated, allowed to recover for an hour, and fixed. Cells were probed for the mitotic marker p-histone H3 S10 [214] using Cell Signaling primary antibody and FITC conjugated secondary antibody (BD Pharmingen). Flow cytometry (Accuri C6, BD Biosciences) was performed as described previously [249].

Immunoprecipitation

10-20 million cells per 14.5-cm plate were lysed with 300 µl 50mM TrisCl, 300mM NaCl, 10% glycerol, and 1% NP-40. Lysates were precleared with protein A agarose beads (Roche); lysate protein concentrations were measured by BCA assay (Thermo Scientific); 20 µg/µl protein solutions were made; beads were incubated with either anti-MRE11 antibody (Cell Signaling), anti-RAD50 antibody (Bethyl), or anti-NBS1 antibody (Novus); and 0.5 mg protein was added along with phosphatase and protease inhibitors (Roche). After an overnight incubation, beads were washed four times. Proteins were eluted from the beads with Laemmli buffer (BioRad), and extracts were heated at 95°C for 10 minutes.

Yeast two-hybrid

Y2HGold (Clontech) were cotransformed using the Yeastmaker Yeast Transformation system (Clontech) per the manufacturer's protocol. To select for cotransformed cells, transformation reactions were plated onto SD-L-W agar (Clontech) plates, and colonies were picked and streaked onto SD-L-W agar plates. To test for interaction by colorimetric assay, the restreaked yeast were picked, grown in SD-L-W (Clontech) overnight, assessed for their density (by OD_{600nm}), and briefly centrifuged. 16 µl of supernatant was aliquoted per reaction, 48 µl assay buffer (2 volumes 0.5M NaOAc, pH 4.5 (aq) and 1 volume 100mM p-nitrophenyl-α-D-galactopyranoside (Sigma-Aldrich) (aq)) was added, and the reactions were incubated at least overnight. Each reaction was quenched with 136 µl 1M Na_2CO_3 (aq), and OD_{410nm} readings were taken by microplate reader. Colony growth was assessed by culturing yeast overnight, normalizing yeast density by OD_{600nm}, and plating five 10X serial dilutions onto SD-L-W (loading control) and SD-L-W-H-ade (interaction test) agar plates.

References

1. Lindahl T, Barnes DE. (2000) Repair of endogenous DNA damage. Cold Spring Harb Symp Quant Biol 65: 127-133.

2. Lindahl T, Nyberg B. (1972) Rate of depurination of native deoxyribonucleic acid. Biochemistry 11: 3610-3618.

3. Nakamura J, Walker VE, Upton PB, Chiang SY, Kow YW, et al. (1998) Highly sensitive apurinic/apyrimidinic site assay can detect spontaneous and chemically induced depurination under physiological conditions. Cancer Res 58: 222-225.

4. Shen JC, Rideout WM,3rd, Jones PA. (1994) The rate of hydrolytic deamination of 5-methylcytosine in double-stranded DNA. Nucleic Acids Res 22: 972-976.

5. Rydberg B, Lindahl T. (1982) Nonenzymatic methylation of DNA by the intracellular methyl group donor S-adenosyl-L-methionine is a potentially mutagenic reaction. EMBO J 1: 211-216.

6. Gates KS. (2009) An overview of chemical processes that damage cellular DNA: Spontaneous hydrolysis, alkylation, and reactions with radicals. Chem Res Toxicol 22: 1747-1760.

7. Valko M, Rhodes CJ, Moncol J, Izakovic M, Mazur M. (2006) Free radicals, metals and antioxidants in oxidative stress-induced cancer. Chem Biol Interact 160: 1-40.

8. Kawanishi S, Hiraku Y, Pinlaor S, Ma N. (2006) Oxidative and nitrative DNA damage in animals and patients with inflammatory diseases in relation to inflammation-related carcinogenesis. Biol Chem 387: 365-372.

9. Reijns MA, Rabe B, Rigby RE, Mill P, Astell KR, et al. (2012) Enzymatic removal of ribonucleotides from DNA is essential for mammalian genome integrity and development. Cell 149: 1008-1022.

10. Li Y, Breaker RR. (1999) Kinetics of RNA degradation by specific base catalysis of transesterification involving the 2-prime hydroxyl group. J Am Chem Soc 121: 5364.

11. Schmitt MW, Matsumoto Y, Loeb LA. (2009) High fidelity and lesion bypass capability of human DNA polymerase delta. Biochimie 91: 1163-1172.

12. Kunkel TA, Bebenek K. (2000) DNA replication fidelity. Annu Rev Biochem 69: 497-529.

13. Takashima H, Boerkoel CF, John J, Saifi GM, Salih MA, et al. (2002) Mutation of TDP1, encoding a topoisomerase I-dependent DNA damage repair enzyme, in spinocerebellar ataxia with axonal neuropathy. Nat Genet 32: 267-272.

14. Pouliot JJ, Yao KC, Robertson CA, Nash HA. (1999) Yeast gene for a tyr-DNA phosphodiesterase that repairs topoisomerase I complexes. Science 286: 552-555.

15. El-Khamisy SF, Saifi GM, Weinfeld M, Johansson F, Helleday T, et al. (2005) Defective DNA single-strand break repair in spinocerebellar ataxia with axonal neuropathy-1. Nature 434: 108-113.

16. Cortes Ledesma F, El Khamisy SF, Zuma MC, Osborn K, Caldecott KW. (2009) A human 5'-tyrosyl DNA phosphodiesterase that repairs topoisomerase-mediated DNA damage. Nature 461: 674-678.

17. Alt FW, Zhang Y, Meng FL, Guo C, Schwer B. (2013) Mechanisms of programmed DNA lesions and genomic instability in the immune system. Cell 152: 417-429.

18. Bolcun-Filas E, Schimenti JC. (2012) Genetics of meiosis and recombination in mice. Int Rev Cell Mol Biol 298: 179-227.

19. Jackson SP, Bartek J. (2009) The DNA-damage response in human biology and disease. Nature 461: 1071-1078.

20. Sinha RP, Hader DP. (2002) UV-induced DNA damage and repair: A review. Photochem Photobiol Sci 1: 225-236.

21. Wogan GN, Hecht SS, Felton JS, Conney AH, Loeb LA. (2004) Environmental and chemical carcinogenesis. Semin Cancer Biol 14: 473-486.

22. Hsieh YH, Hsu JL, Su IJ, Huang W. (2011) Genomic instability caused by hepatitis B virus: Into the hepatoma inferno. Front Biosci 16: 2586-2597.

23. Nitiss JL. (2009) Targeting DNA topoisomerase II in cancer chemotherapy. Nat Rev Cancer 9: 338-350.

24. Pommier Y. (2006) Topoisomerase I inhibitors: Camptothecins and beyond. Nat Rev Cancer 6: 789-802.

25. Helleday T, Petermann E, Lundin C, Hodgson B, Sharma RA. (2008) DNA repair pathways as targets for cancer therapy. Nat Rev Cancer 8: 193-204.

26. Hendry JH, Simon SL, Wojcik A, Sohrabi M, Burkart W, et al. (2009) Human exposure to high natural background radiation: What can it teach us about radiation risks? J Radiol Prot 29: A29-42.

27. Davies HE, Wathen CG, Gleeson FV. (2011) The risks of radiation exposure related to diagnostic imaging and how to minimise them. BMJ 342: d947.

28. Zeissman HA, O'Malley JP, Thrall JH, editors. (2006) Nuclear medicine: The requisites in radiology. Philadelphia, PA: Mosby, An Imprint of Elsevier.

29. Ward JF. (1988) DNA damage produced by ionizing radiation in mammalian cells: Identities, mechanisms of formation, and reparability. Prog Nucleic Acid Res Mol Biol 35: 95-125.

30. Gunderson LL, Tepper JE, editors. (2007) Clinical radiation oncology. Philadelphia, PA: Churchill Livingstone, an imprint of Elsevier Inc.

31. Gerson SL. (2004) MGMT: Its role in cancer aetiology and cancer therapeutics. Nat Rev Cancer 4: 296-307.

32. Kunkel TA, Erie DA. (2005) DNA mismatch repair. Annu Rev Biochem 74: 681-710.

33. Hegde ML, Hazra TK, Mitra S. (2008) Early steps in the DNA base excision/single-strand interruption repair pathway in mammalian cells. Cell Res 18: 27-47.

34. Hoeijmakers JH. (2001) Genome maintenance mechanisms for preventing cancer. Nature 411: 366-374.

35. Masutani C, Kusumoto R, Iwai S, Hanaoka F. (2000) Mechanisms of accurate translesion synthesis by human DNA polymerase eta. EMBO J 19: 3100-3109.

36. Boboila C, Alt FW, Schwer B. (2012) Classical and alternative end-joining pathways for repair of lymphocyte-specific and general DNA double-strand breaks. Adv Immunol 116: 1-49.

37. Chapman JR, Taylor MR, Boulton SJ. (2012) Playing the end game: DNA double-strand break repair pathway choice. Mol Cell 47: 497-510.

38. Dinkelmann M, Spehalski E, Stoneham T, Buis J, Wu Y, et al. (2009) Multiple functions of MRN in end-joining pathways during isotype class switching. Nat Struct Mol Biol 16: 808-813.

39. Bakkenist CJ, Kastan MB. (2004) Initiating cellular stress responses. Cell 118: 9-17.

40. Falck J, Coates J, Jackson SP. (2005) Conserved modes of recruitment of ATM, ATR and DNA-PKcs to sites of DNA damage. Nature 434: 605-611.

41. Zou L, Elledge SJ. (2003) Sensing DNA damage through ATRIP recognition of RPA-ssDNA complexes. Science 300: 1542-1548.

42. Kim ST, Lim DS, Canman CE, Kastan MB. (1999) Substrate specificities and identification of putative substrates of ATM kinase family members. J Biol Chem 274: 37538-37543.

43. O'Neill T, Dwyer AJ, Ziv Y, Chan DW, Lees-Miller SP, et al. (2000) Utilization of oriented peptide libraries to identify substrate motifs selected by ATM. J Biol Chem 275: 22719-22727.

44. Matsuoka S, Ballif BA, Smogorzewska A, McDonald ER,3rd, Hurov KE, et al. (2007) ATM and ATR substrate analysis reveals extensive protein networks responsive to DNA damage. Science 316: 1160-1166.

45. Liu Q, Guntuku S, Cui XS, Matsuoka S, Cortez D, et al. (2000) Chk1 is an essential kinase that is regulated by atr and required for the G(2)/M DNA damage checkpoint. Genes Dev 14: 1448-1459.

46. Matsuoka S, Rotman G, Ogawa A, Shiloh Y, Tamai K, et al. (2000) Ataxia telangiectasia-mutated phosphorylates Chk2 in vivo and in vitro. Proc Natl Acad Sci U S A 97: 10389-10394.

47. Falck J, Petrini JH, Williams BR, Lukas J, Bartek J. (2002) The DNA damage-dependent intra-S phase checkpoint is regulated by parallel pathways. Nat Genet 30: 290-294.

48. Takai H, Tominaga K, Motoyama N, Minamishima YA, Nagahama H, et al. (2000) Aberrant cell cycle checkpoint function and early embryonic death in Chk1(-/-) mice. Genes Dev 14: 1439-1447.

49. Stracker TH, Usui T, Petrini JH. (2009) Taking the time to make important decisions: The checkpoint effector kinases Chk1 and Chk2 and the DNA damage response. DNA Repair (Amst) 8: 1047-1054.

50. Lu X, Nannenga B, Donehower LA. (2005) PPM1D dephosphorylates Chk1 and p53 and abrogates cell cycle checkpoints. Genes Dev 19: 1162-1174.

51. Zhang X, Lin L, Guo H, Yang J, Jones SN, et al. (2009) Phosphorylation and degradation of MdmX is inhibited by Wip1 phosphatase in the DNA damage response. Cancer Res 69: 7960-7968.

52. Song JY, Han HS, Sabapathy K, Lee BM, Yu E, et al. (2010) Expression of a homeostatic regulator, Wip1 (wild-type p53-induced phosphatase), is temporally induced by c-jun and p53 in response to UV irradiation. J Biol Chem 285: 9067-9076.

53. Moon SH, Lin L, Zhang X, Nguyen TA, Darlington Y, et al. (2010) Wild-type p53-induced phosphatase 1 dephosphorylates histone variant gamma-H2AX and suppresses DNA double strand break repair. J Biol Chem 285: 12935-12947.

54. Lindqvist A, de Bruijn M, Macurek L, Bras A, Mensinga A, et al. (2009) Wip1 confers G2 checkpoint recovery competence by counteracting p53-dependent transcriptional repression. EMBO J 28: 3196-3206.

55. Zhang XP, Liu F, Wang W. (2011) Two-phase dynamics of p53 in the DNA damage response. Proc Natl Acad Sci U S A 108: 8990-8995.

56. Loeb LA. (2011) Human cancers express mutator phenotypes: Origin, consequences and targeting. Nat Rev Cancer 11: 450-457.

57. Stracker TH, Petrini JH. (2011) The MRE11 complex: Starting from the ends. Nat Rev Mol Cell Biol 12: 90-103.

58. Chahwan C, Nakamura TM, Sivakumar S, Russell P, Rhind N. (2003) The fission yeast Rad32 (Mre11)-Rad50-Nbs1 complex is required for the S-phase DNA damage checkpoint. Mol Cell Biol 23: 6564-6573.

59. Park YB, Chae J, Kim YC, Cho Y. (2011) Crystal structure of human Mre11: Understanding tumorigenic mutations. Structure 19: 1591-1602.

60. Arthur LM, Gustausson K, Hopfner KP, Carson CT, Stracker TH, et al. (2004) Structural and functional analysis of Mre11-3. Nucleic Acids Res 32: 1886-1893.

61. Hopfner KP, Karcher A, Craig L, Woo TT, Carney JP, et al. (2001) Structural biochemistry and interaction architecture of the DNA double-strand break repair Mre11 nuclease and Rad50-ATPase. Cell 105: 473-485.

62. Williams RS, Moncalian G, Williams JS, Yamada Y, Limbo O, et al. (2008) Mre11 dimers coordinate DNA end bridging and nuclease processing in double-strand-break repair. Cell 135: 97-109.

63. Lim HS, Kim JS, Park YB, Gwon GH, Cho Y. (2011) Crystal structure of the Mre11-Rad50-ATPgammaS complex: Understanding the interplay between Mre11 and Rad50. Genes Dev 25: 1091-1104.

64. Das D, Moiani D, Axelrod HL, Miller MD, McMullan D, et al. (2010) Crystal structure of the first eubacterial Mre11 nuclease reveals novel features that may discriminate substrates during DNA repair. J Mol Biol 397: 647-663.

65. Yu Z, Vogel G, Coulombe Y, Dubeau D, Spehalski E, et al. (2012) The MRE11 GAR motif regulates DNA double-strand break processing and ATR activation. Cell Res 22: 305-320.

66. Lee JH, Ghirlando R, Bhaskara V, Hoffmeyer MR, Gu J, et al. (2003) Regulation of Mre11/Rad50 by Nbs1: Effects on nucleotide-dependent DNA binding and association with ataxia-telangiectasia-like disorder mutant complexes. J Biol Chem 278: 45171-45181.

67. Lammens K, Bemeleit DJ, Mockel C, Clausing E, Schele A, et al. (2011) The Mre11:Rad50 structure shows an ATP-dependent molecular clamp in DNA double-strand break repair. Cell 145: 54-66.

68. Williams GJ, Williams RS, Williams JS, Moncalian G, Arvai AS, et al. (2011) ABC ATPase signature helices in Rad50 link nucleotide state to Mre11 interface for DNA repair. Nat Struct Mol Biol 18: 423-431.

69. Buis J, Stoneham T, Spehalski E, Ferguson DO. (2012) Mre11 regulates CtIP-dependent double-strand break repair by interaction with CDK2. Nat Struct Mol Biol 19: 246-252.

70. Hopfner KP, Putnam CD, Tainer JA. (2002) DNA double-strand break repair from head to tail. Curr Opin Struct Biol 12: 115-122.

71. Hopfner KP, Karcher A, Shin DS, Craig L, Arthur LM, et al. (2000) Structural biology of Rad50 ATPase: ATP-driven conformational control in DNA double-strand break repair and the ABC-ATPase superfamily. Cell 101: 789-800.

72. de Jager M, van Noort J, van Gent DC, Dekker C, Kanaar R, et al. (2001) Human Rad50/Mre11 is a flexible complex that can tether DNA ends. Mol Cell 8: 1129-1135.

73. Schiller CB, Lammens K, Guerini I, Coordes B, Feldmann H, et al. (2012) Structure of Mre11-Nbs1 complex yields insights into ataxia-telangiectasia-like disease mutations and DNA damage signaling. Nat Struct Mol Biol 19: 693-700.

74. Paull TT, Gellert M. (1998) The 3' to 5' exonuclease activity of mre 11 facilitates repair of DNA double-strand breaks. Mol Cell 1: 969-979.

75. Paull TT, Gellert M. (1999) Nbs1 potentiates ATP-driven DNA unwinding and endonuclease cleavage by the Mre11/Rad50 complex. Genes Dev 13: 1276-1288.

76. Buis J, Wu Y, Deng Y, Leddon J, Westfield G, et al. (2008) Mre11 nuclease activity has essential roles in DNA repair and genomic stability distinct from ATM activation. Cell 135: 85-96.

77. Nimonkar AV, Genschel J, Kinoshita E, Polaczek P, Campbell JL, et al. (2011) BLM-DNA2-RPA-MRN and EXO1-BLM-RPA-MRN constitute two DNA end resection machineries for human DNA break repair. Genes Dev 25: 350-362.

78. Mimitou EP, Symington LS. (2009) DNA end resection: Many nucleases make light work. DNA Repair (Amst) 8: 983-995.

79. de Jager M, van Noort J, van Gent DC, Dekker C, Kanaar R, et al. (2001) Human Rad50/Mre11 is a flexible complex that can tether DNA ends. Mol Cell 8: 1129-1135.

80. Lee KC, Padget K, Curtis H, Cowell IG, Moiani D, et al. (2012) MRE11 facilitates the removal of human topoisomerase II complexes from genomic DNA. Biol Open 1: 863-873.

81. Orii KE, Lee Y, Kondo N, McKinnon PJ. (2006) Selective utilization of nonhomologous end-joining and homologous recombination DNA repair pathways during nervous system development. Proc Natl Acad Sci U S A 103: 10017-10022.

82. Park Y, Gerson SL. (2005) DNA repair defects in stem cell function and aging. Annu Rev Med 56: 495-508.

83. Trenz K, Smith E, Smith S, Costanzo V. (2006) ATM and ATR promote Mre11 dependent restart of collapsed replication forks and prevent accumulation of DNA breaks. EMBO J 25: 1764-1774.

84. Sacho EJ, Maizels N. (2011) DNA repair factor MRE11/RAD50 cleaves 3'-phosphotyrosyl bonds and resects DNA to repair damage caused by topoisomerase 1 poisons. J Biol Chem 286: 44945-44951.

85. Verdun RE, Crabbe L, Haggblom C, Karlseder J. (2005) Functional human telomeres are recognized as DNA damage in G2 of the cell cycle. Mol Cell 20: 551-561.

86. Verdun RE, Karlseder J. (2006) The DNA damage machinery and homologous recombination pathway act consecutively to protect human telomeres. Cell 127: 709-720.

87. Dimitrova N, de Lange T. (2009) Cell cycle-dependent role of MRN at dysfunctional telomeres: ATM signaling-dependent induction of nonhomologous end joining (NHEJ) in G1 and resection-mediated inhibition of NHEJ in G2. Mol Cell Biol 29: 5552-5563.

88. Cherry SM, Adelman CA, Theunissen JW, Hassold TJ, Hunt PA, et al. (2007) The Mre11 complex influences DNA repair, synapsis, and crossing over in murine meiosis. Curr Biol 17: 373-378.

89. Moreau S, Ferguson JR, Symington LS. (1999) The nuclease activity of Mre11 is required for meiosis but not for mating type switching, end joining, or telomere maintenance. Mol Cell Biol 19: 556-566.

90. Wiltzius JJ, Hohl M, Fleming JC, Petrini JH. (2005) The Rad50 hook domain is a critical determinant of Mre11 complex functions. Nat Struct Mol Biol 12: 403-407.

91. Lee JH, Paull TT. (2004) Direct activation of the ATM protein kinase by the Mre11/Rad50/Nbs1 complex. Science 304: 93-96.

92. Lee JH, Paull TT. (2005) ATM activation by DNA double-strand breaks through the Mre11-Rad50-Nbs1 complex. Science 308: 551-554.

93. Di Leonardo A, Linke SP, Clarkin K, Wahl GM. (1994) DNA damage triggers a prolonged p53-dependent G1 arrest and long-term induction of Cip1 in normal human fibroblasts. Genes Dev 8: 2540-2551.

94. Campisi J, d'Adda di Fagagna F. (2007) Cellular senescence: When bad things happen to good cells. Nat Rev Mol Cell Biol 8: 729-740.

95. Stucki M, Jackson SP. (2006) gammaH2AX and MDC1: Anchoring the DNA-damage-response machinery to broken chromosomes. DNA Repair (Amst) 5: 534-543.

96. Lou Z, Minter-Dykhouse K, Franco S, Gostissa M, Rivera MA, et al. (2006) MDC1 maintains genomic stability by participating in the amplification of ATM-dependent DNA damage signals. Mol Cell 21: 187-200.

97. Chapman JR, Jackson SP. (2008) Phospho-dependent interactions between NBS1 and MDC1 mediate chromatin retention of the MRN complex at sites of DNA damage. EMBO Rep 9: 795-801.

98. Goldberg M, Stucki M, Falck J, D'Amours D, Rahman D, et al. (2003) MDC1 is required for the intra-S-phase DNA damage checkpoint. Nature 421: 952-956.

99. Dong Z, Zhong Q, Chen PL. (1999) The nijmegen breakage syndrome protein is essential for Mre11 phosphorylation upon DNA damage. J Biol Chem 274: 19513-19516.

100. Yuan SS, Chang HL, Hou MF, Chan TF, Kao YH, et al. (2002) Neocarzinostatin induces Mre11 phosphorylation and focus formation through an ATM- and NBS1-dependent mechanism. Toxicology 177: 123-130.

101. Yuan SS, Su JH, Hou MF, Yang FW, Zhao S, et al. (2002) Arsenic-induced Mre11 phosphorylation is cell cycle-dependent and defective in NBS cells. DNA Repair (Amst) 1: 137-142.

102. Costanzo V, Paull T, Gottesman M, Gautier J. (2004) Mre11 assembles linear DNA fragments into DNA damage signaling complexes. PLoS Biol 2: E110.

103. Di Virgilio M, Ying CY, Gautier J. (2009) PIKK-dependent phosphorylation of Mre11 induces MRN complex inactivation by disassembly from chromatin. DNA Repair (Amst) 8: 1311-1320.

104. Linding R, Jensen LJ, Ostheimer GJ, van Vugt MA, Jorgensen C, et al. (2007) Systematic discovery of in vivo phosphorylation networks. Cell 129: 1415-1426.

105. Yazdi PT, Wang Y, Zhao S, Patel N, Lee EY, et al. (2002) SMC1 is a downstream effector in the ATM/NBS1 branch of the human S-phase checkpoint. Genes Dev 16: 571-582.

106. Gatei M, Young D, Cerosaletti KM, Desai-Mehta A, Spring K, et al. (2000) ATM-dependent phosphorylation of nibrin in response to radiation exposure. Nat Genet 25: 115-119.

107. Wu X, Ranganathan V, Weisman DS, Heine WF, Ciccone DN, et al. (2000) ATM phosphorylation of nijmegen breakage syndrome protein is required in a DNA damage response. Nature 405: 477-482.

108. Zhao S, Weng YC, Yuan SS, Lin YT, Hsu HC, et al. (2000) Functional link between ataxia-telangiectasia and nijmegen breakage syndrome gene products. Nature 405: 473-477.

109. Goodarzi AA, Noon AT, Deckbar D, Ziv Y, Shiloh Y, et al. (2008) ATM signaling facilitates repair of DNA double-strand breaks associated with heterochromatin. Mol Cell 31: 167-177.

110. Gatei M, Jakob B, Chen P, Kijas AW, Becherel OJ, et al. (2011) ATM protein-dependent phosphorylation of Rad50 protein regulates DNA repair and cell cycle control. J Biol Chem 286: 31542-31556.

111. Sartori AA, Lukas C, Coates J, Mistrik M, Fu S, et al. (2007) Human CtIP promotes DNA end resection. Nature 450: 509-514.

112. Limbo O, Chahwan C, Yamada Y, de Bruin RA, Wittenberg C, et al. (2007) Ctp1 is a cell-cycle-regulated protein that functions with Mre11 complex to control double-strand break repair by homologous recombination. Mol Cell 28: 134-146.

113. Bennardo N, Cheng A, Huang N, Stark JM. (2008) Alternative-NHEJ is a mechanistically distinct pathway of mammalian chromosome break repair. PLoS Genet 4: e1000110.

114. Yun MH, Hiom K. (2009) CtIP-BRCA1 modulates the choice of DNA double-strand-break repair pathway throughout the cell cycle. Nature 459: 460-463.

115. Wang H, Shi LZ, Wong CC, Han X, Hwang PY, et al. (2013) The interaction of CtIP and Nbs1 connects CDK and ATM to regulate HR-mediated double-strand break repair. PLoS Genet 9: e1003277.

116. Niida H, Katsuno Y, Banerjee B, Hande MP, Nakanishi M. (2007) Specific role of Chk1 phosphorylations in cell survival and checkpoint activation. Mol Cell Biol 27: 2572-2581.

117. Wilsker D, Petermann E, Helleday T, Bunz F. (2008) Essential function of Chk1 can be uncoupled from DNA damage checkpoint and replication control. Proc Natl Acad Sci U S A 105: 20752-20757.

118. Ziv Y, Bielopolski D, Galanty Y, Lukas C, Taya Y, et al. (2006) Chromatin relaxation in response to DNA double-strand breaks is modulated by a novel ATM- and KAP-1 dependent pathway. Nat Cell Biol 8: 870-876.

119. Goodarzi AA, Kurka T, Jeggo PA. (2011) KAP-1 phosphorylation regulates CHD3 nucleosome remodeling during the DNA double-strand break response. Nat Struct Mol Biol 18: 831-839.

120. Mockel C, Lammens K, Schele A, Hopfner KP. (2012) ATP driven structural changes of the bacterial Mre11:Rad50 catalytic head complex. Nucleic Acids Res 40: 914-927.

121. Lee JH, Mand MR, Deshpande R, Kinoshita E, Yang SH, et al. (2013) ATM kinase activity is regulated by ATP-driven conformational changes in the MRN complex. J Biol Chem .

122. Hohl M, Kwon Y, Galvan SM, Xue X, Tous C, et al. (2011) The Rad50 coiled-coil domain is indispensable for Mre11 complex functions. Nat Struct Mol Biol 18: 1124-1131.

123. McKinnon PJ. (2004) ATM and ataxia telangiectasia. EMBO Rep 5: 772-776.

124. Demuth I, Digweed M. (2007) The clinical manifestation of a defective response to DNA double-strand breaks as exemplified by nijmegen breakage syndrome. Oncogene 26: 7792-7798.

125. Waltes R, Kalb R, Gatei M, Kijas AW, Stumm M, et al. (2009) Human RAD50 deficiency in a nijmegen breakage syndrome-like disorder. Am J Hum Genet 84: 605-616.

126. Stewart GS, Maser RS, Stankovic T, Bressan DA, Kaplan MI, et al. (1999) The DNA double-strand break repair gene hMRE11 is mutated in individuals with an ataxia-telangiectasia-like disorder. Cell 99: 577-587.

127. Delia D, Piane M, Buscemi G, Savio C, Palmeri S, et al. (2004) MRE11 mutations and impaired ATM-dependent responses in an italian family with ataxia-telangiectasia-like disorder. Hum Mol Genet 13: 2155-2163.

128. Fernet M, Gribaa M, Salih MA, Seidahmed MZ, Hall J, et al. (2005) Identification and functional consequences of a novel MRE11 mutation affecting 10 saudi arabian patients with the ataxia telangiectasia-like disorder. Hum Mol Genet 14: 307-318.

129. Uchisaka N, Takahashi N, Sato M, Kikuchi A, Mochizuki S, et al. (2009) Two brothers with ataxia-telangiectasia-like disorder with lung adenocarcinoma. J Pediatr 155: 435-438.

130. Chaki M, Airik R, Ghosh AK, Giles RH, Chen R, et al. (2012) Exome capture reveals ZNF423 and CEP164 mutations, linking renal ciliopathies to DNA damage response signaling. Cell 150: 533-548.

131. Pitts SA, Kullar HS, Stankovic T, Stewart GS, Last JI, et al. (2001) hMRE11: Genomic structure and a null mutation identified in a transcript protected from nonsense-mediated mRNA decay. Hum Mol Genet 10: 1155-1162.

132. Matsumoto Y, Miyamoto T, Sakamoto H, Izumi H, Nakazawa Y, et al. (2011) Two unrelated patients with MRE11A mutations and nijmegen breakage syndrome-like severe microcephaly. DNA Repair (Amst) 10: 314-321.

133. Xiao Y, Weaver DT. (1997) Conditional gene targeted deletion by cre recombinase demonstrates the requirement for the double-strand break repair Mre11 protein in murine embryonic stem cells. Nucleic Acids Res 25: 2985-2991.

134. Luo G, Yao MS, Bender CF, Mills M, Bladl AR, et al. (1999) Disruption of mRad50 causes embryonic stem cell lethality, abnormal embryonic development, and sensitivity to ionizing radiation. Proc Natl Acad Sci U S A 96: 7376-7381.

135. Reina-San-Martin B, Nussenzweig MC, Nussenzweig A, Difilippantonio S. (2005) Genomic instability, endoreduplication, and diminished ig class-switch recombination in B cells lacking Nbs1. Proc Natl Acad Sci U S A 102: 1590-1595.

136. Weissman L, de Souza-Pinto NC, Stevnsner T, Bohr VA. (2007) DNA repair, mitochondria, and neurodegeneration. Neuroscience 145: 1318-1329.

137. Kulkarni A, Wilson DM,3rd. (2008) The involvement of DNA-damage and -repair defects in neurological dysfunction. Am J Hum Genet 82: 539-566.

138. Guo Z, Kozlov S, Lavin MF, Person MD, Paull TT. (2010) ATM activation by oxidative stress. Science 330: 517-521.

139. Oba D, Hayashi M, Minamitani M, Hamano S, Uchisaka N, et al. (2010) Autopsy study of cerebellar degeneration in siblings with ataxia-telangiectasia-like disorder. Acta Neuropathol 119: 513-520.

140. Weemaes CM, The TH, van Munster PJ, Bakkeren JA. (1984) Antibody responses in vivo in chromosome instability syndromes with immunodeficiency. Clin Exp Immunol 57: 529-534.

141. Shiloh Y. (1997) Ataxia-telangiectasia and the nijmegen breakage syndrome: Related disorders but genes apart. Annu Rev Genet 31: 635-662.

142. Lumsden JM, McCarty T, Petiniot LK, Shen R, Barlow C, et al. (2004) Immunoglobulin class switch recombination is impaired in atm-deficient mice. J Exp Med 200: 1111-1121.

143. Gorgoulis VG, Vassiliou LV, Karakaidos P, Zacharatos P, Kotsinas A, et al. (2005) Activation of the DNA damage checkpoint and genomic instability in human precancerous lesions. Nature 434: 907-913.

144. Garcia-Cao I, Garcia-Cao M, Martin-Caballero J, Criado LM, Klatt P, et al. (2002) "Super p53" mice exhibit enhanced DNA damage response, are tumor resistant and age normally. EMBO J 21: 6225-6235.

145. Wooster R, Bignell G, Lancaster J, Swift S, Seal S, et al. (1995) Identification of the breast cancer susceptibility gene BRCA2. Nature 378: 789-792.

146. Miki Y, Swensen J, Shattuck-Eidens D, Futreal PA, Harshman K, et al. (1994) A strong candidate for the breast and ovarian cancer susceptibility gene BRCA1. Science 266: 66-71.

147. Walsh T, King MC. (2007) Ten genes for inherited breast cancer. Cancer Cell 11: 103-105.

148. Athma P, Rappaport R, Swift M. (1996) Molecular genotyping shows that ataxia-telangiectasia heterozygotes are predisposed to breast cancer. Cancer Genet Cytogenet 92: 130-134.

149. Cybulski C, Wokolorczyk D, Kluzniak W, Jakubowska A, Gorski B, et al. (2013) An inherited NBN mutation is associated with poor prognosis prostate cancer. Br J Cancer 108: 461-468.

150. Zuhlke KA, Johnson AM, Okoth LA, Stoffel EM, Robbins CM, et al. (2012) Identification of a novel NBN truncating mutation in a family with hereditary prostate cancer. Fam Cancer 11: 595-600.

151. Ciara E, Piekutowska-Abramczuk D, Popowska E, Grajkowska W, Barszcz S, et al. (2010) Heterozygous germ-line mutations in the NBN gene predispose to medulloblastoma in pediatric patients. Acta Neuropathol 119: 325-334.

152. Seemanova E, Jarolim P, Seeman P, Varon R, Digweed M, et al. (2007) Cancer risk of heterozygotes with the NBN founder mutation. J Natl Cancer Inst 99: 1875-1880.

153. Swift M, Reitnauer PJ, Morrell D, Chase CL. (1987) Breast and other cancers in families with ataxia-telangiectasia. N Engl J Med 316: 1289-1294.

154. Thompson D, Duedal S, Kirner J, McGuffog L, Last J, et al. (2005) Cancer risks and mortality in heterozygous ATM mutation carriers. J Natl Cancer Inst 97: 813-822.

155. Renwick A, Thompson D, Seal S, Kelly P, Chagtai T, et al. (2006) ATM mutations that cause ataxia-telangiectasia are breast cancer susceptibility alleles. Nat Genet 38: 873-875.

156. Fletcher O, Johnson N, dos Santos Silva I, Orr N, Ashworth A, et al. (2010) Missense variants in ATM in 26,101 breast cancer cases and 29,842 controls. Cancer Epidemiol Biomarkers Prev 19: 2143-2151.

157. Boultwood J. (2001) Ataxia telangiectasia gene mutations in leukaemia and lymphoma. J Clin Pathol 54: 512-516.

158. Turner N, Tutt A, Ashworth A. (2004) Hallmarks of 'BRCAness' in sporadic cancers. Nat Rev Cancer 4: 814-819.

159. Zhu J, Petersen S, Tessarollo L, Nussenzweig A. (2001) Targeted disruption of the nijmegen breakage syndrome gene NBS1 leads to early embryonic lethality in mice. Curr Biol 11: 105-109.

160. Yamaguchi-Iwai Y, Sonoda E, Sasaki MS, Morrison C, Haraguchi T, et al. (1999) Mre11 is essential for the maintenance of chromosomal DNA in vertebrate cells. EMBO J 18: 6619-6629.

161. Adelman CA, De S, Petrini JH. (2009) Rad50 is dispensable for the maintenance and viability of postmitotic tissues. Mol Cell Biol 29: 483-492.

162. Demuth I, Frappart PO, Hildebrand G, Melchers A, Lobitz S, et al. (2004) An inducible null mutant murine model of nijmegen breakage syndrome proves the essential function of NBS1 in chromosomal stability and cell viability. Hum Mol Genet 13: 2385-2397.

163. Li A, Swift M. (2000) Mutations at the ataxia-telangiectasia locus and clinical phenotypes of A-T patients. Am J Med Genet 92: 170-177.

164. Micol R, Ben Slama L, Suarez F, Le Mignot L, Beaute J, et al. (2011) Morbidity and mortality from ataxia-telangiectasia are associated with ATM genotype. J Allergy Clin Immunol 128: 382-9.e1.

165. Theunissen JW, Kaplan MI, Hunt PA, Williams BR, Ferguson DO, et al. (2003) Checkpoint failure and chromosomal instability without lymphomagenesis in Mre11(ATLD1/ATLD1) mice. Mol Cell 12: 1511-1523.

166. Boisvert FM, Dery U, Masson JY, Richard S. (2005) Arginine methylation of MRE11 by PRMT1 is required for DNA damage checkpoint control. Genes Dev 19: 671-676.

167. Boisvert FM, Hendzel MJ, Masson JY, Richard S. (2005) Methylation of MRE11 regulates its nuclear compartmentalization. Cell Cycle 4: 981-989.

168. Dery U, Coulombe Y, Rodrigue A, Stasiak A, Richard S, et al. (2008) A glycine-arginine domain in control of the human MRE11 DNA repair protein. Mol Cell Biol 28: 3058-3069.

169. [Anonymous]. (2000) Nijmegen breakage syndrome. the international nijmegen breakage syndrome study group. Arch Dis Child 82: 400-406.

170. Kang J, Bronson RT, Xu Y. (2002) Targeted disruption of NBS1 reveals its roles in mouse development and DNA repair. EMBO J 21: 1447-1455.

171. Williams BR, Mirzoeva OK, Morgan WF, Lin J, Dunnick W, et al. (2002) A murine model of nijmegen breakage syndrome. Curr Biol 12: 648-653.

172. Difilippantonio S, Celeste A, Fernandez-Capetillo O, Chen HT, Reina San Martin B, et al. (2005) Role of Nbs1 in the activation of the atm kinase revealed in humanized mouse models. Nat Cell Biol 7: 675-685.

173. Difilippantonio S, Celeste A, Kruhlak MJ, Lee Y, Difilippantonio MJ, et al. (2007) Distinct domains in Nbs1 regulate irradiation-induced checkpoints and apoptosis. J Exp Med 204: 1003-1011.

174. Stracker TH, Morales M, Couto SS, Hussein H, Petrini JH. (2007) The carboxy terminus of NBS1 is required for induction of apoptosis by the MRE11 complex. Nature 447: 218-221.

175. Xu Y, Ashley T, Brainerd EE, Bronson RT, Meyn MS, et al. (1996) Targeted disruption of ATM leads to growth retardation, chromosomal fragmentation during meiosis, immune defects, and thymic lymphoma. Genes Dev 10: 2411-2422.

176. Barlow C, Hirotsune S, Paylor R, Liyanage M, Eckhaus M, et al. (1996) Atm-deficient mice: A paradigm of ataxia telangiectasia. Cell 86: 159-171.

177. Elson A, Wang Y, Daugherty CJ, Morton CC, Zhou F, et al. (1996) Pleiotropic defects in ataxia-telangiectasia protein-deficient mice. Proc Natl Acad Sci U S A 93: 13084-13089.

178. Spring K, Cross S, Li C, Watters D, Ben-Senior L, et al. (2001) Atm knock-in mice harboring an in-frame deletion corresponding to the human ATM 7636del9 common mutation exhibit a variant phenotype. Cancer Res 61: 4561-4568.

179. Daniel JA, Pellegrini M, Lee BS, Guo Z, Filsuf D, et al. (2012) Loss of ATM kinase activity leads to embryonic lethality in mice. J Cell Biol 198: 295-304.

180. Dumon-Jones V, Frappart PO, Tong WM, Sajithlal G, Hulla W, et al. (2003) Nbn heterozygosity renders mice susceptible to tumor formation and ionizing radiation-induced tumorigenesis. Cancer Res 63: 7263-7269.

181. Spring K, Ahangari F, Scott SP, Waring P, Purdie DM, et al. (2002) Mice heterozygous for mutation in atm, the gene involved in ataxia-telangiectasia, have heightened susceptibility to cancer. Nat Genet 32: 185-190.

182. Chen PL, Liu F, Cai S, Lin X, Li A, et al. (2005) Inactivation of CtIP leads to early embryonic lethality mediated by G1 restraint and to tumorigenesis by haploid insufficiency. Mol Cell Biol 25: 3535-3542.

183. Soderlund K, Stal O, Skoog L, Rutqvist LE, Nordenskjold B, et al. (2007) Intact Mre11/Rad50/Nbs1 complex predicts good response to radiotherapy in early breast cancer. Int J Radiat Oncol Biol Phys 68: 50-58.

184. Choudhury A, Nelson LD, Teo MT, Chilka S, Bhattarai S, et al. (2010) MRE11 expression is predictive of cause-specific survival following radical radiotherapy for muscle-invasive bladder cancer. Cancer Res 70: 7017-7026.

185. Laurberg JR, Brems-Eskildsen AS, Nordentoft I, Fristrup N, Schepeler T, et al. (2012) Expression of TIP60 (tat-interactive protein) and MRE11 (meiotic recombination 11

homolog) predict treatment-specific outcome of localised invasive bladder cancer. BJU Int 110: E1228-36.

186. Stokke T, DeAngelis P, Smedshammer L, Galteland E, Steen HB, et al. (2001) Loss of chromosome 11q21-23.1 and 17p and gain of chromosome 6p are independent prognostic indicators in B-cell non-hodgkin's lymphoma. Br J Cancer 85: 1900-1913.

187. Farmer H, McCabe N, Lord CJ, Tutt AN, Johnson DA, et al. (2005) Targeting the DNA repair defect in BRCA mutant cells as a therapeutic strategy. Nature 434: 917-921.

188. Bryant HE, Schultz N, Thomas HD, Parker KM, Flower D, et al. (2005) Specific killing of BRCA2-deficient tumours with inhibitors of poly(ADP-ribose) polymerase. Nature 434: 913-917.

189. Angele S, Treilleux I, Bremond A, Taniere P, Hall J. (2003) Altered expression of DNA double-strand break detection and repair proteins in breast carcinomas. Histopathology 43: 347-353.

190. D'Errico M, de Rinaldis E, Blasi MF, Viti V, Falchetti M, et al. (2009) Genome-wide expression profile of sporadic gastric cancers with microsatellite instability. Eur J Cancer 45: 461-469.

191. Giannini G, Ristori E, Cerignoli F, Rinaldi C, Zani M, et al. (2002) Human MRE11 is inactivated in mismatch repair-deficient cancers. EMBO Rep 3: 248-254.

192. Viana-Pereira M, Almeida I, Sousa S, Mahler-Araujo B, Seruca R, et al. (2009) Analysis of microsatellite instability in medulloblastoma. Neuro Oncol 11: 458-467.

193. O'Driscoll M, Ruiz-Perez VL, Woods CG, Jeggo PA, Goodship JA. (2003) A splicing mutation affecting expression of ataxia-telangiectasia and Rad3-related protein (ATR) results in seckel syndrome. Nat Genet 33: 497-501.

194. Hassan MJ, Chishti MS, Jamal SM, Tariq M, Ahmad W. (2008) A syndromic form of autosomal recessive congenital microcephaly (jawad syndrome) maps to chromosome 18p11.22-q11.2. Hum Genet 123: 77-82.

195. Miquel C, Jacob S, Grandjouan S, Aime A, Viguier J, et al. (2007) Frequent alteration of DNA damage signalling and repair pathways in human colorectal cancers with microsatellite instability. Oncogene 26: 5919-5926.

196. Falchetti M, Saieva C, Lupi R, Masala G, Rizzolo P, et al. (2008) Gastric cancer with high-level microsatellite instability: Target gene mutations, clinicopathologic features, and long-term survival. Hum Pathol 39: 925-932.

197. Ham MF, Takakuwa T, Luo WJ, Liu A, Horii A, et al. (2006) Impairment of double-strand breaks repair and aberrant splicing of ATM and MRE11 in leukemia-lymphoma cell lines with microsatellite instability. Cancer Sci 97: 226-234.

198. Mongiat-Artus P, Miquel C, Van der Aa M, Buhard O, Hamelin R, et al. (2006) Microsatellite instability and mutation analysis of candidate genes in urothelial cell carcinomas of upper urinary tract. Oncogene 25: 2113-2118.

199. Viana-Pereira M, Lee A, Popov S, Bax DA, Al-Sarraj S, et al. (2011) Microsatellite instability in pediatric high grade glioma is associated with genomic profile and differential target gene inactivation. PLoS One 6: e20588.

200. Gaymes TJ, Mohamedali AM, Patterson M, Matto N, Smith A, et al. (2013) Microsatellite instability induced mutations in DNA repair genes ctip and MRE11 confer hypersensitivity to poly (ADP-ribose) polymerase (PARP) inhibitors in myeloidmalignancies. Haematologica .

201. Giannini G, Rinaldi C, Ristori E, Ambrosini MI, Cerignoli F, et al. (2004) Mutations of an intronic repeat induce impaired MRE11 expression in primary human cancer with microsatellite instability. Oncogene 23: 2640-2647.

202. Alemayehu A, Fridrichova I. (2007) The MRE11/RAD50/NBS1 complex destabilization in lynch-syndrome patients. Eur J Hum Genet 15: 922-929.

203. Leary RJ, Lin JC, Cummins J, Boca S, Wood LD, et al. (2008) Integrated analysis of homozygous deletions, focal amplifications, and sequence alterations in breast and colorectal cancers. Proc Natl Acad Sci U S A 105: 16224-16229.

204. Ouillette P, Fossum S, Parkin B, Ding L, Bockenstedt P, et al. (2010) Aggressive chronic lymphocytic leukemia with elevated genomic complexity is associated with multiple gene defects in the response to DNA double-strand breaks. Clin Cancer Res 16: 835-847.

205. Fukuda T, Sumiyoshi T, Takahashi M, Kataoka T, Asahara T, et al. (2001) Alterations of the double-strand break repair gene MRE11 in cancer. Cancer Res 61: 23-26.

206. Heikkinen K, Karppinen SM, Soini Y, Makinen M, Winqvist R. (2003) Mutation screening of Mre11 complex genes: Indication of RAD50 involvement in breast and ovarian cancer susceptibility. J Med Genet 40: e131.

207. Bartkova J, Tommiska J, Oplustilova L, Aaltonen K, Tamminen A, et al. (2008) Aberrations of the MRE11-RAD50-NBS1 DNA damage sensor complex in human breast cancer: MRE11 as a candidate familial cancer-predisposing gene. Mol Oncol 2: 296-316.

208. Wang Z, Cummins JM, Shen D, Cahill DP, Jallepalli PV, et al. (2004) Three classes of genes mutated in colorectal cancers with chromosomal instability. Cancer Res 64: 2998-3001.

209. Schuetz JM, MaCarthur AC, Leach S, Lai AS, Gallagher RP, et al. (2009) Genetic variation in the NBS1, MRE11, RAD50 and BLM genes and susceptibility to non-hodgkin lymphoma. BMC Med Genet 10: 117-2350-10-117.

210. Sjoblom T, Jones S, Wood LD, Parsons DW, Lin J, et al. (2006) The consensus coding sequences of human breast and colorectal cancers. Science 314: 268-274.

211. Siegel R, Naishadham D, Jemal A. (2013) Cancer statistics, 2013. CA Cancer J Clin 63: 11-30.

212. Ziv Y, Bielopolski D, Galanty Y, Lukas C, Taya Y, et al. (2006) Chromatin relaxation in response to DNA double-strand breaks is modulated by a novel ATM- and KAP-1 dependent pathway. Nat Cell Biol 8: 870-876.

213. Beamish H, Lavin MF. (1994) Radiosensitivity in ataxia-telangiectasia: Anomalies in radiation-induced cell cycle delay. Int J Radiat Biol 65: 175-184.

214. Van Hooser A, Goodrich DW, Allis CD, Brinkley BR, Mancini MA. (1998) Histone H3 phosphorylation is required for the initiation, but not maintenance, of mammalian chromosome condensation. J Cell Sci 111 (Pt 23): 3497-3506.

215. Uziel T, Lerenthal Y, Moyal L, Andegeko Y, Mittelman L, et al. (2003) Requirement of the MRN complex for ATM activation by DNA damage. EMBO J 22: 5612-5621.

216. Cuadrado M, Martinez-Pastor B, Murga M, Toledo LI, Gutierrez-Martinez P, et al. (2006) ATM regulates ATR chromatin loading in response to DNA double-strand breaks. J Exp Med 203: 297-303.

217. Limbo O, Moiani D, Kertokalio A, Wyman C, Tainer JA, et al. (2012) Mre11 ATLD17/18 mutation retains Tel1/ATM activity but blocks DNA double-strand break repair. Nucleic Acids Res 40: 11435-11449.

218. van der Linden E, Sanchez H, Kinoshita E, Kanaar R, Wyman C. (2009) RAD50 and NBS1 form a stable complex functional in DNA binding and tethering. Nucleic Acids Res 37: 1580-1588.

219. Boboila C, Jankovic M, Yan CT, Wang JH, Wesemann DR, et al. (2010) Alternative end-joining catalyzes robust IgH locus deletions and translocations in the combined absence of ligase 4 and Ku70. Proc Natl Acad Sci U S A 107: 3034-3039.

220. Yan CT, Boboila C, Souza EK, Franco S, Hickernell TR, et al. (2007) IgH class switching and translocations use a robust non-classical end-joining pathway. Nature 449: 478-482.

221. Wang JH, Gostissa M, Yan CT, Goff P, Hickernell T, et al. (2009) Mechanisms promoting translocations in editing and switching peripheral B cells. Nature 460: 231-236.

222. Della-Maria J, Zhou Y, Tsai MS, Kuhnlein J, Carney JP, et al. (2011) Human Mre11/human Rad50/Nbs1 and DNA ligase IIIalpha/XRCC1 protein complexes act together in an alternative nonhomologous end joining pathway. J Biol Chem 286: 33845-33853.

223. Tobin LA, Robert C, Nagaria P, Chumsri S, Twaddell W, et al. (2012) Targeting abnormal DNA repair in therapy-resistant breast cancers. Mol Cancer Res 10: 96-107.

224. Tobin LA, Robert C, Rapoport AP, Gojo I, Baer MR, et al. (2013) Targeting abnormal DNA double-strand break repair in tyrosine kinase inhibitor-resistant chronic myeloid leukemias. Oncogene 32: 1784-1793.

225. Robert I, Dantzer F, Reina-San-Martin B. (2009) Parp1 facilitates alternative NHEJ, whereas Parp2 suppresses IgH/c-myc translocations during immunoglobulin class switch recombination. J Exp Med 206: 1047-1056.

226. Wang M, Wu W, Wu W, Rosidi B, Zhang L, et al. (2006) PARP-1 and ku compete for repair of DNA double strand breaks by distinct NHEJ pathways. Nucleic Acids Res 34: 6170-6182.

227. Her C, Vo AT, Wu X. (2002) Evidence for a direct association of hMRE11 with the human mismatch repair protein hMLH1. DNA Repair (Amst) 1: 719-729.

228. Vo AT, Zhu F, Wu X, Yuan F, Gao Y, et al. (2005) hMRE11 deficiency leads to microsatellite instability and defective DNA mismatch repair. EMBO Rep 6: 438-444.

229. Zhao N, Zhu F, Yuan F, Haick AK, Fukushige S, et al. (2008) The interplay between hMLH1 and hMRE11: Role in MMR and the effect of hMLH1 mutations. Biochem Biophys Res Commun 370: 338-343.

230. Linzer DI, Levine AJ. (1979) Characterization of a 54K dalton cellular SV40 tumor antigen present in SV40-transformed cells and uninfected embryonal carcinoma cells. Cell 17: 43-52.

231. Lane DP, Crawford LV. (1979) T antigen is bound to a host protein in SV40-transformed cells. Nature 278: 261-263.

232. Lane DP. (1992) Cancer. p53, guardian of the genome. Nature 358: 15-16.

233. Stracker TH, Carson CT, Weitzman MD. (2002) Adenovirus oncoproteins inactivate the Mre11-Rad50-NBS1 DNA repair complex. Nature 418: 348-352.

234. Orazio NI, Naeger CM, Karlseder J, Weitzman MD. (2011) The adenovirus E1b55K/E4orf6 complex induces degradation of the bloom helicase during infection. J Virol 85: 1887-1892.

235. Pellegrini M, Celeste A, Difilippantonio S, Guo R, Wang W, et al. (2006) Autophosphorylation at serine 1987 is dispensable for murine atm activation in vivo. Nature 443: 222-225.

236. Bakkenist CJ, Kastan MB. (2003) DNA damage activates ATM through intermolecular autophosphorylation and dimer dissociation. Nature 421: 499-506.

237. Dupre A, Boyer-Chatenet L, Sattler RM, Modi AP, Lee JH, et al. (2008) A forward chemical genetic screen reveals an inhibitor of the Mre11-Rad50-Nbs1 complex. Nat Chem Biol 4: 119-125.

238. Boisvert FM, Cote J, Boulanger MC, Richard S. (2003) A proteomic analysis of arginine-methylated protein complexes. Mol Cell Proteomics 2: 1319-1330.

239. Boisvert FM, Rhie A, Richard S, Doherty AJ. (2005) The GAR motif of 53BP1 is arginine methylated by PRMT1 and is necessary for 53BP1 DNA binding activity. Cell Cycle 4: 1834-1841.

240. Adams MM, Wang B, Xia Z, Morales JC, Lu X, et al. (2005) 53BP1 oligomerization is independent of its methylation by PRMT1. Cell Cycle 4: 1854-1861.

241. Rai R, Zheng H, He H, Luo Y, Multani A, et al. (2010) The function of classical and alternative non-homologous end-joining pathways in the fusion of dysfunctional telomeres. EMBO J 29: 2598-2610.

242. Lottersberger F, Bothmer A, Robbiani DF, Nussenzweig MC, de Lange T. (2013) Role of 53BP1 oligomerization in regulating double-strand break repair. Proc Natl Acad Sci U S A 110: 2146-2151.

243. Mitchell TR, Glenfield K, Jeyanthan K, Zhu XD. (2009) Arginine methylation regulates telomere length and stability. Mol Cell Biol 29: 4918-4934.

244. Deng Z, Norseen J, Wiedmer A, Riethman H, Lieberman PM. (2009) TERRA RNA binding to TRF2 facilitates heterochromatin formation and ORC recruitment at telomeres. Mol Cell 35: 403-413.

245. Bothmer A, Robbiani DF, Di Virgilio M, Bunting SF, Klein IA, et al. (2011) Regulation of DNA end joining, resection, and immunoglobulin class switch recombination by 53BP1. Mol Cell 42: 319-329.

246. Zimmermann M, Lottersberger F, Buonomo SB, Sfeir A, de Lange T. (2013) 53BP1 regulates DSB repair using Rif1 to control 5' end resection. Science 339: 700-704.

247. Escribano-Diaz C, Orthwein A, Fradet-Turcotte A, Xing M, Young JT, et al. (2013) A cell cycle-dependent regulatory circuit composed of 53BP1-RIF1 and BRCA1-CtIP controls DNA repair pathway choice. Mol Cell 49: 872-883.

248. van Steensel B, Smogorzewska A, de Lange T. (1998) TRF2 protects human telomeres from end-to-end fusions. Cell 92: 401-413.

249. Theunissen JW, Petrini JH. (2006) Methods for studying the cellular response to DNA damage: Influence of the Mre11 complex on chromosome metabolism. Methods Enzymol 409: 251-284.